

COMPACTION ANALYSIS OF AGRICULTURAL
SOIL USING GAMMA RAY TECHNIQUES

By

WANGXING LI

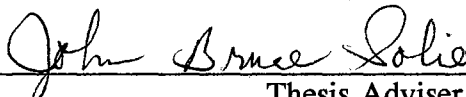
Bachelor of Science
in Agricultural Engineering
Jilin University of Technology
Changchun, Jilin Province
People's Republic of China
1982

Master of Science
in Agricultural Engineering
University of Nebraska-Lincoln
Lincoln, Nebraska
1986

Submitted to the Faculty of the
Graduate College of the
Oklahoma State University
in partial fulfillment of
the requirements for
the Degree of
DOCTOR OF PHILOSOPHY
December, 1994

COMPACTION ANALYSIS OF AGRICULTURAL
SOIL USING GAMMA RAY TECHNIQUES

Thesis Approved:

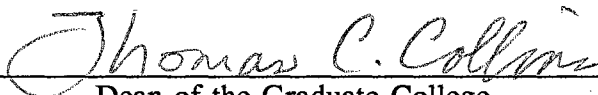


Thesis Adviser









Dean of the Graduate College

PREFACE

This research concerns the relationship among the load, track width and resulting density profiles in soil samples. Four experiments were conducted, and gamma ray techniques were used to detect the density distribution in soil samples. I am grateful to Dr. John Solie, my research adviser, for his invaluable advice throughout this program and his many suggestions on this dissertation.

I am indebted to other committee members; Dr. Glenn Kranzler, Dr. Glenn Brown, Biosystems and Agricultural Engineering Department and Dr. William Raun, Agronomy Department. I also acknowledge the contribution of Dr. Glenn Brown for allowing me to use the Gamma Ray Technique System and assisting me in the process of scanning soil samples.

I express my appreciation to the Biosystems and Agricultural Engineering Department for supplying experimental equipment and financial support. I also thank many fellow graduate students in the department for helping my experiment, sharing their experience and, of course, friendship.

My parents and my brothers deserve special gratitude for their support and their confidence in me during my study in the United States. Last but not least, I would like to thank my wife, Chunhua, for her love, encouragement, patience and sacrifice during this program.

TABLES OF CONTENTS

Chapter	Page
I. INTRODUCTION	1
II. LITERATURE REVIEW	4
Effects of Soil Properties on Soil Strength	4
Compaction Modeling	6
Finite Element Models	15
Gamma Ray Transmission Method	15
Effects of Soil Compaction on Plant Growth	18
III. EXPERIMENTAL EQUIPMENT AND PROCEDURE	24
Laboratory Experiment	25
Experimental Analysis	25
Soil Bin Experiment	28
Field Experiments	30
Force Transducers	31
Speed Transducer	33
Data Acquisition System	34
IV. RESULTS AND DISCUSSION	37
Theoretical Considerations	38
Analysis of Laboratory Controlled Experiment	42
Modeling Single Iso-Density Line	43
Determination of Y_{offset}	47
Determination of Parameter A	47
Determination of Parameter B	50
Calculate Iso-Density Lines	51
Calculate Density Value at Any Location	53
Analysis of Area Enclosed by Iso-Density Lines	60
Maximum Width of Compaction	61
Analysis of Soil Bin Experiment	61
Contact Area between Press Wheel and Soil Surface	65
Properties of Soil Bin Experiment Samples	65
Elimination of Linear Trend	66

Chapter	Page
Compensation for the Effect of Moisture Content	66
Cause of the Linear Trend of Soil Density Profile	73
Analysis of Field Experiments	73
Forces Exerted on the Press Wheel	77
First Field Experiment	77
Second Field Experiment	79
Analysis of Soil Attenuation Coefficients	81
 V. SUMMARY, CONCLUSIONS AND RECOMMENDATIONS	 87
Summary	87
Conclusions	89
Recommendations for Future Research	91
 REFERENCES	 93
 APPENDIX A - PROGRAMS FOR DATA ACQUISITION AND PROCESSING	 98
 APPENDIX B - DESIGN DRAWINGS FOR FORCE TRANSDUCER, CALIBRATION BRACKETS	 116
 APPENDIX C - CONTOUR MAPS OF ORIGINAL DENSITY PROFILES OF LABORATORY EXPERIMENT SAMPLES	 121
 APPENDIX D - FIGURES OF FITTING LABORATORY EXPERIMENT SAMPLES FOR DENSITY LEVEL OF 1.2, 1.25 AND 1.3 g/cm ³	 134
 APPENDIX E - MAPS OF EXPERIMENTAL DESIGNS	 147

LIST OF TABLES

Table	Page
I. Parameters for Equation (1)	5
II. Density Deviations Caused by Inaccuracies of Five Component Members	18
III. Critical Bulk Density Values (g/cm ³) Calculated from PR and WC	19
IV. Incomplete Factorial Design of Experiments	30
V. Characteristics of Laboratory Experiment Samples	43
VI. Fitting Single Density Lines for Density 1.20 g/cm ³	47
VII. Fitting Single Density Lines for Density 1.25 g/cm ³	48
VIII. Fitting Single Density Lines for Density 1.30 g/cm ³	49
IX. Determination of Parameter A	49
X. General Linear Model Procedure for Parameter A	50
XI. Determination of Parameter B	51
XII. General Linear Model Procedure for Parameter B	52
XIII. Validation of Modeling Iso-Density Line of 1.25 g/cm ³	55
XIV. Summary of Calculation Errors for Laboratory Test Samples	57
XV. Characteristics of Soil Bin Experiment Samples	67
XVI. Fitting of Linear Trend of Density for Soil Bin Experiment	68
XVII. Summary of Prediction Errors for Soil Bin Experiment	69
XVIII. Average Properties of Field Experiment No. 1	77

Table	Page
XIX. Average Properties of Field Experiment No. 2 And Prediction Errors for Zone 3	81
XX. Average Soil Attenuation Coefficients (cm ² /g)	86

LIST OF FIGURES

Figure	Page
1. Lines of Equal Bulk Density (g/cm^3) Caused by a Rigid Cylinder	14
2. Schematic of Gamma Ray Scanning System	26
3. Press Wheel System with Force Transducers	32
4. Load Transducer with Strain Gage Location and Wiring Configuration . . .	33
5. Integration of Area Enclosed by an Iso-Density Line	40
6. Contour of Sample #112 with 25 mm Wide Track and 5 kg Ballast	45
7. Fitting of Sample #112 with 25 mm Wide Track and 5 kg Mass	46
8. Calculating $1.25 \text{ g}/\text{cm}^3$ Iso-Density Line of Sample #112 With Parameters A and B Generated for This Sample and Whole Experiment	54
9. Contour Lines of Density Generated from the Calculated Data for Sample #111 with 25 mm Wide Track and 5 kg Mass	58
10. Contour Lines of Errors (%) of Calculated Density for Sample #111 with 25 mm Wide Track and 5 kg Mass	59
11. Cross Sectional Area Enclosed by Iso-Density Lines as a Function of Soil Density for Several Simulated Wheel Tracks and Press Wheel Ballasts . .	62
12. Maximum Penetration Depth as a Function of Soil Density for Several Simulated Wheel Tracks and Press Wheel Ballasts	63
13. Maximum Compaction Width as a Function of Soil Density for Several Simulated Wheel Tracks and Press Wheel Ballasts	64
14. Schematic of Soil and Wheel Contact Area and Its Effective Length	66
15. Contour Lines of Original Density Data of Sample #151 with 51 mm Press Wheel and 28.5 kPa Load	70

Figure	Page
16. Contour Lines of Density Generated from Predicted Data for Sample #151 with 51 mm Press Wheel and 28.5 kPa Load	71
17. Contour Lines of Errors (%) of Predicting Density for Sample #151 with 51 mm Press Wheel and 28.5 kPa Load	72
18. Contour Lines of the Sample Packed Directly in Laboratory	74
19. Contour Lines of the Sample Packed in Soil Bin and Transported Horizontally with Plaster of Paris on the Top	75
20. Contour Lines of the Sample Packed in Soil Bin and Transported Vertically	76
21. Forces Exerted on Press Wheel for Plot #105 of Field Experiment No. 2 with 10 kg Ballast and 51 mm Press Wheel	78
22. Contour of Density Profiles for Sample #142 of Field Experiment No. 1 with 10 kg Ballast and 25 mm Press Wheel	80
23. Contour of Original Density Profiles of Sample #152 of Field Experiment No. 2 with 10 kg Ballast and 25 mm Press Wheel	82
24. Contour of Simulated Density Profiles of Sample #152 of Field Experiment No. 2 with 10 kg Ballast and 25 mm Press Wheel	83
25. Contour of Simulation Errors of Sample #152 of Field Experiment No. 2 with 10 kg Ballast and 25 mm Press Wheel	84

CHAPTER I

INTRODUCTION

Researchers and manufacturers of planting machines have contributed numerous efforts to design and test individual components and their combinations to improve the reliability of germination, emergence and establishment of crop plants. In general, the following planting functions are considered in designing a planting machine (Erbach et al., 1983):

1. Residue cutting or clearing,
2. Opening a soil furrow,
3. Metering and depositing seed,
4. Covering the soil opening,
5. Compacting the soil under, over or around the seed,
6. Applying extraneous materials to the seeded area, and
7. Controlling planting depth.

Compacting the soil by the rear press wheel and ballast, compared to other components of the planting machine, has not received enough attention. Though some attempts have been made to relate the effects of press wheel and ballast on the establishment of crops (Morrison, 1989), very little has been learned about how the press wheel and ballast apply stress to soil layers and then compact the soil. When

approaching the compaction problem, most literature deals with only general agricultural machinery and about compaction much deeper and ballast loads much higher than those exerted by planting machines. Therefore, it is very beneficial to understand the mechanism of soil compaction around the seed zone.

Modeling is a powerful tool to theorize the compaction process and the related phenomena. The general goal of an agricultural soil compaction model is to be used to design systems for effective management of soil physical condition for improving cropping systems. To achieve this, it is necessary to have a complete understanding of the following facets (Schafer et al., 1991):

1. The sources of the force systems causing the compaction,
2. The propagation and distribution of the stresses within the soil mass which are caused by these force systems,
3. The soil's response to the stresses (compaction behavior), and
4. The relationship (and consequences) of the resulting compaction state to the cropping system (the plant, the fluid and gaseous movements and the biological and chemical activities).

Soil compaction of a planting system depends mainly on the rear press wheel geometry and its ballast (or load), and may be influenced by the opener and the coulter. Soil properties, especially moisture content, are known to significantly affect soil compaction. However, the relationships among these factors and the resulting soil compaction are not well defined. Therefore, the specific objectives of this research were:

1. Develop a model to predict the soil compaction under the different track widths and ballasts, and derive a better understanding of how the compaction process affects

density distribution in soil,

2. Determine the effects of the rear press wheel and the ballast on the soil compaction as measured by soil density around the seed zone in controlled laboratory conditions,

3. Develop and evaluate the use of gamma ray techniques to measure density profile in soil samples compacted by press wheels, and

4. Conduct soil bin and field experiments to test the model's applicability under different conditions.

CHAPTER II

LITERATURE REVIEW

Effects of Soil Properties on Soil Strength

To evaluate the effects of traffic on soil condition, Blackwell et al. (1986) conducted an experiment with three treatments: unwheeled soil, moderately wheeled soil and heavily wheeled soil. They measured the change of soil porosity and determined that the same change trend occurred for soil strengths. This relationship suggested that the percentage amount of air-filled pores within soil could be related to soil strength, and that it could be utilized as an index to predict soil strength.

Ball and O'Sullivan (1982) found that cone resistance and vane shear strength tended to decrease with increasing water content and decreasing bulk density down to 1300 kg/m³, but at lower density, they were not related to bulk density. Cone resistance and vane shear strength tended to decrease with increasing coarseness of texture, but also depended on soil structure and organic matter content.

Ayers (1987) conducted a torsional shear test to investigate the moisture and density effects on soil shear strength parameters for coarse-grained soils. Soil shear strength parameters included soil cohesion and soil friction angle. The conclusions were: 1) Generally, for all soil types, values for both soil cohesion and friction angle increased with increasing soil density, 2) Lower soil cohesion values were found in soil types with

lower clay content, 3) Loamy sands tended to exhibit peak strength parameter values at intermediate moisture contents for constant density soil conditions, and 4) Except at low moisture levels, the soil friction angle values for sands were relatively independent of moisture content. One of their prediction equations was

$$c, \phi = a + bBD + dBD^2 + eBD^3 + fMC + gMC^2 + hMC^3 + iBDMC + jBD^2MC + kBDMC^2 \quad (1)$$

where c is soil cohesion, ϕ is soil internal friction angle, BD is bulk density (g/cm^3), MC is moisture content (% dry basis) and $a, b, d, e, f, g, h, i, j$ and h are constants. Their values are listed in Table I.

TABLE I
PARAMETERS FOR EQUATION (1)

Constants	c	ϕ
a	-897.04	-21.67
b	1922.17	72.94
c	-1382.61	-61.48
d	335.39	15.08
e	-6.811	-4.656
f	0.0315	0.6506
g	0.01305	-0.00955
h	16.743	-0.169
i	-4.231	2.114
j	-0.4725	-0.3211
R-Square	0.93	0.95

Equation (1) was determined for normal stresses of 0, 20.7 and 34.5 kPa, moisture content from 1.7 to 14.5 percent dry basis, and soil bulk density from 1.22 to 1.64 g/cm^3 . The soil was loamy sand type, with 79% sand, 14% silt and 7% clay.

Perumpral (1983) reviewed and summarized the applications of cone penetrometers. Many important conclusions were made, including the following three:

- 1) Penetration resistance decreased as moisture content increased,
- 2) At high moisture content, density had minimal effect on penetration resistance.

However, the reverse was true at low moisture content, and

- 3) Penetration resistance was influenced by soil type.

Compaction Modeling

Compaction modeling was attempted by many researchers in many ways. The Finite Element Method (FEM) is a relatively new approach, but it has been validated primarily by laboratory test data.

The modeling of compaction usually takes the form of relating the force or stress exerted on the soil to the final density or strength of soil. For example, the following equation, based on triaxial tests, describes the density-stress behavior of soil (Bailey and Vanden Berg, 1968):

$$(1/BD) = m \log \sigma + b \quad (2)$$

where

BD = bulk density,

m = compressibility coefficient,

σ = applied stress, and

b = (1/BD) at an applied stress of 1.0.

Equation (2) is widely used, but it is invalid when applied stress, σ , approaches zero. Another equation based on a hydrostatic model solves this problem (Bailey, 1986):

$$\ln(V/V_i) = (A+B\sigma_h) (1-e^{-C\sigma_h}) \quad (3)$$

where

V_i = initial volume,

V = volume,

σ_h = hydrostatic stress, and

A, B, C = compactibility coefficients.

In terms of bulk density, equation (3) becomes

$$\ln\left(\frac{BD_i}{BD}\right) = (A+B\sigma_h) (1-e^{-C\sigma_h}) \quad (4)$$

where

BD_i = bulk density at zero pressure, and

BD = bulk density.

Equations (3) and (4) are valid for the data at both low and high stresses. Nevertheless, they were derived from hydrostatic load conditions and need to be expanded for complex loading conditions. Grisso et al. (1987) modified them by including a multiplicative factor, β , which was a function of principal stress ratio (PSR), and by replacing σ_h with octahedral normal stress, σ_{oct} . This equation was:

$$\ln(V/V_i) = \beta (A+B\sigma_{oct}) (1-e^{-C\sigma_{oct}}) \quad (5)$$

where

$$\beta = M_f(PSR-1) + (M_o-M_f) (PSR-1) (e^{-F\sigma_{oct}}) + 1 \quad (6)$$

and

σ_{oct} = octahedral normal stress,

PSR = principal stress ratio (σ_1/σ_3),

M_f , M_0 , F = soil parameters, and

A , B , C = compactibility coefficients which were determined from hydrostatic tests.

Equation (5) described the compaction of the cylindrical triaxial test samples well for each PSR < 3.0, and it omitted the effects of shear stress. Bailey and Johnson (1988) proceeded to further develop the model so that it better described the compaction behavior of soil subjected to a stress state which included shear stresses. The equation was:

$$\ln(V/V_i) = (A+B\sigma_{oct}) (1-e^{-C\sigma_{oct}}) + D(\gamma_{oct}/\sigma_{oct}) \quad (7)$$

where D = coefficient for the component of natural volumetric strain due to shearing stress.

To use the relationships between the stress and volumetric changes, the relationships between the stress state and the applied forces must be known. Various approaches for different circumstances have been recorded. Assuming that soil is homogeneous, isotropic, linearly elastic and using the theory of elasticity, Jumikis (1984) reported that Boussinesq (1885) developed an equation to calculate the vertical stress distribution resulting from a point load acting perpendicular to the surface. The equation was:

$$\sigma_z = \frac{Q(3z^3)}{2\pi(r^2+z^2)^{5/2}} \quad (8)$$

where

σ_z = the vertical compressive stress due to the point load at a point under the

surface,

Q = the point load applied at the surface,

z = the depth to the point in question, and

r = the horizontal distance from the point load to the point in question.

Boussinesq's stress distribution theory was based on the result given by the mathematical theory of elasticity for the simplest case of loading of a solid, homogeneous, elastic-isotropic, semi-infinite medium: namely, the case of a single, vertical, point load applied at a point on the horizontal boundary surface (or ground surface). Boussinesq's stress distribution theory gave all normal and shear stress components. In dealing with compaction, only the vertical, normal, compressive stress, σ_z , acting on a horizontal area is of interest.

Agricultural soils distribute stresses differently from the above assumptions. The point-load equation was modified to incorporate a concentration factor to account for agricultural soils (Soehne, 1958):

$$\sigma_z = \frac{\nu Q}{2\pi z^2} \cos^{(\nu+2)} \theta \quad (9)$$

where

ν = concentration factor; suggested values 4, 5 and 6 for hard, medium and soft soils respectively, and

θ = angle between the point load vector and the radial arm connecting the point in question to the intersection of the point load and the surface.

If the concentration factor, ν , is set to 3, equation (9) becomes equation (8). This fact indicates that agricultural soil is too soft to be modeled directly by equation (8).

Johnson and Burt (1986) applied the point-load equation (8) to determine the

complete stress state due to tractor loads in agricultural soils. An area of uniformly distributed load is sometimes used to represent the tire load on the soil surface. Double integration of the point-load equation was used to derive the following equation to calculate stress distribution under the corner of a uniformly loaded rectangular area:

$$\sigma_z = q_0 \frac{1}{4\pi} \left\{ \frac{2mn(m^2+n^2+1)^{1/2}}{m^2+n^2+1+m^2n^2} \times \frac{(m^2+n^2+2)}{(m^2+n^2+1)} + \arctan \frac{2mn(m^2+n^2+1)^{1/2}}{m^2+n^2+1-m^2n^2} \right\} \quad (10)$$

where

q_0 = surface or contact stress,

$m = W/z$,

$n = L/z$, and

L, W = length and width of the uniformly loaded area, respectively.

Because equation (10) was derived from the point-load equation, which uses a concentration factor of 3, there may be inaccuracies in utilizing it for predicting subsurface stress distribution in agricultural soils where concentration factors of 4, 5 and 6 are expected. Using two software packages, Macsyma and Maple (LISP based, symbolic manipulation programs), Ayers and Riper (1991) integrated the point-load equation (9) with concentration factors of 4, 5 and 6. The resulting equations were:

Concentration factor of 4 (hard soil):

$$\sigma_z = \frac{q_0}{4\pi} \left\{ n(m^2+1)^{3/2} (m^2+n^2+1) (2n+3) \arctan \left(\frac{m}{(n^2+1)^{1/2}} \right) + m(n^2+1)^{3/2} (m^2+n^2+1) (2m^2+3) \arctan \left(\frac{n}{(m^2+1)^{1/2}} \right) + mn(m^2+1)^{1/2} (n^2+1)^{1/2} (m^2+n^2+2) \right\} / \left\{ (m^2+1)^{3/2} (n^2+1)^{3/2} (m^2+n^2+1) \right\} \quad (11)$$

Concentration factor of 5 (medium soil):

$$\sigma_z = \frac{q_0}{12\pi} \left\{ 2mn [5(m^6+n^6) + 19(m^4+n^4) + 26(m^2+n^2) + 3(m^2n^6+m^6n^2) + 21(m^2n^4+m^4n^2) + 6m^4n^4 + 42m^2n^2 + 12] / [(m^2+1)^2(n^2+1)^2(m^2+n^2+1)^{3/2}] + 3 \arctan \left(\frac{2mn(m^2+n^2+1)^{1/2}}{m^2+n^2+1-m^2n^2} \right) \right\} \quad (12)$$

Concentration factor of 6 (soft soil):

$$\sigma_z = \frac{q_0}{16\pi} \left\{ n(m^2+1)^{5/2}(m^2+n^2+1)^2(8m^4+20m^2+15) \arctan \left(\frac{m}{(n^2+1)^{1/2}} \right) + m(n^2+1)^{5/2}(m^2+n^2+1)^2 (8n^4+20n^2+15) \arctan \left(\frac{n}{(m^2+1)^{1/2}} \right) + mn(m^2+1)^{1/2}(n^2+1)^{1/2} [38(m^2+n^2) + 27(m^4+n^4) + 7(m^6+n^6) + 29(m^4n^2+m^2n^4) + 60m^2n^2 + 8m^4n^4 + 4(m^2n^6+m^6n^2) + 18] \right\} / [(m^2+1)^{5/2}(n^2+1)^{5/2}(m^2+n^2+1)^2] \quad (13)$$

Nevertheless, there were no experimental data to verify the accuracy of equations (11) to (13), except for a successful match with the point-load equation.

In addition to point load, the shear load (or horizontal direction load) on the applied point affected the stress state. Johnson and Burt (1990) proposed the following equation:

$$\sigma_r = v(P \cos^{v-2} \varphi + H \sin^{v-2} \varphi \cos \theta) / 2\pi R^2 \quad (14)$$

where

σ_r = normal stress at a soil element,

v = Froehlich's concentration factor, $v \geq 3.0$,

P = normal point load,

H = shear point load,

φ = angle between the normal load vector and the position vector from the point

load to the desired point,

θ = angle between the shear load vector and the vertical plane that contains the position vector from the shear load to the desired point, and

R = radial distance from point load to a desired point.

When predicting the soil stress state under a tractor tire, equation (14) was integrated numerically, assuming different types of applied force patterns. For the normal force, three types of force distributions under the tire were evaluated. Type I was a uniform distribution. Types II and III were similar to each other, with the exception of having different ratios of pressure at the sideline to the pressure at the centerline. The formula for the Types II and III was:

$$\begin{aligned} p_i &= [A + (B-A) (y/y_{\max})^n] [1 - (x/x_{\max})^n] \\ B &= rA \\ A &= (n+1)^2 p_{\text{ave}} / [n(n+r)] \\ r &> 0 \end{aligned} \tag{15}$$

where

p_i = normal pressure at any point within footprint,

A = normal pressure at the center of footprint,

B = normal pressure at the sides of footprint,

r = ratio of B to A, $r=0.5$ for type II and $r=2$ for type III,

n = power for parabolic pressure distribution,

p_{ave} = average normal pressure over footprint,

x, y = x and y coordinates of i^{th} point within footprint, and

X_{\max} , Y_{\max} = one-half of foot print length and width at the x-y coordinates, respectively.

The normal force for a small area, A_i , was:

$$P_i = p_i A_i \quad (16)$$

The shear component, H_i , aligned in the direction of travel was assumed uniformly distributed over the tire footprint or modeled as:

$$H_i = A_i (c + p_i \tan \delta) (1 - e^{-j_i/k}) \quad (17)$$

where

c = soil cohesion,

δ = soil internal friction angle,

j_i = shear displacement at A_i , and

k = shear displacement coefficient.

The shear displacement, j , was assumed to vary linearly from zero at the leading front edge of the tire footprint to a maximum value equal to the product of the footprint length and travel reduction at the trailing rear edge of the footprint. Since a flat footprint was assumed, the dynamic load on the tire was ΣP_i , and the net traction was ΣH_i . Therefore, this model was useful for predicting the stress state from the tire dynamic load and traction.

All the models mentioned above will predict that the maximum density occurs on the soil surface where the applied stress is larger than any other location below the soil surface. However, the highest density sometimes occurs at a location some distance below the soil surface. Chancellor et al. (1962) measured changes in bulk density in a Yolo sandy loam at 14.7 percent water by weight when a 7.6 cm piston was forced 6.3 cm into the soil at the rate of 1.2 cm/min. Larson et al. (1971) presented the lines of equal bulk density following the treatment (Figure 1). Maximum density occurred at the point of a cone beneath the piston. The volume of soil forming the cone beneath the face

of the cylinder and the point of maximum density acted as a portion of the cylinder as it was forced into the soil. Shear failure occurred on the surface of the cone. This was also called the soil wedge effect. Chancellor et al. (1962) concluded that this effect was more apparent in soil samples of high initial porosity (low density) and high moisture contents. The wider the pressing cylinder, the higher the value of density produced.

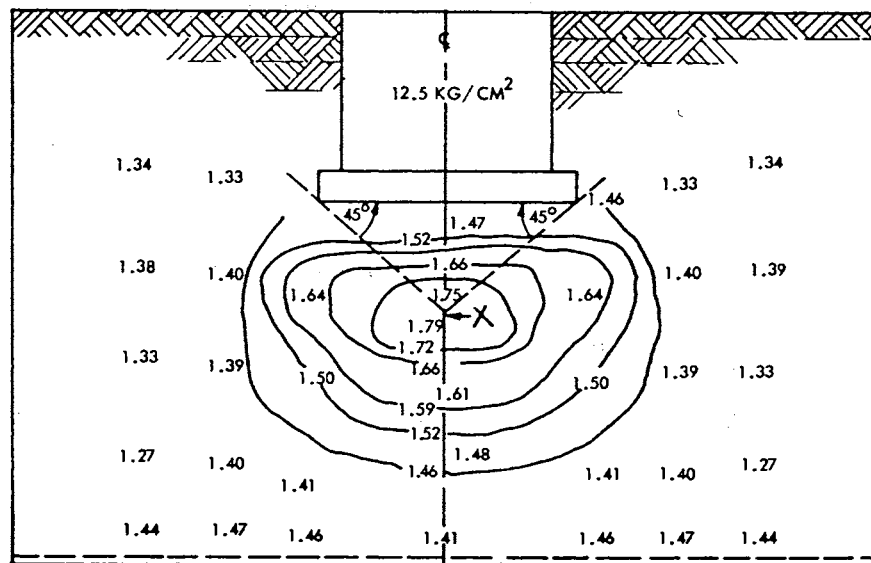


Figure 1. Lines of Equal Bulk Density (g/cm³) Caused by a Rigid Cylinder.

As noted by Wolf and Hadas. (1984) after trying several models, the stress-strain relationships of loose soil subjected to wheeled or crawler traffic were complex and not fully understood. Thus, predictive modeling of soil compaction failed quantitatively, although it showed the expected trend. Therefore, modeling loose soil less than 10 cm deep was a trial-and-error process. There has been was no firm conclusion on this matter.

Finite Element Models

Based on the Terzaghi's passive earth pressure theory, several analytical models were developed. These were fairly simple equations to evaluate forces on the tools, but could not account for the effect of different kinds of shapes of tillage blades. An FEM model was developed by Yong & Henna (1977) for two-dimensional soil failure with a wide blade and a three-dimensional model by Chi & Kushwaha (1988a, 1988b, 1990) for a narrow cutting blade. Those models provided the force distribution, stress field, displacement field and failure zone. However, FEM models require measurement of many parameters of soil properties and soil-tool interactions. Since parameters of soil-tool interaction were variable, the applicability of FEM models was limited.

Gamma Ray Transmission Method

The gamma-ray transmission method has been used to measure the water content and dry bulk density of soil for many years, both in field and laboratory. Assuming a uniform sample separating a monoenergetic source and a detector, the gamma-ray attenuation law is (Van Bavel et al., 1957):

$$C = C_0 e^{-x(\rho_d \mu_s + \rho_w \mu_w \theta)} \quad (18)$$

where

C = number of counts per unit time (counts/s),

C_0 = incident number of counts per unit time (counts/s),

x = soil attenuation length (cm),

μ_s = soil mass attenuation coefficient (cm^2/g),

μ_w = water mass attenuation coefficient (cm^2/g),

ρ_s = dry soil bulk density of soil (g/cm³),

ρ_w = water specific mass (g/cm³), and

θ = volumetric water content (cm³/cm³).

Given that

$$\theta = \frac{\rho_s W}{\rho_w} \quad (19)$$

where W is the gravimetric water content (g/g). Combining above equations:

$$C = C_0 e^{-x\rho_s(\mu_s + \mu_w W)} \quad (20)$$

Applying the above standard gamma-ray transmission law, Bertuzzi et al. (1987) derived relationships that were usable in soil moisture and density measurement. Introducing the mass attenuation coefficient of a reference material having a mass attenuation coefficient, μ_c , equation (20) was written as:

$$C = C_0 e^{-x\mu_c[(\mu_s/\mu_c) + (\mu_w/\mu_c)W] \rho_s} \quad (21)$$

or

$$C = C_0 e^{-x\mu_c \rho_c} \quad (22)$$

where

$$\rho_c = \left(\frac{\mu_s}{\mu_c} + \frac{\mu_w}{\mu_c} W \right) \rho_s \quad (23)$$

Equations (22) and (23) show that any soil having a dry bulk density, ρ_s , a gravimetric water content, W, and a mass attenuation coefficient, μ_s , has the same gamma-ray attenuation characteristics as reference material having mass attenuation coefficient, μ_c , and a referenced bulk density, ρ_c . Thus, with calibration of a reference

material and knowing the water content of soil and the water attenuation coefficient, μ_w , the bulk density of soil, ρ_s , can be obtained. From equation (20), the relationship is derived as:

$$\rho_s = -\ln\left(\frac{C}{C_0}\right) \frac{1}{x(\mu_s + \mu_w W)} \quad (24)$$

Assuming proper instrument tuning, photon statistics obeys the Poisson distribution. For counts greater than 30, any measurement will be a random variable with a normal distribution and:

$$\sigma = \sqrt{C^*} \quad (25)$$

where σ is the standard deviation and C^* is the mean gamma ray count in this study. C ranged from 25,000 to 50,000 for the laboratory experiment. The standard deviation of the count was thus $\sqrt{25,000} = 158$. The maximum relative error was $158/25,000 = 0.6\%$.

The prediction of dry bulk density, ρ_s , is a factor of five variables, C , x , μ_s , μ_w and W . The variation of density, caused by errors in each of these parameters can be calculated by the partial derivative of equation (24):

$$\begin{aligned} \frac{\Delta \rho_s}{\Delta C} &= -\frac{1}{C} \frac{1}{x(\mu_s + \mu_w W)} \\ \frac{\Delta \rho_s}{\Delta x} &= \ln \frac{C}{C_0} \frac{1}{x^2(\mu_s + \mu_w W)} \\ \frac{\Delta \rho_s}{\Delta \mu_s} &= \ln \frac{C}{C_0} \frac{1}{x(\mu_s + \mu_w W)^2} \\ \frac{\Delta \rho_s}{\Delta \mu_w} &= \ln \frac{C}{C_0} \frac{W}{x(\mu_s + \mu_w W)^2} \\ \frac{\Delta \rho_s}{\Delta W} &= \ln \frac{C}{C_0} \frac{\mu_w}{x(\mu_s + \mu_w W)^2} \end{aligned} \quad (26)$$

With $C_0 = 50,000$, $C = 25,000$ and the standard deviation of 158, density

deviations caused by five members are calculated and listed in table II.

TABLE II
DENSITY DEVIATIONS CAUSED BY INACCURACIES OF
FIVE COMPONENT MEMBERS

Components	Original Values	Deviation	$\Delta\rho$ (g/cm ³)
C_0	50,000		
C (counts)	25,000	158	-0.01
x (cm)	7.62	0.5	-0.07
μ_s	0.0752	0.00752	-0.10
μ_w	0.0831	0.00831	-0.01
W (%)	10	5	-0.05

Effects of Soil Compaction on Plant Growth

Root growth of crops depends on many plant and ecological factors. When root growth is not restricted by physical properties of the soil such as temperature and aeration, the main physical factor controlling root growth seems to be soil strength, which varies with bulk density and water content or metric potential (Ehlers et al., 1983). They observed that the soil bulk density increased sharply in tilled soil at a depth of about 25-30 cm, which indicated the presence of a traffic pan, whereas in untilled soil, the bulk density remained constant. Differences in soil strength could have modified rooting density of oats with profiles of tilled and untilled soil. During most of the vegetative period, rooting density in tilled soil was higher within the 5-25 cm layer, but lower within 25-45 cm layer compared with untilled soil. The relation between rooting densities in tilled and untilled soil changed with the position of traffic pan (25-30 cm), which apparently impeded rooting growth within and below this compacted layer.

To relate soil strength to bulk density and water content, a multiple regression analysis was performed. This analysis was based on the data of averaged penetration resistance, moisture contents and bulk density for three layers (1-5 cm, 11-15 cm and 16-20 cm). The relation, with $R^2=0.81$, was:

$$PR = 0.472 WC + 16.26 BD - 0.461 BD \times WC - 17.34 \quad (27)$$

where PR is the penetration resistance (MPa), WC is water content (%g/g) and BD is soil bulk density (g/cm^3). Equation (27) can be rewritten as:

$$BD = \frac{PR - 0.472 WC + 17.34}{16.26 - 0.46 WC} \quad (28)$$

and therefore, some critical bulk density values can be calculated (see Table III). For most of our samples, the WC was 10-15%. From the literature, the critical penetrometer resistance is about 2-3 MPa. Therefore, our critical bulk density will be in the range of 1.26 to 1.42 g/cm^3 .

TABLE III

CRITICAL BULK DENSITY VALUES (g/cm^3)
CALCULATED FROM PR AND WC

PR (MPa)	Water Content (%)			
	5	10	15	20
2	1.22	1.26	1.31	1.41
3	1.29	1.34	1.42	1.55
4	1.36	1.43	1.53	1.69

Hamblin et al. (1982) conducted an experiment monitoring above- and below-ground growth of a wheat crop in a long-term tillage trial in a loamy sand in

Western Australia. The grain yield was 20% greater in the crop sown after plowing than in those crops sown by direct drilling. The plowed treatment had lower soil strength, not only in the seedbed but also to 50 cm in the subsoil, until 8 weeks after seeding. The lower soil strength coincided with more-rapid wetting of the subsoil under plowing, and higher root extension rates. He concluded that the critical value for root growth in the subsoil could be estimated to be between 2.5 and 3.0 MPa of penetrometer resistance. A 2.5 MPa value in penetrometer resistance was sufficient to cause severe reduction in root growth in the traffic pan zone.

Ohu et al. (1985) planted bush beans in three soil textures having varying organic matter contents that were subjected to three levels of compaction energy. Measurements were made of some plant and yield parameters in a controlled environment. They found that soil compaction decreased fresh yields of the crop, plant height and root dry matter, but increased the plant diameters. On the other hand, organic matter incorporation, which tended to reduce compaction, increased the fresh and dry yields of the crop, plant height, leaf area index and root dry matter.

Voorhees et al. (1975) measured primary root elongation rates of pea seedlings and the soil resistance to penetration of a probe in remolded cores of sandy loam and clay soils over a soil water suction range of 0.1-1.0 bar. Physical soil resistance can be varied by varying bulk density and water content. It was also noted that there was a need to develop a probe technology that more closely simulated the resistance offered to a plant root. Primary root elongation was more closely correlated with soil resistance for a 10° probe than a 60° probe. It was also more closely correlated with soil resistance normal to the probe, neglecting soil-metal friction, than with total probe resistance which does include the friction component. The conclusion was that, when normal point

resistance of the soil on a 10^0 probe increased, root elongation rates decreased.

Whitely and Dexten (1982) conducted a field experiment on red-brown earth soils at two sites in South Australia. The effects of different amounts and types of tillage on root growth and plant development were compared for linseed, pea, rape, safflower soybean, sunflower and wheat. All seven plant species benefitted from some loosening of the soil below the depth of sowing. Wheat benefitted the most. The results implied that decreasing soil resistance increased the plant growth. They reported that the bulk density of top soil (20-100 mm depth) was 1.23-1.31 g/cm³, 25-35 days after planting. Water content (50-100 mm depth) was 15.7-21.4% (d.b.) 8-10 days after planting.

Ellington (1986) studied the effects of deep ripping, direct drilling, gypsum and lime on soils, wheat growth and yield. Among the five conclusions, one stated that the hard pan below the cultivation layer can impede penetration of water and roots into the subsoil and contribute to stunted growth of wheat.

Ball and O'Sullivan (1982) measured cone resistance and shear strength in the top 50-100 mm of seven soils. Bulk density and water content were also measured in the same layer by coring. They found that plant populations, mainly spring barley, were reduced in soil with cone resistance and vane shear strength greater than 2500 kPa and 65 kPa respectively. Such high strength in undisturbed soil was associated with wheeling during harvesting, and was apparently independent of soil type. At the only site of measurement, soil strength apparently decreased during weathering in subsequent seasons. They also noticed that soil bulk densities had little dependence on soil type. Increase of bulk density in drilled soil was usually associated with increased soil strength due to compaction by wheels, mainly during harvesting. Seedbed bulk densities ranged from 1.08 to 1.46 g/cm³ for average depths of 10-60 mm. For the top layer (0-50 mm)

of one particular seedbed, bulk density was changed from 1.13 to 1.33 g/cm³ after compaction.

Taylor (1971) observed that, when other plant growth conditions were adequate, increases in soil strength reduced the rate of seedling emergence or the rate of root elongation. High strength also reduced the proportion of seedlings that emerge or the proportion of roots that penetrate the impeding layer. Plant yields would be reduced by a high-strength layer if an adequate plant population was not established, or if the layer caused the plant to undergo substantial additional stress for water or nutrients.

After two-year experiment, Chaplin et al. (1986) concluded that an accepted range of soil compaction before corn root penetration ceased was 2400 kPa (highest mean corn value) for no-till at 24 cm below the soil surface. Taylor et al. (1963, 1968) stated the accepted range was 2000-2500 kPa.

Chu et al. (1991a), in a laboratory experiment, studied the cotton emergence force as affected by soil temperature, moisture and soil crust compression which was simulated by applied static weights. In the temperature range of 22°C to 32°C, the emergence force was in the range of 5.5 N to 11.4 N. The authors noted that the maximum emergence force was almost twice as large as the maximum force previously reported (i.e., 11.4 vs. 5.88 N). The result was probably due to firmer lateral support to the hypocotyl. Chu et al. (1991b) demonstrated this result even further in their second experiment. It was observed that seedling roots growing in soil compacted to 13.8 kPa in penetration resistance and a bulk density of 1.3 Mg/m³ were damaged under loads of 60 g and 132 g by buckling of the root due to inadequate soil support. The injured seedlings did elongate, but at a much slower rate than healthy seedlings. Therefore, the ability of the soil to support the root could be a limiting factor for seedling emergence under soil

crusts. This showed that the ability of soil to provide adequate root support when seedling elongation is impeded by a crust is another important aspect of the crusting problem.

CHAPTER III

EXPERIMENTAL EQUIPMENT AND PROCEDURE

The following variables were identified as affecting the performance of the planting system: press wheel width, press wheel ballast, soil type and soil moisture. Other factors may include forward speed, planting depth and original density of soil. Due to limited availability of resources, this research focused on the effect of press wheel width and ballast.

Four experiments were conducted; one laboratory experiment, one soil bin experiment and two field experiments. The laboratory experiment took place at the Oklahoma State University Groundwater Laboratory, Agricultural Hall. The soil bin experiment was conducted at Agricultural Engineering West. In the above two experiments, the soil used was an Asher silty clay loam with approximately 5% sand, 65% silt and 30% clay. Two field experiments were conducted at the Agronomy Experiment Station, Stillwater, Oklahoma. The soil type was Zaneis loam with approximately 25% sand, 50% silt and 25% clay.

Gamma ray techniques were used to detect density profiles in soil samples. The results from laboratory experiment samples were used to develop a prediction model, and the results from soil bin and field experiments were utilized to test the applicability of the model in different conditions.

Laboratory Experiment

The design of laboratory experiment is shown in Appendix E-4. The experiment number IV was assigned since it was conducted after the two field experiments and the soil bin experiment. The plot number represented only one replicate rather than a physical field plot. The test was conducted by packing soil directly into soil samplers. Three wooden blocks were used to simulate the wheel tracks by being pressed into the soil with applied static weights. Two ballast levels (5 kg and 10 kg) and three track width levels (25, 51 and 102 mm) were used in this experiment.

Samplers used in this research were aluminum rectangular boxes of 25.4 cm length, 15.2 cm height and 7.6 cm width. To guarantee uniform compaction, a calculated amount of soil (245 g) was packed into a 1-cm layer, with an approximate dry bulk density of 1.1 g/cm³, assuming 15% moisture content (d.b.). After packing, the sample was sealed in plastic and scanned immediately. Soil moisture content was similar for all the samples. However, samples for measuring moisture content were taken, and moisture contents were recorded.

Experimental Analysis

The gamma ray technique was used to analyze the density distribution of the soil sample. The gamma ray scanning system (Brown et al., 1993) consisted of a photon source, a detector, motion controller and data acquisition computer (Figure 2). Photons emitted from the 1.2 Ci ¹³⁷Cs source passed through the soil sample, and were received by the NaI(Tl) detector. The detector signal was amplified, and sent to a multichannel analyzer which was installed inside of an EVEREX 386sx PC. The sample was moved

by two stepper motors which moved the sample to horizontally and vertically. This arrangement enabled the whole rectangular sample to be scanned as a matrix of 31 rows and 49 columns, with 5 mm increments in both directions. Positioning accuracy in both horizontal and vertical directions was 0.005 mm.

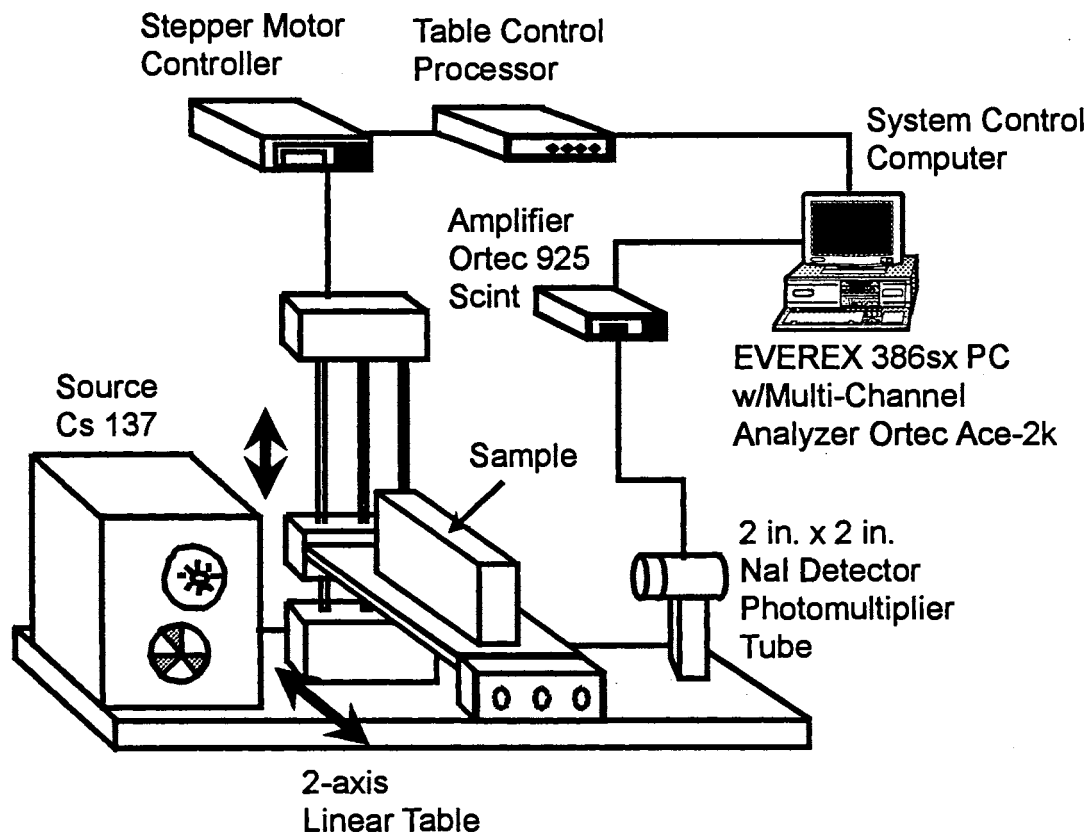


Figure 2. Schematic of Gamma Ray Scanning System.

Two 50 mm long tungsten collimators with 2 mm diameters were used in both source and detector. The collimators were aligned by passing a neon laser clearly through both the source and detector collimators, while the detector was removed. Previously measured quartz mass attenuation coefficient of the system was $0.0752 \text{ cm}^2/\text{g}$.

Luo and Wells (1992) showed that the mass attenuation coefficients were insensitive to soil composition at the energy of the 662 keV ^{137}Cs photons. Therefore, the soil mass attenuation was assumed to be $0.0752\text{ cm}^2/\text{g}$ throughout this research.

Scanning data from each column was stored as an individual file. Later, the density profile of the sample was reconstructed using a C program (see Appendix A). Typical time to scan one sample was about 3.5 hours. After scanning, the net weight of sample soil was measured and the moisture content was determined by oven-drying for 24 hours at the temperature of 104°C .

When reconstructing the 49 data files of photon counts of one sample into an integrated file, it was assumed that the attenuation factor of soil was $0.0752\text{ cm}^2/\text{g}$ and the sample moisture content as 7.6% d.b.. The attenuation factor of water was known to be $0.0831\text{ cm}^2/\text{g}$, and the sample path was 7.62 cm. The top three rows were treated as reference photon counts, C_0 , because in these rows there was no soil, only the aluminum box walls in the way of photon travel. An initial soil density map was constructed assuming a nominal packing water content of 10%. Due to moisture variation among samples, this initial density profile was not exact, but was in proportion to the average density of the sample. Finally, the average initial dry density, ρ_D , was calculated.

After obtaining the initial density profiles, a program was written to manually digitize the soil surface line and write the boundary data into files. Simultaneously, this program set all the density values above the boundary line to zero, but kept the density values below this line unchanged.

The total dry weight and volume were needed to obtain the average bulk density of a sample. Dry weight was calculated using the measured total wet weight and oven-

dried moisture content of each sample. With a known sample width of 7.62 cm, the total volume was obtained using the cross section area. The cross section area was calculated using the software Surfer. With known sample area, sample width, wet weight and moisture content, the average bulk density, ρ_R , was calculated.

The initial density profiles were then divided by the ratio of ρ_I to ρ_R . The resulting density profile obtained was the actual distribution independent of the soil attenuation coefficient. It's major limitation is the assumption of constant water content. That assumption was unavoidable with a single energy source system as was used here.

Contour lines of density profile, at this state, showed some noise. That noise can be attributed to both actual soil variation and photon statistics (Brown et al., 1994). Further analysis of density distribution pattern required the removal of these local anomalies. A low-pass filter was implemented with:

$$\rho_{new}[i, j] = \frac{1}{9} \sum_{a=i-1}^{a=i+1} \sum_{b=j-1}^{b=j+1} \rho_{old}[a, b] \quad (29)$$

Density data were completed for the analysis of results.

Soil Bin Experiment

A soil bin experiment was conducted because soil condition in this experiment was between that of the laboratory and the field experiments. The design of the soil bin experiment is shown in Appendix E-3. Experiment number III was assigned since it was conducted after the two field experiments.

A 182 cm long, 32.4 cm high and 50.8 cm wide soil bin was constructed of wood. It was wide enough to operate the press wheel and long enough to collect two replicate samples. Loadcells for the press wheel system were not used in this test, and

the press wheel system was moved manually.

The soil was assumed to be uniform in moisture content. Large clods were removed. A measured volume of soil was uniformly poured into the soil bin over the horizontal area, and then a wooden block was used to compact the soil. The block was positioned about 5 cm above the soil surface and dropped. This process was repeated until the whole area was compacted. Another layer was then added and compacted. Because of the large size of the soil bin, there was still some variation in density.

After the soil bin was prepared, the press wheel was put on one end of the soil bin and pulled manually to the other end. As in the previous experiments, the rectangular samplers were used to collect two samples for each run. To measure initial soil surface density and moisture content, an aluminum ring was used as a sampler. The ring had an inner diameter of 59 mm and a height of 36 mm. After pushing the ring fully into the soil, a scraper was used to clear the top of the ring. Soil surrounding the ring was then cleared, and the scraper was used to cut the ring out of the ground. The volume of the ring was the volume of soil sampled. The soil inside the ring was put into a marked can for measuring the surface density and moisture content using the procedure described in the previous section. Two samples were taken from each plot and were used to calculate the surface density and moisture content. After finishing one run, the soil in the bin was removed, loosened and repacked into the soil bin.

Small wooden chips were poured on the top of samples to preserve the soil surface profile. The sample was then sealed in plastic and transported to the scanning laboratory. Because the moisture was initially the same throughout the sample in this experiment, samples were not held for moisture equilibration.

Field Experiments

Field experiments consisted of a factorial arrangement of treatments, with two major factors in a randomized block design. The two major factors were press wheel width (three levels: 25, 51 and 102 mm) and press wheel ballast (four levels: 0, 5, 10 and 15 kg). Three blocks were included in each experiment for replication and two subsamples for each plot. This design required

$$3(\text{wheels}) * 4(\text{ballasts}) * 3(\text{reps}) * 2(\text{subs}) = 72 \text{ samples}$$

which was physically impractical to handle. Since there is no interaction between the press wheel widths and ballasts, only selected plots were tested. Table IV shows the incomplete factorial design. Those plots marked by ✓ were tested. Thus, a total of

$$6(\text{plots}) * 3(\text{reps}) * 2(\text{subs}) = 36 \text{ samples}$$

was collected.

TABLE IV
INCOMPLETE FACTORIAL DESIGN OF EXPERIMENTS

Wheel Width (mm)	Ballast (kg)			
	0	5	10	15
25.4			✓	
50.8	✓	✓	✓	✓
101.6			✓	

Maps of two field experiments are shown in Appendix E-1 and E-2, with plot numbers assigned as 101, 102, etc. The field was 64 m long and 18.3 m wide. Each plot was 3 m wide, which was adequate for a tractor to pass, and 15.2 m long, which was sufficient for collecting data by the data acquisition system. The two alleys were

9.1 m long, which permitted tractor maneuvering.

For each plot, a set of numbers was used to represent different replication and treatment combinations. The first Roman numeral represented the experiment number; the second the replication number, or block number (1 through 3); the third the press wheel width level (1 = 25, 2 = 51 and 3 = 102 mm); the fourth the press wheel ballast level (1 = 0, 2 = 5, 3 = 10 and 4 = 15 kg). For example, plot II124 represents the second experiment, with 51 mm wide wheel and 15 kg ballast of the first replicate (first block).

Field experiments were conducted using a press wheel system (Figure 3) which was connected to a testing frame. This frame was attached to the three-point hitch system of a tractor (John Deere 2520) and supplied a platform for the data acquisition system. A hydraulic cylinder was installed at the front of the tractor to push a soil sampler boxes into the ground.

The instrumentation system for field experiments consisted of two force transducers, a speed transducer and data acquisition boards and computer.

Force Transducers

The press wheel and the coulter were both connected with a loadcell such that the dynamic vertical and horizontal forces acting on them were recorded. The loadcell was an extended split ring transducer designed based on Hoag and Yoerger (1974). Figure 4 shows the transducer and the wiring configuration.

The transducers were machined from 7075-T6 aluminum, which had a yield strength of 480 MPa and a modulus of elasticity of 70 MPa. A detailed design diagram is shown in Appendix B. Dimensions of the transducers were calculated based on the

total load of 45 kg, which satisfied the test condition. The strain gages applied to the transducers were WK-13-250BG-350 (Micro-Measurements Division, Measurement Group, Inc.) due to their suitability for harsh environment applications. A protective coating (Micro-Measurement M-Coat F) was also applied to protect the strain gages and wiring.

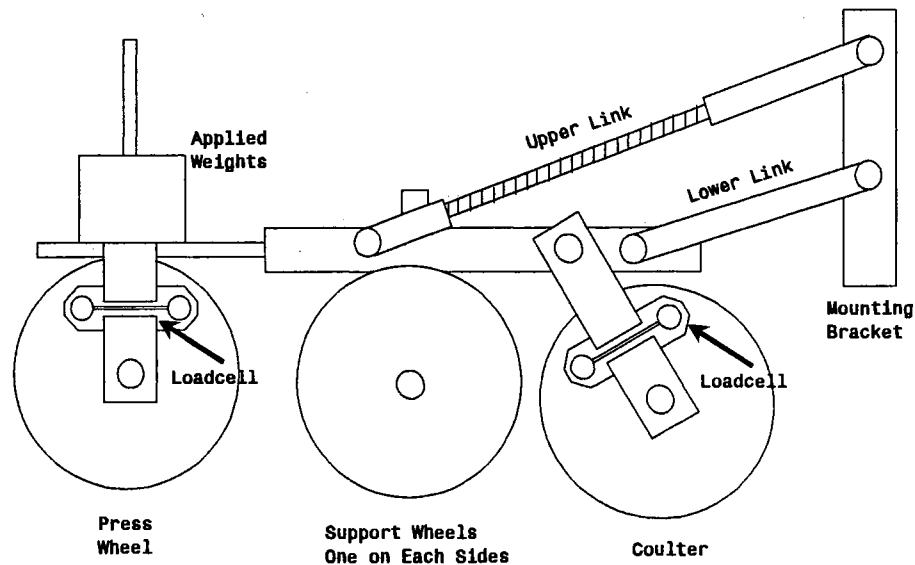


Figure 3. Press Wheel System with Force Transducers.

The transducers were calibrated by statically applying known weights in the appropriate directions. Designs of the brackets for the calibration and the calibration data are shown in Appendix B. Four calibration relationships are shown in equations (30) through (33), where WV, WH, CV and CH represent the relationships among vertical (V) and horizontal (H) forces (Newtons) on the press wheel (W) and coulter (C) and computer digital readings (A/D). The coefficient of determination (R^2) was found to be greater than 0.99 for all four equations.

$$WV = -1107.9 + 0.6327 x (A/D) \quad (30)$$

$$WH = 1526.4 - 0.6339 x (A/D) \quad (31)$$

$$CV = -95.3 + 0.8211 x (A/D) \quad (32)$$

$$CH = -1426.1 + 0.6474 x (A/D) \quad (33)$$

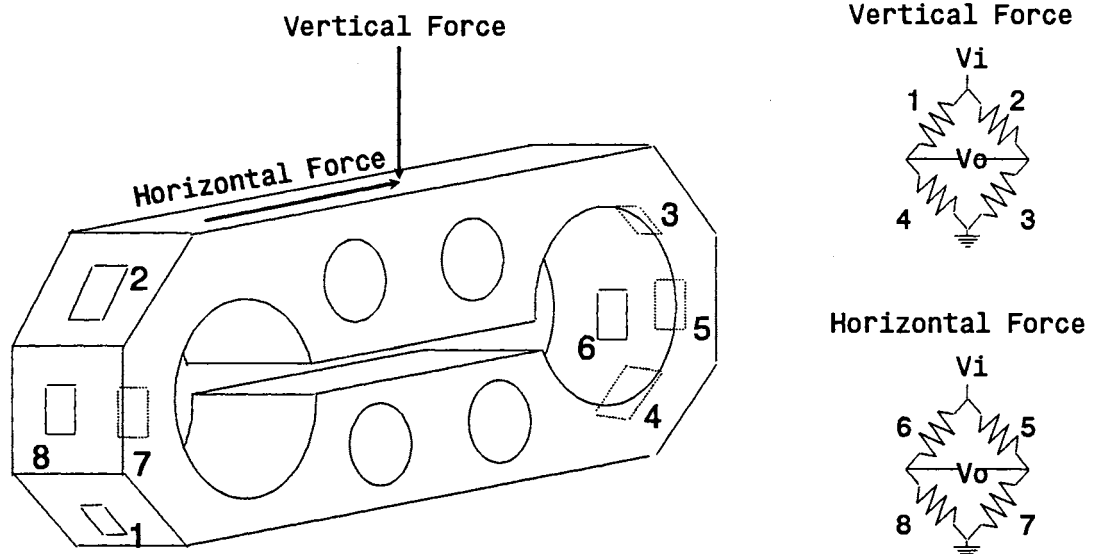


Figure 4. Load Transducer with Strain Gage Location and Wiring Configuration.

Speed Transducer

Vehicle travel speed was sensed by a GX-12M proximity sensor (General Engineering, Inc.). The sensor was installed on the testing frame with a sprocket was installed nearby so the teeth of the sprocket were close to the head of the sensor. When

the sprocket was driven by the wheel of the testing frame through a connecting chain, the teeth of the sprocket would pass close to the sensor. This proximity caused electrical pulses which were counted by the data acquisition board to indicate vehicle speed. Calibration indicated that a 1 Hz pulse frequency was equivalent to a velocity of 0.038 m/s. The predominant frequency was about 20 Hz, which was equivalent to speed of 2.7 km/hr.

Data Acquisition System

The data acquisition system (PCI Systems, Burr-Brown Co.) consisted of an analog input module, a digital input module, a carrier module, two terminations, and one personal computer (Industrial Computer).

The analog input module (PCI-20002M) was utilized with terminations PCI-20044 and PCI-20045T. Total gain of hardware gain and software gain was 1000. An RC low-pass filter with a cutoff frequency of 100 Hz was used.

The digital input module (PCI-20007M) supported two rate-generator channels and four digital inputs. One rate-generator was utilized as an internal clock, and one digital input channel was used to receive the signal from the proximity sensor. With these two inputs, the frequency of the input pulses can be calculated. Between the digital module and the sensor was digital termination PCI-20025T as a convenient connecting board.

The two input modules were inserted into the carrier module (PCI-20001C) which was installed directly in the computer mother board. A shop-made instrumentation box was utilized to house the two terminations. It provided a convenient way of connecting sensors to the computer and supplied power to the two terminations.

The computer had a 1.4Mb floppy disk drive which was adequate for storing

computer programs and data files. The analog and digital input modules were accompanied by a software driver written in PASCAL. Therefore, the application programs were also written in PASCAL (See Appendix A). Due to the harsh field environment, a light and compact Radio Shack computer (TRS-80, Model 100) was used as a monitor, which was connected to the Industrial Computer through RS-232C interfacing.

Sampling frequency was set to 340 Hz, which was adequate for the highest probable frequency passing through the low-pass filter which had a cut-off frequency of 100 Hz. For each run, the total number of sampled data was 1024. With the measured speed and time period between data points (1/340 seconds), the distance traveled can be calculated. Assuming the speed was equivalent to 20 Hz from the speed sensor, the total distance was: $20 * 0.038 / 340 * 1024 = 2.3$ meters.

Plots were tilled to a desired condition for planting and marked one day before the experiments. Like the soil bin experiment, three small samples were collected using the circular sampling ring for measuring the soil surface density and moisture content.

Before collecting force data from each plot, zero-force readings were taken with the data acquisition system as reference for later force analysis. The press wheel was then pulled through the plot at a velocity of 2.7 kmh, and a pressed furrow was formed. Forces acting on the coulter and press wheel in both horizontal and vertical directions, and the forward speed were recorded. The computer program was designed to record data in the following order: vehicle velocity, forces on the coulter, forces on the press wheel and, finally, vehicle velocity again.

After pressing furrows for all the plots, the press wheel system was disconnected from the testing frame. Using a hydraulic cylinder mounted on the front of the tractor,

a sampler was pushed into the soil until the distance between the soil surface and the top of the box was approximately 5 cm. A slurry of plaster of paris and water was poured onto the top layer of the soil inside the sampler to preserve the top profile of the soil sample. However, about 2 cm of clearance was left on top of the sample which was needed as a reference for later gamma ray scanning. After the slurry hardened, the soil sample was taken out of soil and sealed in plastic. The sample was then transported to the laboratory for scanning. Two samples were taken for each plot.

After transporting samples to the laboratory, they were placed horizontally for several days before scanning, so that moisture was equilibrated throughout each sample. This reduced the effect of varying moisture distribution on the measurement of density profile.

CHAPTER IV

RESULTS AND DISCUSSION

There have been many efforts by researchers to find the relationship between soil compaction and its causes, especially the applied load. Unfortunately, most of these experiments were conducted as triaxial tests, which have little resemblance to the compaction of agricultural top soil when planting or drilling seed. Relationships are mostly nonlinear, and require many experimentally obtained parameters. They are not easily adapted to situations where the soil density profile varies. Nevertheless, those experiments reveal that the resulting compaction, or increased soil bulk density, is related to the soil stress caused by applied loads. Unfortunately, only limited research has been conducted to relate density directly to loading environment.

Most research has concentrated on relating applied load to the stress status within soil. Attempts to relate observed soil density to these models were not successful. However, density profiles from data collected in the research were similar to the stress profiles calculated using theoretical formulae. Density was a function of stress in all previously derived models. It was logical to adapt the stress model to the density profile model. The stress model was modified by adding two parameters. Those parameters were determined by fitting iso-density lines. This approach was successfully used to modify the stress model into a density model. Iso-density lines in the soil profile are also

important, because they define how deep the compaction will penetrate and how wide it will spread. They also defines the high-density zones where root elongation can be retarded.

Theoretical Considerations

Results of controlled laboratory tests indicated that Boussinesq's point-load equation for soil stress reasonably approximated the data, though the equation predicted the stress in the soil profile rather than density. To improve the fit to the data, the equation was modified by introducing two parameters A and B, i.e.,

$$\rho = \frac{BP}{y^2} \frac{1}{\left[1 + \left(\frac{x}{Ay}\right)^2\right]^{\frac{5}{2}}} \quad (34)$$

where ρ is density, P is applied load, x and y are the coordinates of a point in soil and A and B are parameters to be determined empirically.

To obtain the iso-density line, equation (34) was rewritten as:

$$x = Ay \sqrt{\left(\frac{BP}{\rho y^2}\right)^{\frac{2}{5}} - 1} \quad (35)$$

This equation implies that iso-density lines are symmetrical about a vertical axis extending through the center of the imposed load.

Equation (35) predicts several properties of iso-density lines; namely, the maximum depth an iso-density line can penetrate, the maximum width the line can spread horizontally, its distance from the center line of the imposed load, and the area this line encloses.

The maximum depth, y_{\max} , is determined by setting equation (35) equal to 0:

$$y_{\max} = \sqrt{\frac{BP}{\rho}} \quad (36)$$

The equation predicts that higher applied loads will cause an iso-density line to penetrate deeper. Compared to higher density lines, lower density lines will penetrate deeper for the same load.

To obtain the maximum distance an iso-density line can spread across horizontally, the derivative of equation (35) is calculated, i.e.,

$$\frac{dx}{dy} = \frac{1}{5} \frac{3 \left(\frac{BP}{\rho y^2} \right)^{\frac{2}{5}} - 5}{\sqrt{\left(\frac{BP}{\rho y^2} \right)^{\frac{2}{5}} - 1}} = 0 \quad (37)$$

Therefore,

$$\begin{aligned} y_{x\max} &= \left(\frac{3}{5} \right)^{\frac{5}{4}} \sqrt{\frac{BP}{\rho}} \\ &= 0.528 \sqrt{\frac{BP}{\rho}} \\ &= 0.528 y_{\max} \end{aligned} \quad (38)$$

where $y_{x\max}$ is the y coordinate corresponding to $x=x_{\max}$. Substituting equation (38) into equation (35):

$$\begin{aligned} x_{\max} &= \left(\frac{2}{3} \right)^{\frac{1}{2}} \left(\frac{3}{5} \right)^{\frac{5}{4}} A \sqrt{\frac{BP}{\rho}} \\ &= 0.431 A \sqrt{\frac{BP}{\rho}} \\ &= 0.431 A y_{\max} \end{aligned} \quad (39)$$

To obtain the area enclosed by an iso-density line between y_0 and y_1 , the equation for the iso-density curve was integrated (Figure 5):

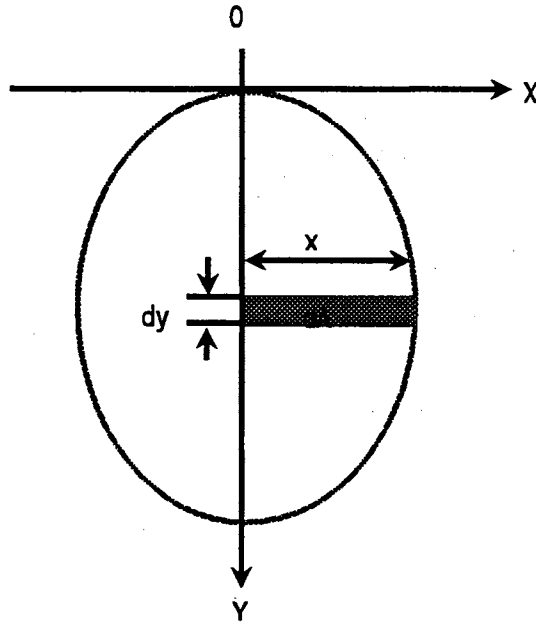


Figure 5. Integration of Area Enclosed by an Iso-Density Line.

$$\begin{aligned}
 \text{area} &= \int_{y_0}^{y_1} d(\text{area}) \\
 &= \int_{y_0}^{y_1} x dy
 \end{aligned}
 \tag{40}$$

Substituting equation (35) into equation (40) yields:

$$\begin{aligned}
 \text{area} &= \int_{y_0}^{y_1} Ay \sqrt{Ty^{-\frac{2}{5}} - 1} dy \\
 &= \int_{y_0}^{y_1} A \sqrt{Ty^{\frac{6}{5}} - y^2} dy
 \end{aligned}
 \tag{41}$$

where:

$$T = \left(\frac{BP}{\rho} \right)^{\frac{2}{5}}
 \tag{42}$$

Equation (41) was integrated using MathCad version 3.1 (MathSoft, Inc., 1992).

However, the form was not recognized by the program. To integrate the equation, the following substitutions were made: Let $y=z^5$, then $y^{6/5}=z^6$, $y^2=z^{10}$ and $dy=5z^4dz$; when $y \rightarrow y_0$, $z \rightarrow y_0^{1/5}$, and when $y \rightarrow y_1$, $z \rightarrow y_1^{1/5}$. These substitutions yielded the equation:

$$\begin{aligned}
 \text{area} &= \int_{y_0^{1/5}}^{y_1^{1/5}} A \sqrt{Tz^6 - z^{10}} 5z^4 dz \\
 &= 5A \int_{y_0^{1/5}}^{y_1^{1/5}} \sqrt{T - z^4} z^7 dz \\
 &= -\frac{5A}{30} \left\{ \left(2T^2 - 3y_1^{8/5} + Ty_1^{4/5} \right) \sqrt{T - y_1^{4/5}} + \left(-2T^2 + 2y_0^{8/5} - Ty_0^{4/5} \right) \sqrt{T - y_0^{4/5}} \right\}
 \end{aligned} \tag{43}$$

If $y_1 = y_{\max}$, (i.e., integrating to the deepest possible point), the area is obtained by entering equation (36) to equation (43):

$$\text{area} = \frac{A}{6} \left\{ 2T^2 - 2y_0^{8/5} + Ty_0^{4/5} \right\} \sqrt{T - y_0^{4/5}} \tag{44}$$

where

$$T = \left(\frac{BP}{\rho} \right)^{2/5} \tag{45}$$

If $y_0=0$, the total area is:

$$\begin{aligned}
 \text{area} &= \frac{A}{3} T^{5/2} \\
 &= \frac{A}{3} \left(\left(\frac{BP}{\rho} \right)^{2/5} \right)^{5/2} \\
 &= \frac{ABP}{3\rho}
 \end{aligned} \tag{46}$$

The area calculated with equation (46) is half of the total area. The total area

enclosed by a greater iso-density line will be smaller than that enclosed by a lower iso-density line. Because parameters A and B vary for different densities, the effect of change in density can be predicted by taking the derivative of area function, with respect to density. Taking derivatives of both sides of equation (44):

$$\begin{aligned} \frac{d(\text{area})}{d\rho} &= \frac{1}{6} \left(\frac{dA}{d\rho} \right) \left\{ 2T^2 - 2y_0^{\frac{8}{5}} + y_0^{\frac{4}{5}} T \right\} \sqrt{T - y_0^{\frac{4}{5}}} \\ &+ \frac{A}{6} \left\{ 4T + y_0^{\frac{4}{5}} \right\} \frac{dT}{d\rho} \sqrt{T - y_0^{\frac{4}{5}}} \\ &+ \frac{A}{12} \frac{\left\{ 2T^2 - 2y_0^{\frac{8}{5}} + T y_0^{\frac{5}{4}} \right\}}{\sqrt{T - y_0^{\frac{4}{5}}}} \frac{dT}{d\rho} \end{aligned} \quad (47)$$

where

$$\frac{dT}{d\rho} = \frac{2}{5} \left(\frac{BP}{\rho} \right)^{-\frac{3}{5}} P \left(\frac{1}{\rho} \frac{dB}{d\rho} - \frac{B}{\rho^2} \right) \quad (48)$$

and $dA/d\rho$ and $dB/d\rho$ will be determined later.

Analysis of Laboratory Controlled Experiment

The basic characteristics of samples from this test was shown in Table V. The computer program, Surfer version 4.0 (Golden Software, Inc., 1989), was used to generate contour lines of density profiles for each data set. Figure 6 shows the contour map of sample #112 with 25 mm wide track and 5 kg ballast. This is a typical contour map generated from the data of this experiment. Contour maps of all other samples are contained in Appendix C. The results from this experiment were well behaved and fit the theoretically predicted pattern.

TABLE V
CHARACTERISTICS OF LABORATORY EXPERIMENT SAMPLES

Sample No.	Width (mm)	Mass (kg)	Load P (kPa)	Y_{offset} (mm)	MC (%)
111	25	5	25.3	5	14.4
112	25	5	25.3	5	13.3
121	51	5	12.7	10	13.4
122	51	5	12.7	10	12.9
131	102	5	6.3	45	11.6
132	102	5	6.3	45	13.0
141	25	10	50.7	5	14.4
142	25	10	50.7	5	13.7
151	51	10	25.3	10	16.6
152	51	10	25.3	10	14.2
161	102	10	12.7	45	15.3
162	102	10	12.7	45	12.5

Modeling Single Iso-Density Line

The initial efforts to model the whole density profile of each sample failed, because there were no suitable formulas available to account for the different loading and load widths for each sample. The next reasonable approach was to generate a model to fit a single density line by varying parameters A and B. Parameters A and B are then modeled with respect to the loading variables of each sample. This method proved to be successful.

A program was written to digitize x, y coordinate data for specified density levels, and these data were used to draw the iso-density lines. Iso-densities of 1.20, 1.25

and 1.30 kg/cm³ from all the samples were used for this purpose. Equation (35) cannot be used directly to predict x values, because loads were distributed across a horizontal surface of finite width, rather than imposed at a point. Therefore, a new factor was introduced to account for this effect and the equation was modified to:

$$x = A(y + y_{offset}) \sqrt{\left(\frac{BP}{\rho (y + y_{offset})^2} \right)^{\frac{2}{5}} - 1} \quad (49)$$

where, y_{offset} is the variable that accounts for the effect of the load imposed with a finite width instead of a point load.

For each pair of observed values x and y, the predicted x was obtained using equation (35). Error was the difference between the observed and predicted x values. Total error was the absolute summation of all the errors over the applicable y range. The best fit was obtained by changing y_{offset} , A and B until the error between observed and predicted x values was minimized. The y_{offset} was related to the width of the compacted track. The data from three different levels of density were fitted individually and therefore, each one of the three levels had different A and B values. The observed and predicted data were plotted. Figure 7 shows the example data and fitted curves for sample #112 with 25 mm wide track and 5 kg ballast. Curves for all other data sets are contained in Appendix D. Observed and predicted x values were regressed into a straight line to determine how well the curve fit the data. Results of fitting density lines of 1.20, 1.25 and 1.30 g/cm³ are shown in Table VI to Table VIII.

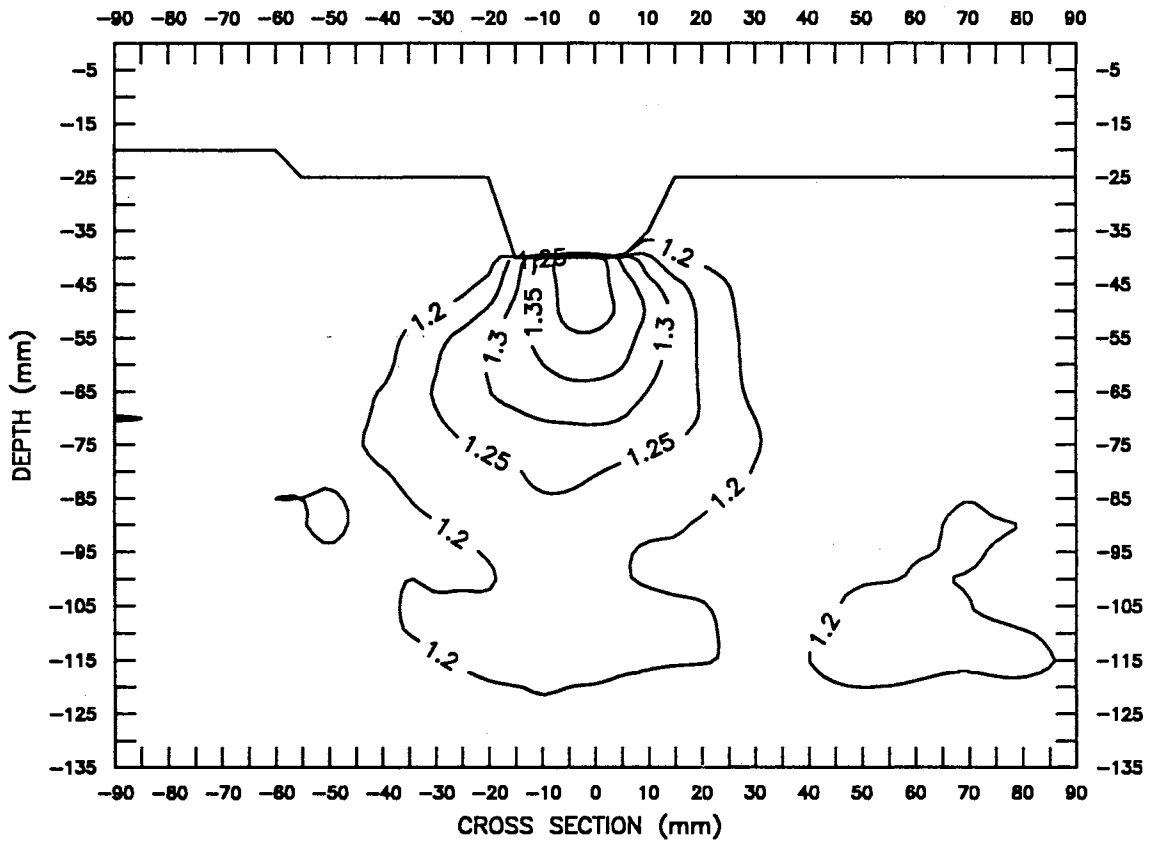


Figure 6. Contour of Sample #112 with 25 mm Wide Track and 5 kg Ballast.

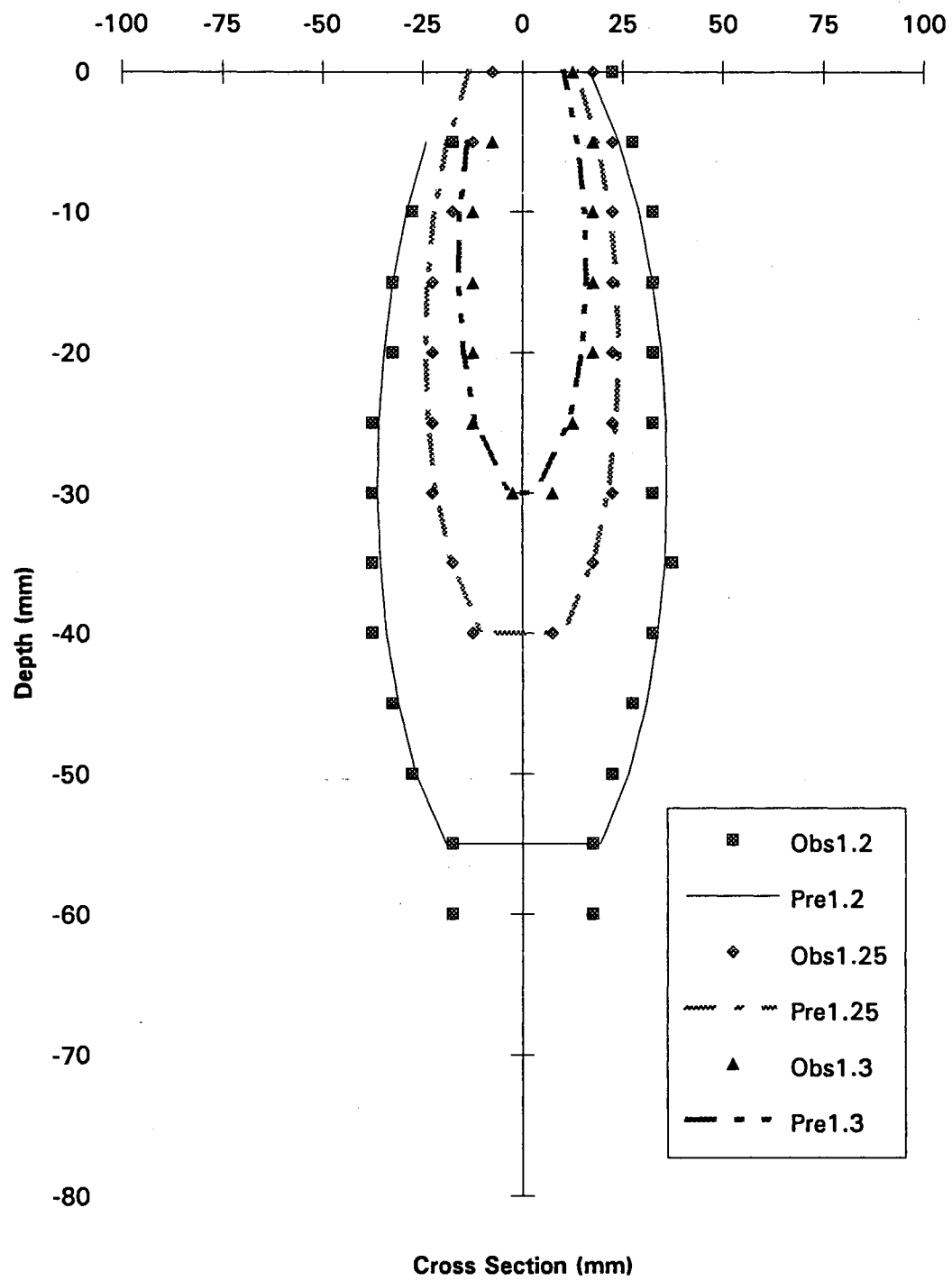


Figure 7. Fitting of Sample #112 with 25 mm Wide Track and 5 kg Mass.

TABLE VI
FITTING SINGLE DENSITY LINES FOR DENSITY 1.20 g/cm³

Sample No.	A	B	Intercept	Slope	R ²
111	1.30	543	-8.6	0.98	0.99
112	1.30	197	-2.7	0.77	0.83
121	1.20	715	-10.4	0.81	0.91
122	1.30	740	3.1	0.93	0.95
131	1.20	1381	5.3	0.92	0.89
132	1.20	2565	7.3	0.93	0.96
141	1.35	202	-1.6	0.81	0.93
142	1.25	271	-3.9	0.79	0.95
151	1.30	592	2.0	0.96	0.99
152	1.20	543	1.3	0.96	0.99
161	1.25	1850	-7.9	0.92	0.97
162	1.20	1258	-2.1	0.86	0.96

Determination of Y_{offset}

The parameter Y_{offset} was found to be related to the track width only, and the relationship between them is polynomial. The regression formula was

$$Y_{offset} = 3.2053 + 4.0086 * 10^{-4} * width^{2.5} \quad (50)$$

where Y_{offset} and width have units of mm. The coefficient of determination (R²) is 0.99.

Determination of Parameter A

To determine the parameter A, the SAS General Linear Model was used to relate parameter A to six independent variables; namely, width, weight, load, density, Y_{offset}

and moisture content (MC). The independent variables were eliminated one-by-one according to their low correlation with parameter A. Finally, it was determined that only density was closely related to parameter A ($r = -0.91$). This process is summarized in Table IX and the general linear model procedure for parameter A is shown in Table X. The relationship was:

$$A = 3.723 - 2.044 \rho \quad (51)$$

TABLE VII

FITTING SINGLE DENSITY LINES FOR DENSITY 1.25 g/cm³

Sample No.	A	B	Intercept	Slope	R ²
111	1.20	133	-5.4	0.77	0.96
112	1.20	109	-1.3	1.03	0.98
121	1.20	306	-4.7	0.93	0.96
122	1.35	252	-3.3	1.01	0.97
131	*	*	*	*	*
132	1.25	1431	4.7	0.89	0.96
141	1.15	123	-0.6	1.03	0.98
142	1.10	187	-2.8	0.88	0.94
151	1.20	543	1.0	0.99	0.99
152	1.10	321	-1.0	0.96	0.97
161	1.15	1726	-2.3	1.01	0.99
162	1.10	888	-1.1	1.05	0.84

* Data were not available, because density did not exceed 1.25 g/cm³ in this sample.

TABLE VIII

FITTING SINGLE DENSITY LINES FOR DENSITY 1.30 g/cm³

Sample No.	A	B	Intercept	Slope	R ²
111	1.20	84	-3.4	1.02	0.98
112	1.00	64	-2.4	0.96	0.98
121	0.90	212	-2.2	0.84	0.94
122	*	*	*	*	*
131	*	*	*	*	*
132	*	*	*	*	*
141	1.05	80	-0.7	1.03	0.97
142	0.90	80	-2.2	0.92	0.95
151	1.25	345	-1.6	1.09	0.99
152	1.00	217	-1.2	0.99	0.95
161	0.95	1361	-1.0	0.95	0.99
162	*	*	*	*	*

* Data are not available, because the density line did not exceed 1.3 g/cm³.

TABLE IX

DETERMINATION OF PARAMETER A

Step	Correlation Coefficient Between A and Variables						Root MSE	C.V.	R ²
	Width	Weight	Load	Density	Y _{offset}	MC(%)			
1	0.05*	-0.21	-0.11	-0.91	-0.10	-0.07	0.030	2.53	0.91
2		-0.21	-0.11	-0.91	-0.10	-0.07*	0.029	2.49	0.91
3		-0.21	-0.11	-0.91	-0.10*		0.035	2.95	0.87
4		-0.21	-0.11*	-0.91			0.034	2.90	0.87
5		-0.21*		-0.91			0.035	2.94	0.86
6				-0.91			0.038	3.20	0.83

* The variable was eliminated at this step due to low correlation with A.

TABLE X
GENERAL LINEAR MODEL PROCEDURE FOR PARAMETER A

Source	DF	Sum of Squares	Mean Square	F Value	Pr > F
Model	1	0.216	0.216	152.54	0.0001
Error	31	0.044	0.001		
Corrected Total	32	0.260			
	R-Square	C.V.	Root MSE		A Mean
	0.83	3.20	0.038		1.18
Source	DF	Type I SS	Mean Square	F Value	Pr > F
DENSITY	1	0.216	0.216	152.54	0.0001
Source	DF	Type III SS	Mean Square	F Value	Pr > F
DENSITY	1	0.216	0.216	152.54	0.0001
Parameter	Estimate	T for H0: Paramtr=0	Pr > T	Std Error of Estimate	
INTERCEPT	3.72	18.05	0.0001	0.206	
DENSITY	-2.044	-12.35	0.0001	0.165	

Determination of Parameter B

The process of determining parameter B was essentially the same, but the linear model did not fit the data. After transforming the data of B and six independent variables to logarithmic scale, the data fit a linear model. The process of determining parameter B after data transformation is summarized in Table XI. Three variables were closely related to B; namely, width, load and density. The general linear model

procedure for the parameter B is shown in Table XII. The relationship was:

$$B = e^{1.625} \text{width}^{1.724} \text{load}^{0.167} \rho^{-12.997} \quad (52)$$

with $R^2=0.91$. The unit of width is mm, load is kPa, and density is g/cm^3 .

TABLE XI
DETERMINATION OF PARAMETER B

Step	Correlation Coefficient Between B and Variables						Root MSE	C.V.	R ²
	Width	Weight	Load	Density	Y _{offset}	MC(%)			
1	0.87	0.05*	-0.68	-0.52	0.84	-0.10	0.30	4.97	0.94
2	0.87		-0.68	-0.52	0.84	-0.10*	0.32	5.31	0.96
3	0.87		-0.68	-0.52	0.84#		0.34	5.66	0.91
4	0.87		-0.68	-0.52			0.33	5.57	0.91

* The variable was eliminated in this step due to low correlation with B.

Y_{offset} was eliminated because of its high correlation with width (0.94).

Calculate Iso-Density Lines

The parameters needed to utilize equation (49) to calculate any iso-density line for any given density and any loading conditions have been determined. If the applied load, block width and density are specified, parameters A, B and Y_{offset} can be calculated using equations (51), (52) and (50), respectively. Then, x values can be calculated using equation (49) for any given y values. However, the given y values cannot be greater than y_{max}. To consider the effect of y_{offset}, equation (36) is modified to:

$$y_{\max} = \sqrt{\frac{BP}{\rho}} - Y_{\text{offset}} \quad (53)$$

TABLE XII

GENERAL LINEAR MODEL PROCEDURE FOR PARAMETER B

Source	DF	Sum of Squares	Mean Square	F Value	Pr > F
Model	3	33.690	11.230	102.87	0.0001
Error	29	3.166	0.109		
Corrected Total	32	36.856			
	R-Square	C.V.	Root MSE		B Mean
	0.91	5.569	0.330		5.93

Source	DF	Type I SS	Mean Square	F Value	Pr > F
WIDTH	1	28.058	28.058	257.03	0.0001
LOAD	1	0.150	0.150	1.38	0.2502
DENSITY	1	5.482	5.482	50.21	0.0001

Source	DF	Type III SS	Mean Square	F Value	Pr > F
WIDTH	1	9.517	9.517	87.18	0.0001
LOAD	1	0.127	0.127	1.17	0.2888
DENSITY	1	5.482	5.482	50.21	0.0001

Parameter	Estimate	T for H0: Paramtr=0	Pr > T	Std Error of Estimate
INTERCEPT	1.625	1.34	0.1914	1.214
WIDTH	1.724	9.34	0.0001	0.184
LOAD	0.170	1.08	0.2888	0.155
DENSITY	-12.997	-7.09	0.0001	1.834

To validate the model, the calculated x values using equation (49) were compared with observed x values. Then, they were plotted against the original fitted line generated using A and B for that specific sample. The two lines were close for most samples. Figure 8 shows this result for sample no. 112 with 25 mm wide track width and 5 kg mass.

To quantify the validation, calculated x values and observed x values were regressed, and the coefficients of determination values were examined. Generally, they fit a straight line. R^2 values were mostly over 0.95, and the standard errors were mostly less than 5 mm. Table XIII shows the validation summary for 1.25 g/cm³ iso-density lines.

Calculate Density Value at Any Location

To calculate density values at a location, it was necessary to re-formulate equation (49) to:

$$\rho = \frac{BP}{(y+y_{offset})^2} \frac{1}{\left[1 + \left(\frac{x}{A(y+y_{offset})}\right)^2\right]^{\frac{5}{2}}} \quad (54)$$

This formula contained parameters A and B , which varied for different density values. After substituting the equations for A and B , equations (51) and (52) respectively, the equation was solved numerically.

A program was written to calculate the density values at any given location for any loading environment, using a Newton-Raphson method (Press et al., 1992). This method was intended to solve for a root of a function, within given low and high bounds. It was necessary to re-define equation (54) to:

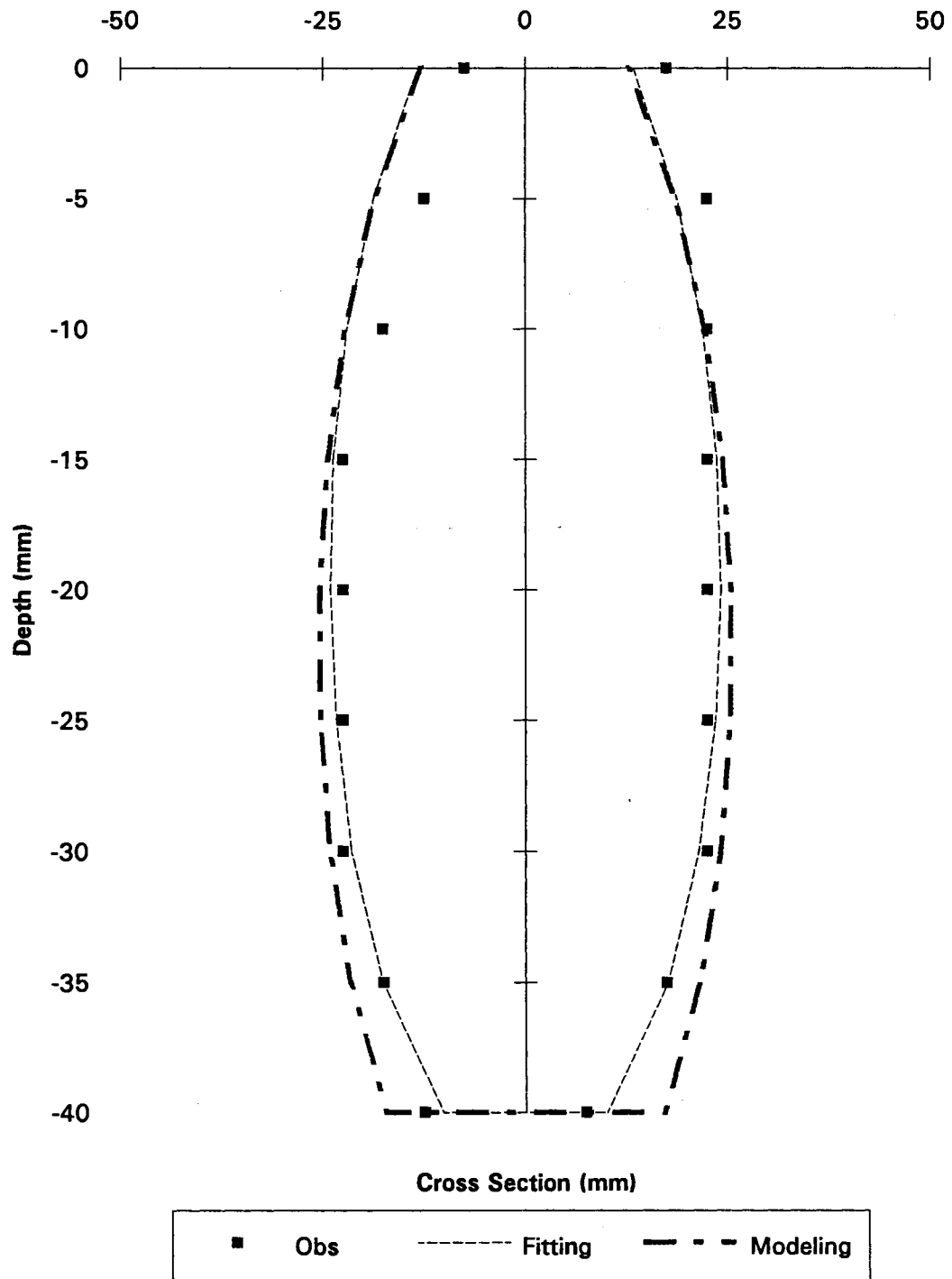


Figure 8. Calculating 1.25 g/cm³ Iso-Density Line of Sample #112 With Parameters A and B Generated for This Sample and Whole Experiment.

TABLE XIII

VALIDATION OF MODELING ISO-DENSITY LINE OF 1.25 g/cm³

Sample No.	Intercept	Slope	R ²	MSE
111	-5.0	0.72	0.96	4.54
112	-1.2	1.11	0.95	3.68
121	-5.4	1.06	0.99	3.12
122	-4.0	1.16	0.99	3.86
131	*	*	*	*
132	1.8	0.68	0.99	3.70
141	-0.9	1.05	0.98	5.08
142	-2.8	0.78	0.96	6.90
151	0.9	0.86	0.98	5.63
152	-1.2	1.23	0.99	4.26
161	-3.0	0.74	0.93	13.16
162	-2.9	1.30	0.99	3.72

* Data are not available because density did not exceed 1.25 g/cm³.

$$f(\rho) = \rho - \frac{BP}{(y+y_{offset})^2} \frac{1}{\left[1 + \left(\frac{x}{A(y+y_{offset})}\right)^2\right]^{\frac{5}{2}}} \quad (55)$$

The Newton-Raphson method also requires the first derivative of the function, which was:

$$\frac{df(\rho)}{d\rho} = 1 - \frac{dB}{d\rho} \frac{P}{(y+y_{offset})^2} \frac{1}{\left[1 + \left(\frac{x}{A(y+y_{offset})}\right)^2\right]^{\frac{5}{2}}} - \frac{dA}{d\rho} \frac{5BPx^3}{A^3(y+y_{offset})^4} \frac{1}{\left[1 + \left(\frac{x}{A(y+y_{offset})}\right)^2\right]^{\frac{7}{2}}} \quad (56)$$

where

$$\frac{dA}{d\rho} = -2.044 \quad (57)$$

and

$$\frac{dB}{d\rho} = -12.997 e^{1.625} \text{width}^{1.724} \text{load}^{0.167} \rho^{-13.997} \quad (58)$$

To compare the calculated and the measured density values for all the samples, errors between them were calculated for four zones. The first zone was a rectangular area of 200 mm cross and 80 mm deep; the second zone was a 60 x 60 mm square area; the third zone was a 30 x 30 mm square area and the fourth zone was a 25 x 25 mm square area but 25 mm below the applied load point. The first three zones were located directly below the applied load point. The first zone was almost the whole area scanned except the two extreme sides. The fourth zone was located in the seed zone. For each of the four zones, the average errors between the measured and calculated density values, both for net errors and absolute errors, were calculated. The result of this analysis is summarized in Table XIV. The results showed that the least error occurred at the fourth zone, which coincided with the seed zone. This was not accidental, because the model is based on the density data near this zone. For the third zone, the model tended to overestimate the density values, since the net-error terms had many negative numbers. Generally, the model fit the data very well.

The calculated density data and their errors were plotted as contours using the, program, Surfer. Figure 9 and Figure 10 show the result of calculated density and their errors for sample #111 with 25 mm block and 5 kg ballast. The calculated density lines of the central part were very close to the density lines generated from the measured data.

Maximum errors occurred immediately below the imposed load, at points where density approached the density of the undisturbed soil, and near the bottom of the soil profile. The model was not intended to predict soil densities of the far right and left sides of undisturbed soil samples, and large errors occurred. The lower part of the sample was mostly out of the reach of the loading variables, and large errors also occurred. Large errors occurred at the point directly below the load applied point, because the model predicted that this point had the maximum density. In reality, the top surface had the maximum density most of time, and sometimes maximum density occurred at a short distance below the load point. This fact caused relatively large errors at that point.

TABLE XIV

SUMMARY OF CALCULATION ERRORS FOR LABORATORY TEST SAMPLES

Smpl	Zone1 Error (%)		Zone2 Error (%)		Zone3 Error (%)		Zone4 Error (%)	
	Net	Abs	Net	Abs	Net	Abs	Net	Abs
111	7.06	7.20	1.27	1.90	0.04	2.16	1.38	1.39
112	5.32	5.93	-0.83	1.47	-2.02	2.05	-1.05	1.11
121	2.10	3.84	-1.23	2.33	-4.54	4.69	0.18	1.03
122	2.97	4.56	-2.91	3.04	-7.54	7.54	-2.72	2.72
131	-1.89	2.44	-3.15	3.17	-5.37	5.37	-1.45	1.45
132	2.18	2.73	0.94	2.36	-1.88	2.13	1.40	1.70
141	4.95	5.66	0.04	1.23	0.65	1.57	0.63	1.04
142	4.58	4.93	-0.35	1.17	-1.19	1.77	-0.26	0.41
151	2.55	3.24	2.15	3.18	-0.87	2.88	2.29	2.32
152	-0.32	2.91	-3.24	3.42	-8.23	8.24	-0.52	1.00
161	2.39	3.23	2.93	3.65	-0.16	2.01	3.51	3.51
162	-4.40	4.56	-5.87	5.87	-8.72	8.72	-4.13	4.13

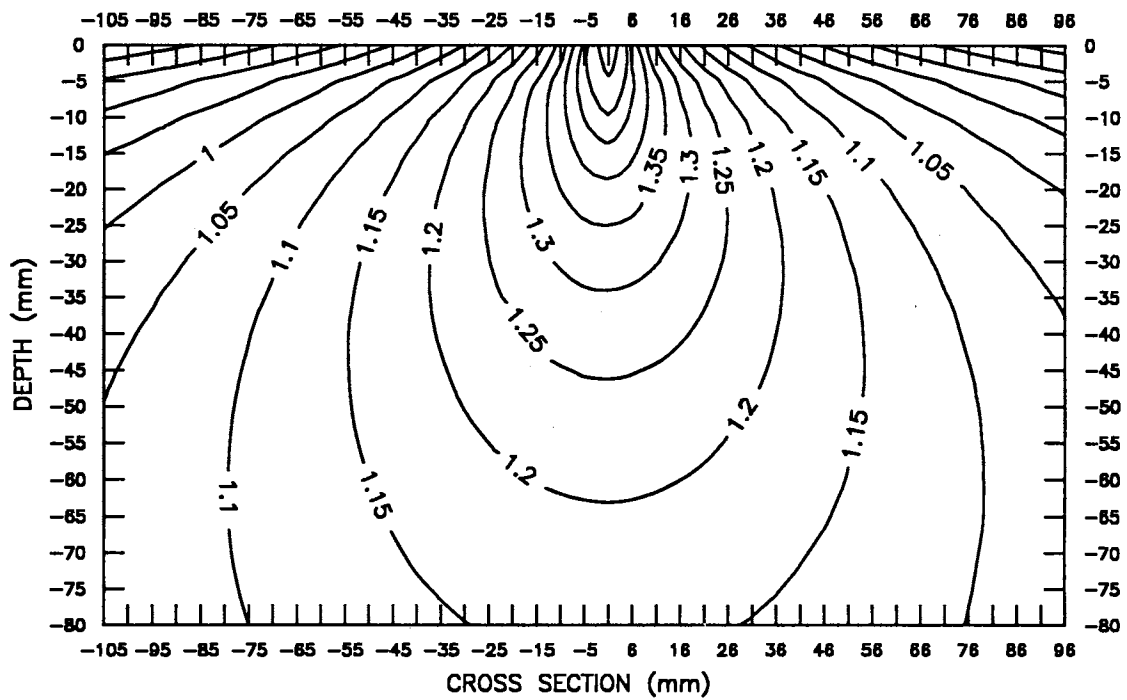


Figure 9. Contour Lines of Density Generated from the Calculated Data for Sample #111 with 25 mm Wide Track and 5 kg Mass.

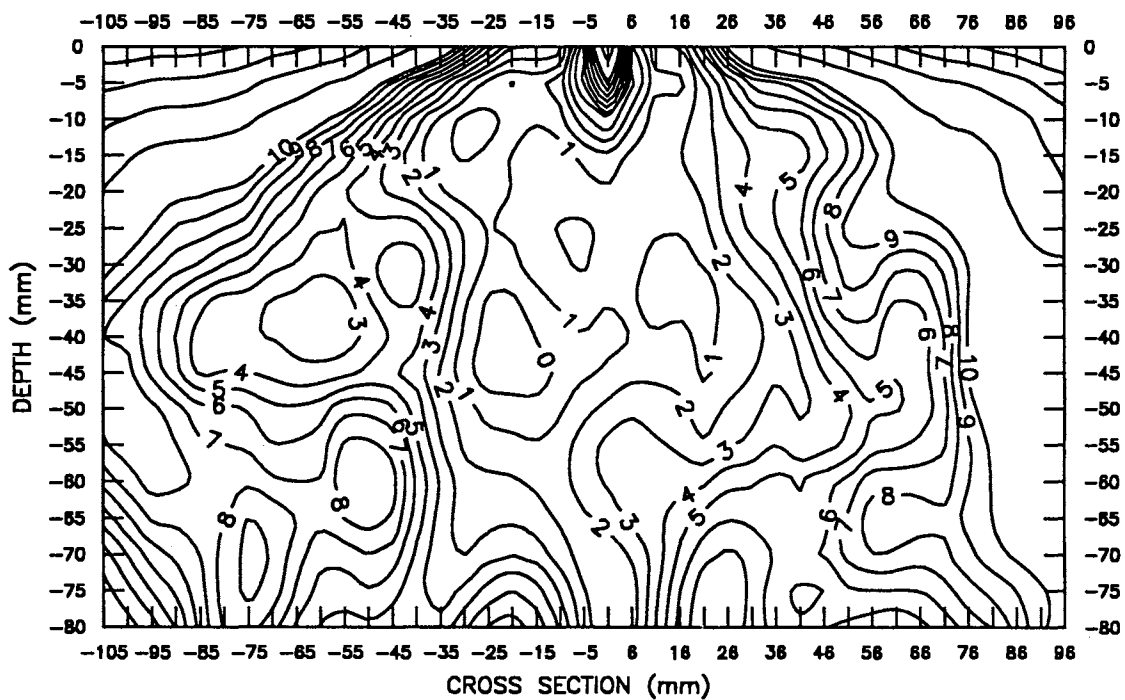


Figure 10. Contour Lines of Errors (%) of Calculated Density for Sample #111 with 25 mm Wide Track and 5 kg Mass.

Analysis of Area Enclosed by Iso-Density Lines

The area enclosed by iso-density lines was calculated using equation (44) with $y_0 = y_{\text{offset}}$ and the T-term calculated from equation (45). Parameters A and B were calculated with equation (51) and equation (52), respectively. Figure 11 shows that the area enclosed by an iso-density line decreases as the density increases. It was true for all loading conditions. For a specified density level, the enclosed area increased as the load increased. For cases of the same applied loads, the area was determined by track width, but not in a uniform way. For example, for an applied ballast of 98 N, 102 mm wide track compacted a larger area than the 51 mm block for density less than 1.27 g/cm³. For density values above 1.27 g/cm³, the situation was reversed. The same was true for 102 mm wide track and 25 mm wide track at a density about 1.34 (g/cm³). A similar response occurred for 49 N ballast cases.

Equation (53) was used to study the change of penetration depth as a function of density. Figure 12 shows maximum penetration depth as the function of density. The analysis of depth was similar to the situation with area. For a specified density level, more ballast mass caused deeper depths. For the same ballast mass, narrower blocks caused deeper penetration. However, it was not always true. For example, in the case of the 98 N ballast mass, the 51 mm wide track caused deeper penetration than the 25 mm block for density levels less than 1.45 g/cm³. This trend was reversed for density levels higher than 1.45 g/cm³. Therefore, using wider press wheels causes deeper compaction, but less severely in term of density level.

Maximum Width of Compaction

The ratio of maximum width to maximum depth of compaction was calculated using equations (39), (53) and (51), i.e.,

$$\frac{X_{\max}}{Y_{\max} + Y_{\text{offset}}} = 0.431A \quad (59)$$

$$= 1.605 - 0.881\rho$$

This ratio determined the geometric relation of width-to-depth, and it is the function of density. As the density increased, the ratio of width-to-depth of the compacted zone enclosed by this density level became smaller. For the same reason, the compacted zone enclosed by a higher density level tended to be relatively narrower comparing its penetrating depth. Figure 13 shows maximum compaction width as a function of soil density for several simulated wheel track widths and press wheel ballasts. Higher ballast or wider track caused a wider compaction zone, but a wider track cannot compact soil to high density. For example, the 100 mm track caused the highest density (1.42 g/cm³) for a 98-N weight, and 1.35 g/cm³ for a 49-N weight. Other tracks of narrower width caused even higher densities.

Analysis of Soil Bin Experiment

The soil bin experiment was conducted to test the portability of the model and to gain an understanding of the effect of loading variables on the density profile in soil, especially in the seed zone. Grain drill press wheels, instead of wooden blocks, were used in this test. Therefore, this test was closer to the real field conditions than the laboratory controlled experiment.

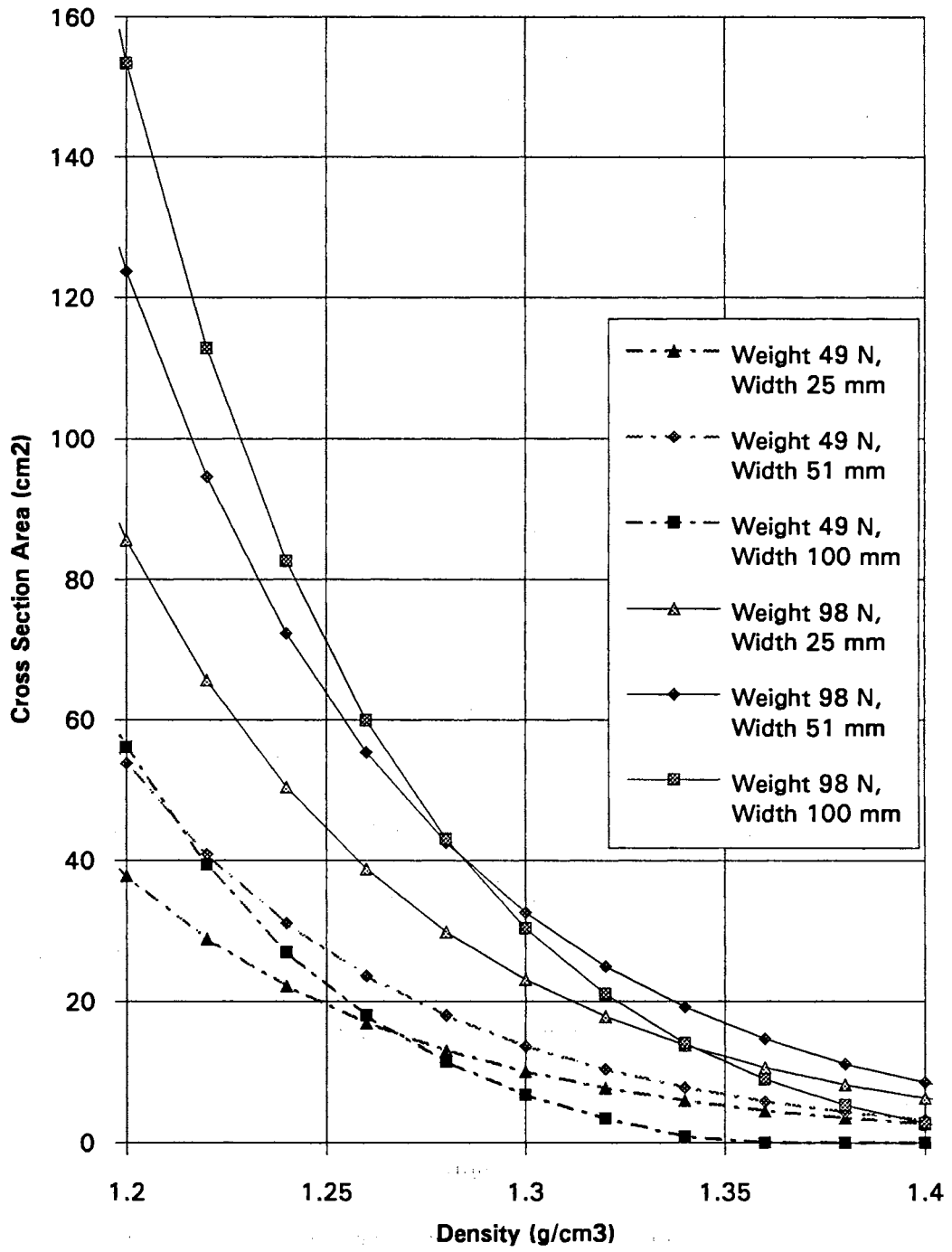


Figure 11. Cross Sectional Area Enclosed by Iso-Density Lines as a Function of Soil Density for Several Simulated Wheel Tracks and Press Wheel Ballasts.

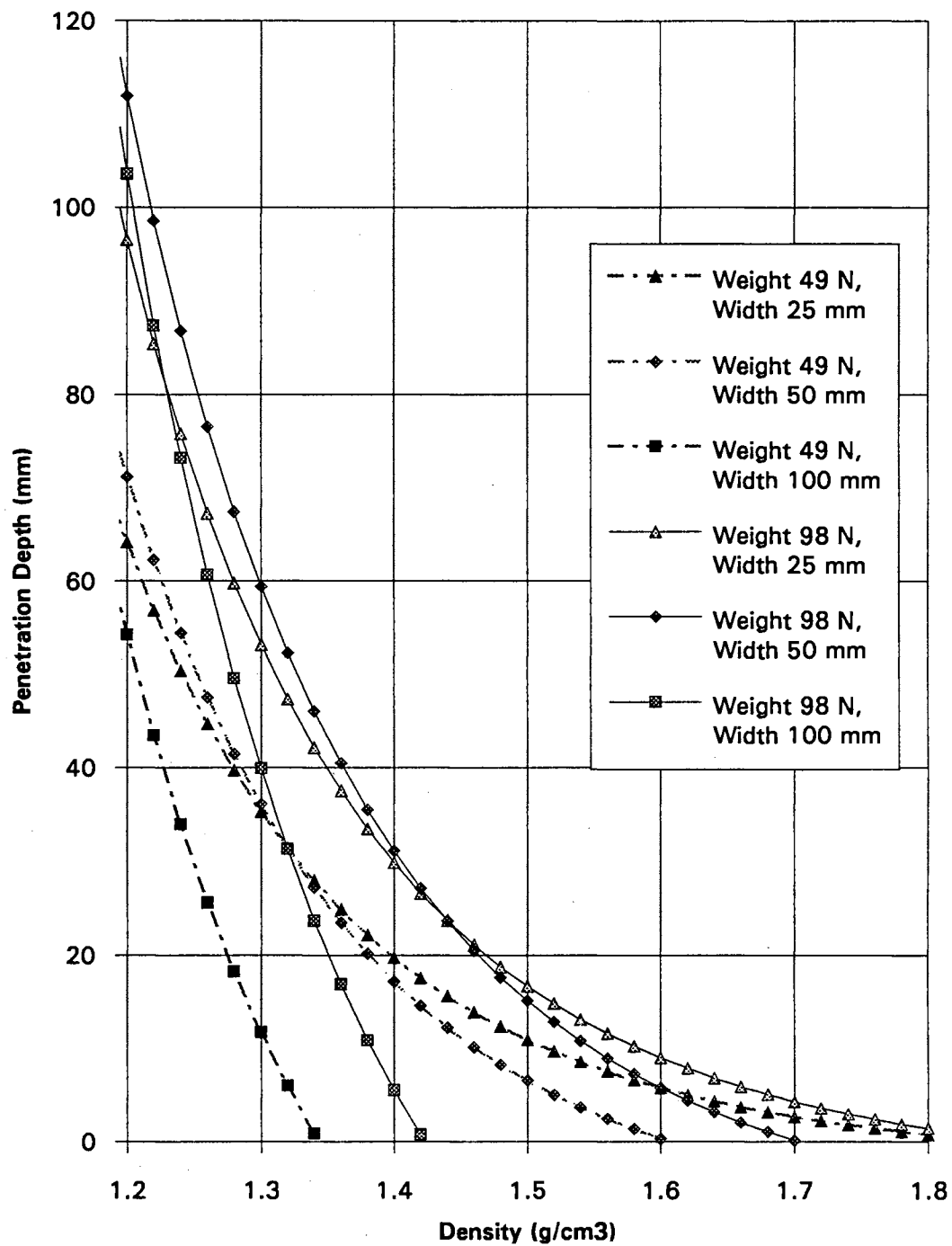


Figure 12. Maximum Penetration Depth as a Function of Soil Density for Several Simulated Wheel Tracks and Press Wheel Ballasts.

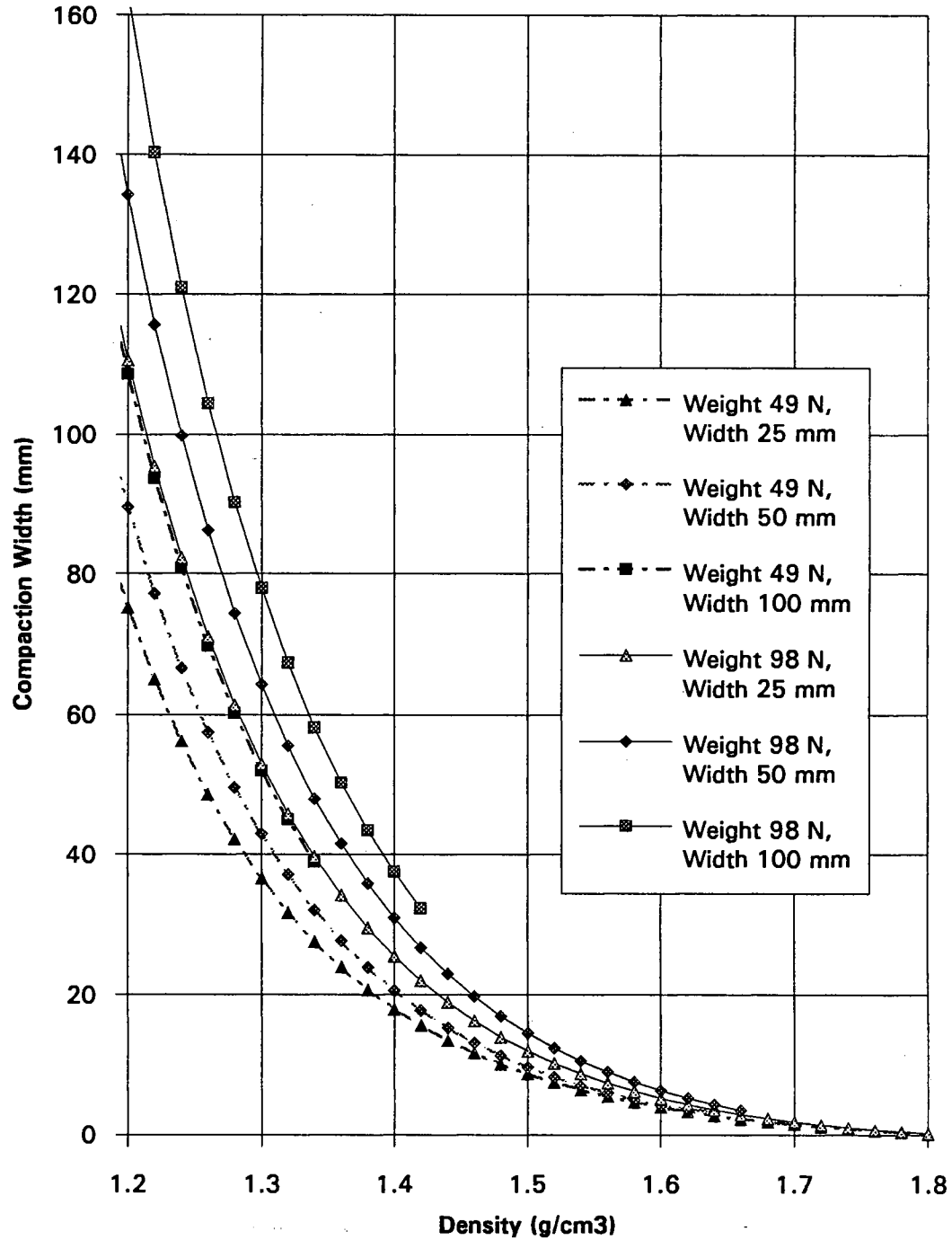


Figure 13. Maximum Compaction Width as a Function of Soil Density for Several Simulated Wheel Tracks and Press Wheel Ballasts.

Contact Area between Press Wheel and Soil Surface

The contact area between press wheel and soil surface must be calculated to determine the applied pressure on the soil surface. For agricultural tractor tires, Soehne (1958) suggested using an elliptical area to estimate the contact area. However, this approach was suitable only for tires on a relatively hard surface. In the case of a grain drill, the press wheels were made of hard rubber and the soil surface layer was very soft. The press wheel sank to a relatively great depth (Figure 14). The average contact surface was a square area with the width of the wheel, w , and the length, l , which was the projection length of the contacting arc on the horizontal surface. Because the wheel moved horizontally, only the right half of the arc contacted the soil. With sinkage, z , and wheel radius, R , the projection length l was calculated as:

$$l = \sqrt{2Rz - z^2} \quad (60)$$

Thus, the contact area was $w \times l$ and it was used to find the applied pressure.

Properties of Soil Bin Experiment Samples

After calculating the contact area and the applied total mass (mass of ballast and press wheel), the applied pressure was computed. The properties of samples are shown in Table XV. The mass of the press wheels also contributed to the total mass applied to the soil surface.

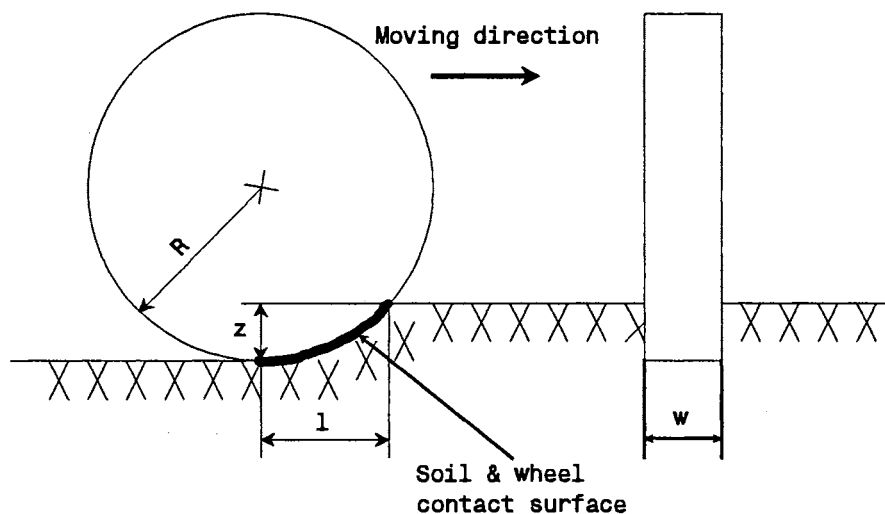


Figure 14. Schematic of Soil and Wheel Contact Area and Its Effective Length.

Elimination of Linear Trend

After plotting the density profiles, it was noted that the data did not have as clear a pattern as the laboratory experiments. There was an obvious linear trend, for most of the samples, of increasing density with increasing depth. The cause of this linear trend will be discussed later.

To eliminate the linear trend, bands of data from far right and far left sides of the sample were used. The density data of those points were regressed linearly with depth, y , as the independent variable. The fitted results are shown in Table XVI. This procedure removed the linear trend from most of the samples.

Compensation for the Effect of Moisture Content

Like the analysis of the laboratory experiments, the predicted and observed

density data were compared and their differences were calculated for four different zones. At this stage, the errors were very large for all zones, and the errors were mostly in the range of 20-30%, which were not acceptable. It appeared that the moisture content affected density.

TABLE XV
CHARACTERISTICS OF SOIL BIN EXPERIMENT SAMPLES

Smpl No.	Sinkage (mm)	Radius (mm)	Contact Area			Mass		MC (%)	Load (kPa)
			Width (mm)	Length (mm)	Area (mm ²)	Ballast (kg)	Wheel (kg)		
111	40	153	25	103	2624	10	2.25	7.4	45.8
112	40	153	25	103	2624	10	2.25	7.7	45.8
121	5	140	102	37	3763	10	4.50	6.5	37.8
122	5	140	102	37	3763	10	4.50	6.7	37.8
131	15	165	51	69	3493	0	4.00	7.9	11.2
132	15	165	51	69	3493	0	4.00	7.9	11.2
141	40	165	51	108	5473	5	4.00	7.6	16.1
142	20	165	51	79	4001	5	4.00	7.8	22.1
151	30	165	51	95	4821	10	4.00	8.4	28.5
152	20	165	51	79	4001	10	4.00	8.0	34.8
161	35	165	51	102	5164	15	4.00	7.6	36.1
162	40	165	51	108	5473	15	4.00	7.3	34.1

When modeling the soil strength factors c and ϕ , Ayers and Bowen (1987) noted that when soil was dry, the model tended to overestimate. They proposed the following formula to compensate for the effect of moisture content:

$$CF = 0.5 + \frac{3.0}{MC} \quad (61)$$

where CF=correction factor, and MC=soil moisture content, % dry basis. By

observing the moisture content of the two experiments, and by the process of trial-and-error, the following correction relationship was developed:

$$CF = 0.5 + 0.75 \frac{MC}{14.0} \quad (62)$$

TABLE XVI

FITTING OF LINEAR TREND OF DENSITY FOR SOIL BIN EXPERIMENT

Sample No.	Intercept	Slope	R ²
111	1.0	-0.0034	0.81
112	1.1	-0.0031	0.85
121	1.1	-0.0027	0.77
122	1.0	-0.0033	0.70
131	0.7	-0.0064	0.45
132	0.6	-0.0069	0.50
141	1.0	-0.0034	0.93
142	1.0	-0.0034	0.83
151	1.1	-0.0028	0.81
152	0.7	-0.0065	0.45
161	1.1	-0.0032	0.91
162	1.1	-0.0031	0.85

After making this correction, the differences between the predicted and observed density values were compared for the four zones. The results are shown in Table XVII. The errors in this experiment were about one order of magnitude higher than the errors of the laboratory-controlled experiment. The prediction error was mostly less than 15%. With an average of 10% error, and for density in range of 1.0 to 1.4, the difference in

magnitude of the densities was about 0.1 g/cm^3 . Even though the experimental data differed greatly from the predicted data, the results approximated the general pattern of density distribution. The inaccuracy of prediction was due in part to the inaccuracy of measuring the wheel-soil contact area. The model was justified by this experiment, with a relatively large room for improvement.

TABLE XVII
SUMMARY OF PREDICTION ERRORS FOR SOIL BIN EXPERIMENT

Smpl	Zone1 (%)		Zone2 (%)		Zone3 (%)		Zone4 (%)	
	Net	Abs	Net	Abs	Net	Abs	Net	Abs
111	13.69	14.16	2.99	5.00	-3.07	4.37	1.33	1.54
112	16.50	16.68	7.23	7.99	2.35	5.19	7.00	7.00
121	7.33	7.52	4.15	4.65	0.09	0.94	6.23	6.37
122	4.33	5.81	0.74	4.51	-4.24	4.90	4.35	4.50
131	-11.26	11.84	-17.13	17.13	-19.67	19.67	-13.64	13.64
132	-11.33	11.56	-15.37	15.37	-19.30	19.30	-10.46	10.46
141	15.95	16.03	8.72	9.08	3.00	4.34	9.48	9.48
142	8.56	9.17	2.30	5.05	-3.87	5.38	4.64	4.64
151	7.19	8.01	0.17	3.82	-5.82	5.91	0.99	2.15
152	-17.44	17.55	-22.70	22.70	-27.37	27.38	-23.30	23.30
161	11.45	11.70	4.932	6.033	-0.42	3.67	6.21	6.21
162	14.23	14.55	6.814	8.232	0.07	5.33	8.46	8.46

Figure 15 shows the original lines of original density, while Figure 16 and Figure 17 show the results of predicted density profiles and their errors for sample #151, with 25 mm press wheel and 28.5 kPa load. Density lines of the central part of the sample were close to the measured ones. The main errors occurred at the two sides and at the very top part near the load-applying point.

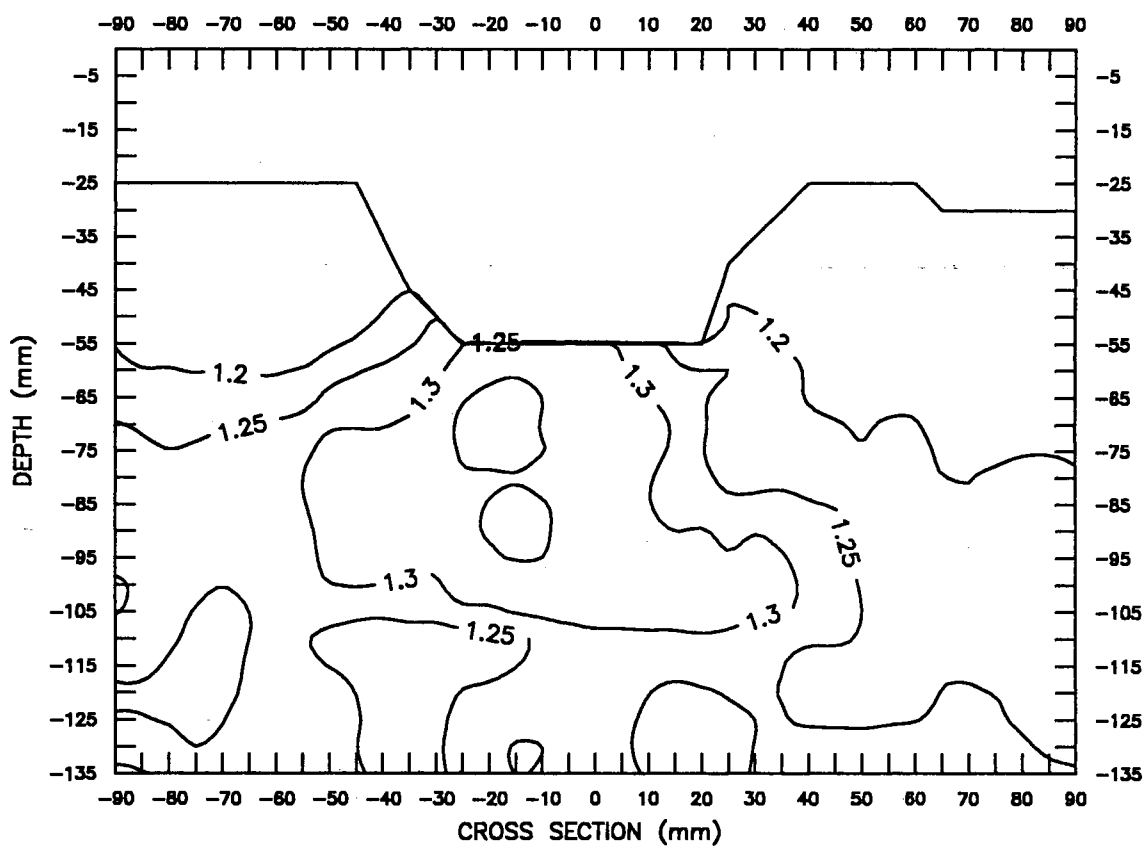


Figure 15. Contour Lines of Original Density Data of Sample #151 with 51 mm Press Wheel and 28.5 kPa Load.

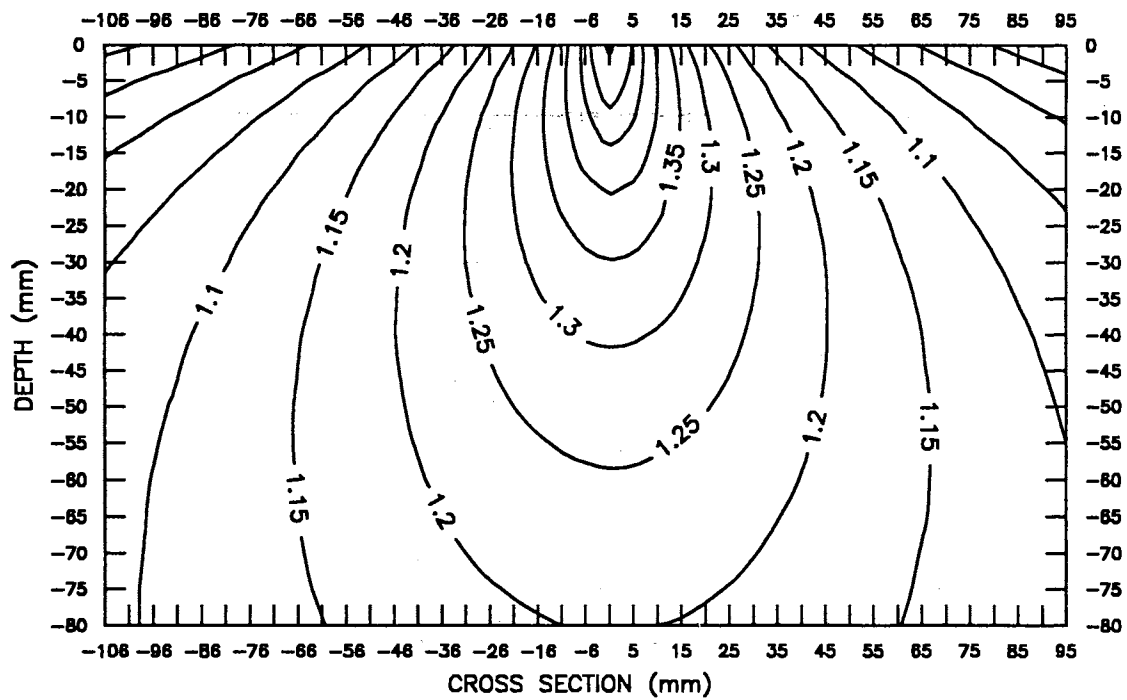


Figure 16. Contour Lines of Density Generated from Predicted Data for Sample #151 with 51 mm Press Wheel and 28.5 kPa Load.

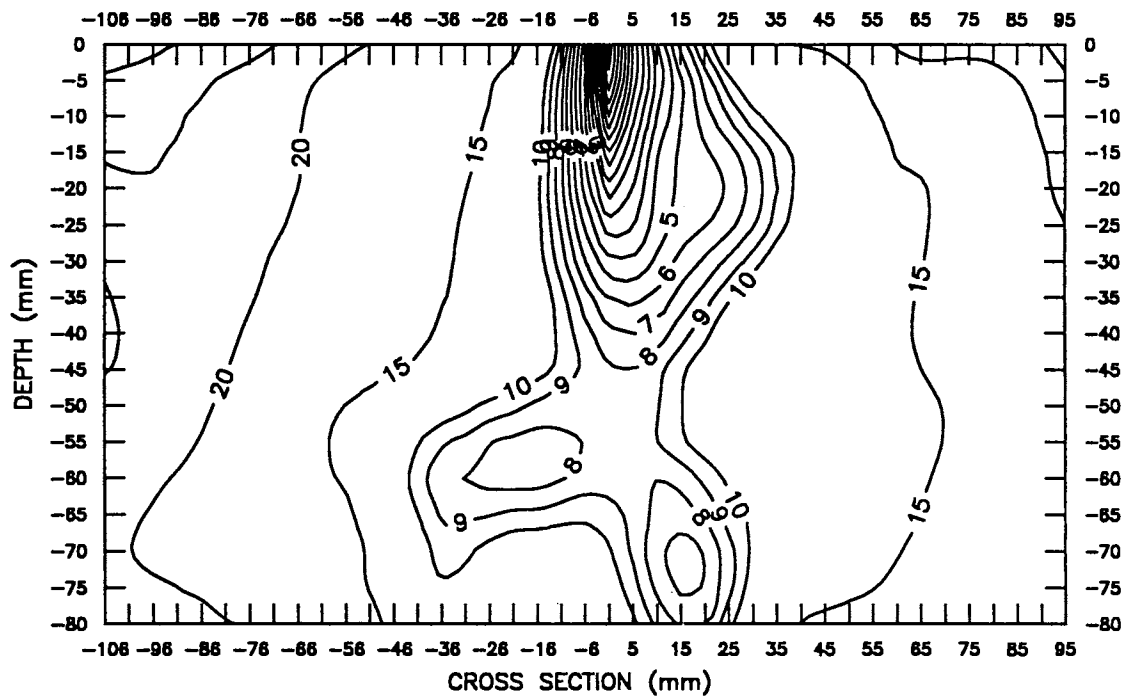


Figure 17. Contour Lines of Errors (%) of Predicting Density for Sample #151 with 51 mm Press Wheel and 28.5 kPa Load.

Cause of the Linear Trend of Soil Density Profile

To determine the cause of the density linear trend, three more samples were taken and scanned. One sample was prepared in the laboratory by packing the soil directly into the sampler, as was the case in the laboratory experiment. The other two samples were collected in soil bin, as in the case of the soil bin experiment. One of these samples was transported vertically, and the other one was transported horizontally with top portion secured with plaster of paris to preserve the soil surface. Asher silty clay loam soil was used in all samples. Moisture content was 8.47%, d.b.. No external forces were applied to the samples. Contour maps of the three samples are shown in Figure 18 to Figure 20. Compared to the other two samples, the sample that was packed in the soil bin and transported vertically showed a clear linear density pattern. The sinkage of the soil surface line of this sample indicated that transporting the sample vertically caused increasing density with increasing depth.

Analysis of Field Experiments

Two field experiments were conducted on the same location at different times and with different moisture contents. The forces exerted on the press wheel were recorded. The data from these two experiments were so variable that it was impossible to draw definite conclusions. Especially in the case of the first experiment, no meaningful density profiles were observed. This condition was probably due to the low moisture content, so that density change caused by the loading variables was over-shadowed by the variable soil condition. However, the second experiment still exhibited some of the characteristics of density profile pattern that existed in the laboratory experiment.

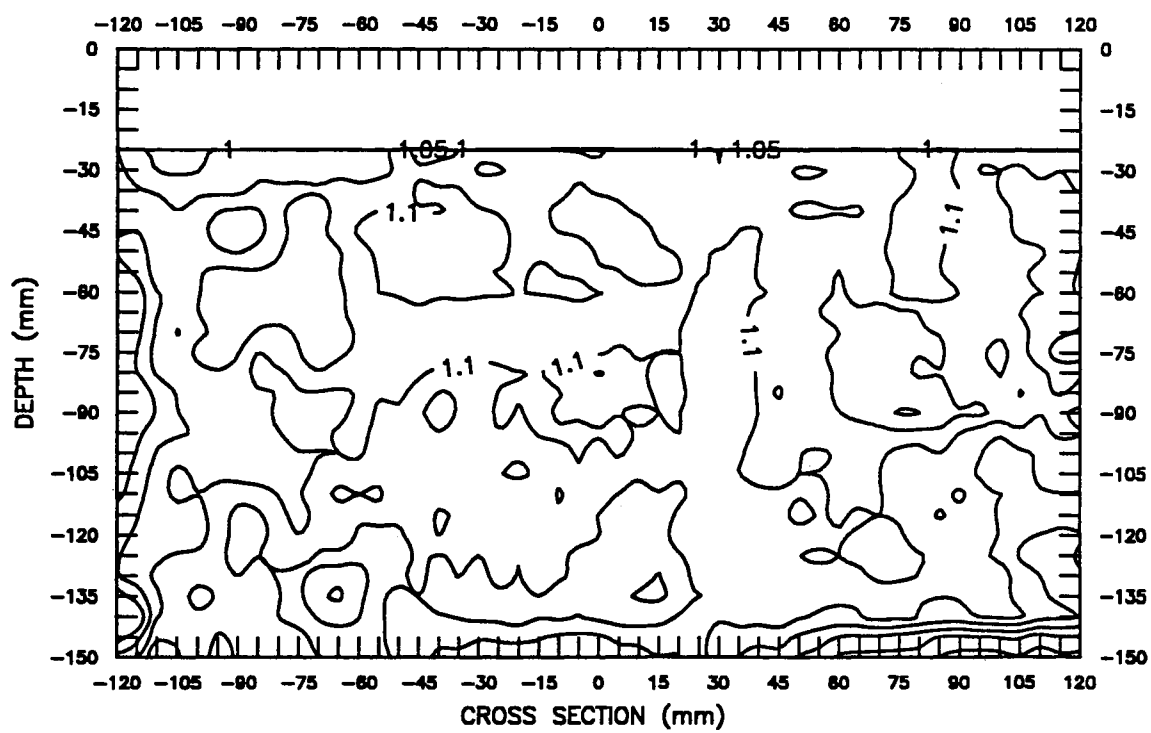


Figure 18. Contour Lines of the Sample Packed Directly in Laboratory.

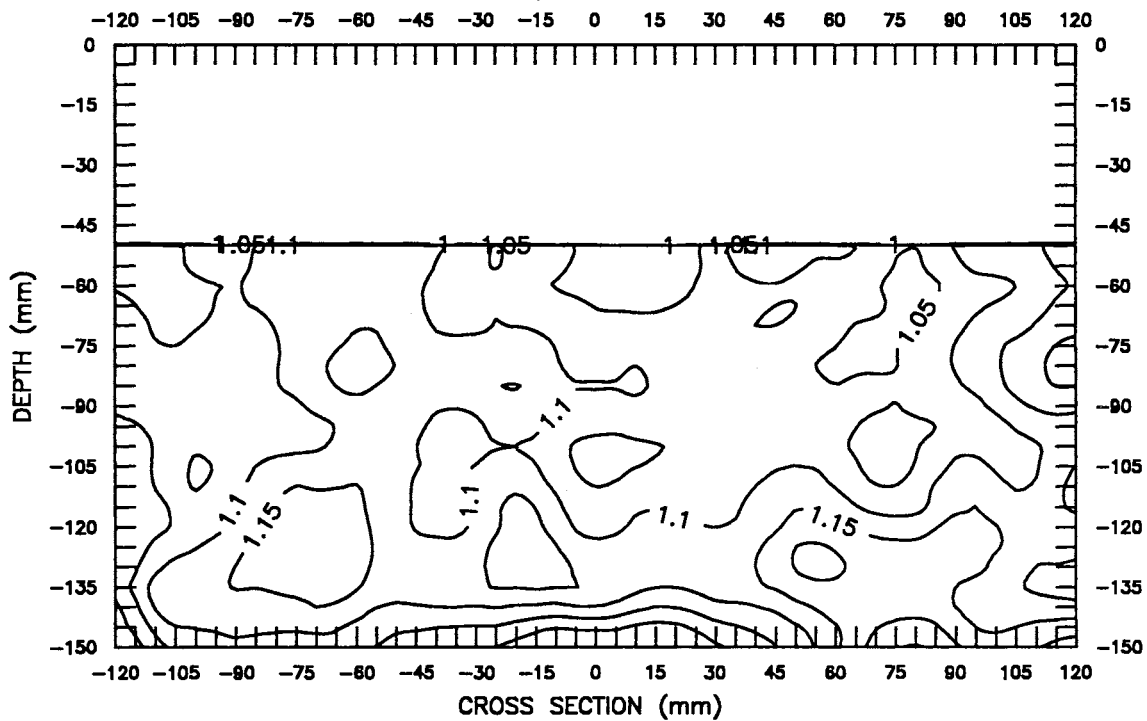


Figure 19. Contour Lines of the Sample Packed in Soil Bin and Transported Horizontally with Plaster of Paris on the Top.

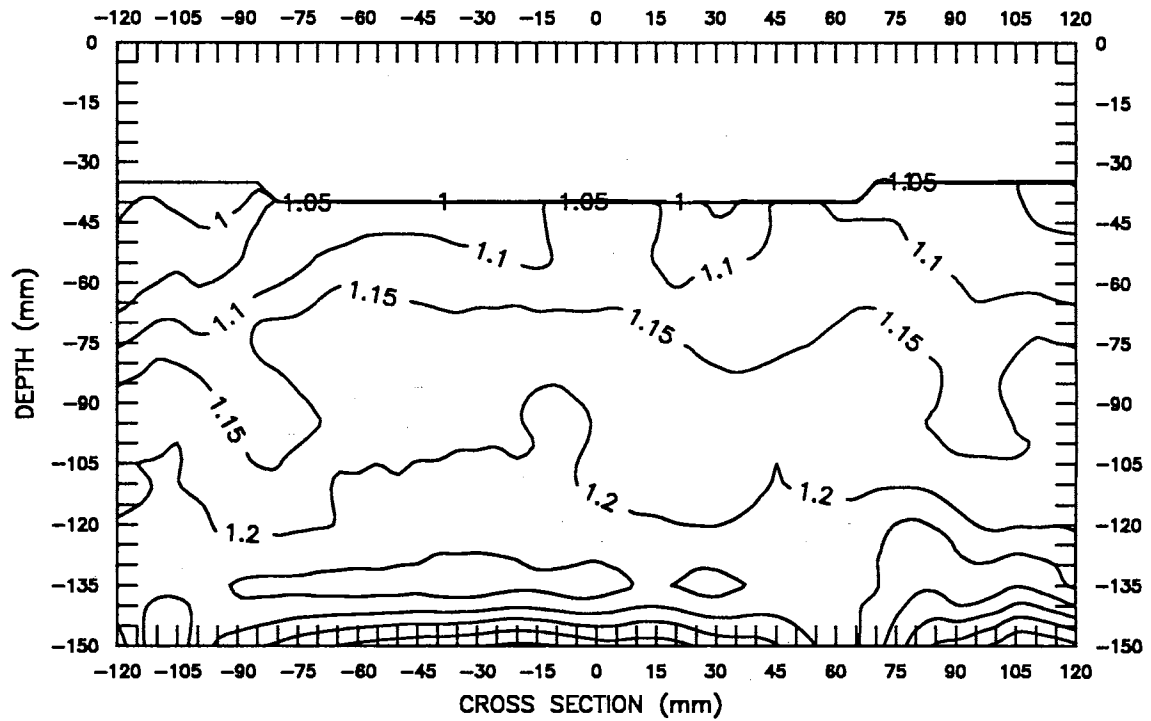


Figure 20. Contour Lines of the Sample Packed in Soil Bin and Transported Vertically.

Forces Exerted on the Press Wheel

As an example of measured forces exerted on press wheel, Figure 21 shows the forces exerted on a press wheel in plot #105 of field experiment no. 2 with 10 kg ballast and 51 mm press wheel. The forces oscillated and had peak values much higher than the average values. For most of the plots, the average vertical forces were close to the summation of ballast and press wheel weights. This phenomenon justified using the summation weight as the load in the prediction model. However, the difference between the static weight and the dynamic load may be a factor contributing to the inconsistency between the measured and predicted density profiles.

First Field Experiment

The first field experiment had 31 valid samples with different loading conditions and soil moisture content. The properties of this test are shown in Table XVIII.

TABLE XVIII

AVERAGE PROPERTIES OF FIELD EXPERIMENT NO. 1

Width (mm)	Ballast (kg)	Reps	MC (%)	Sinkage (mm)
25	10	3	6.3	22
51	0	6	6.8	13
51	5	5	6.0	13
51	10	6	5.6	13
51	15	5	8.4	16
102	10	6	5.5	8

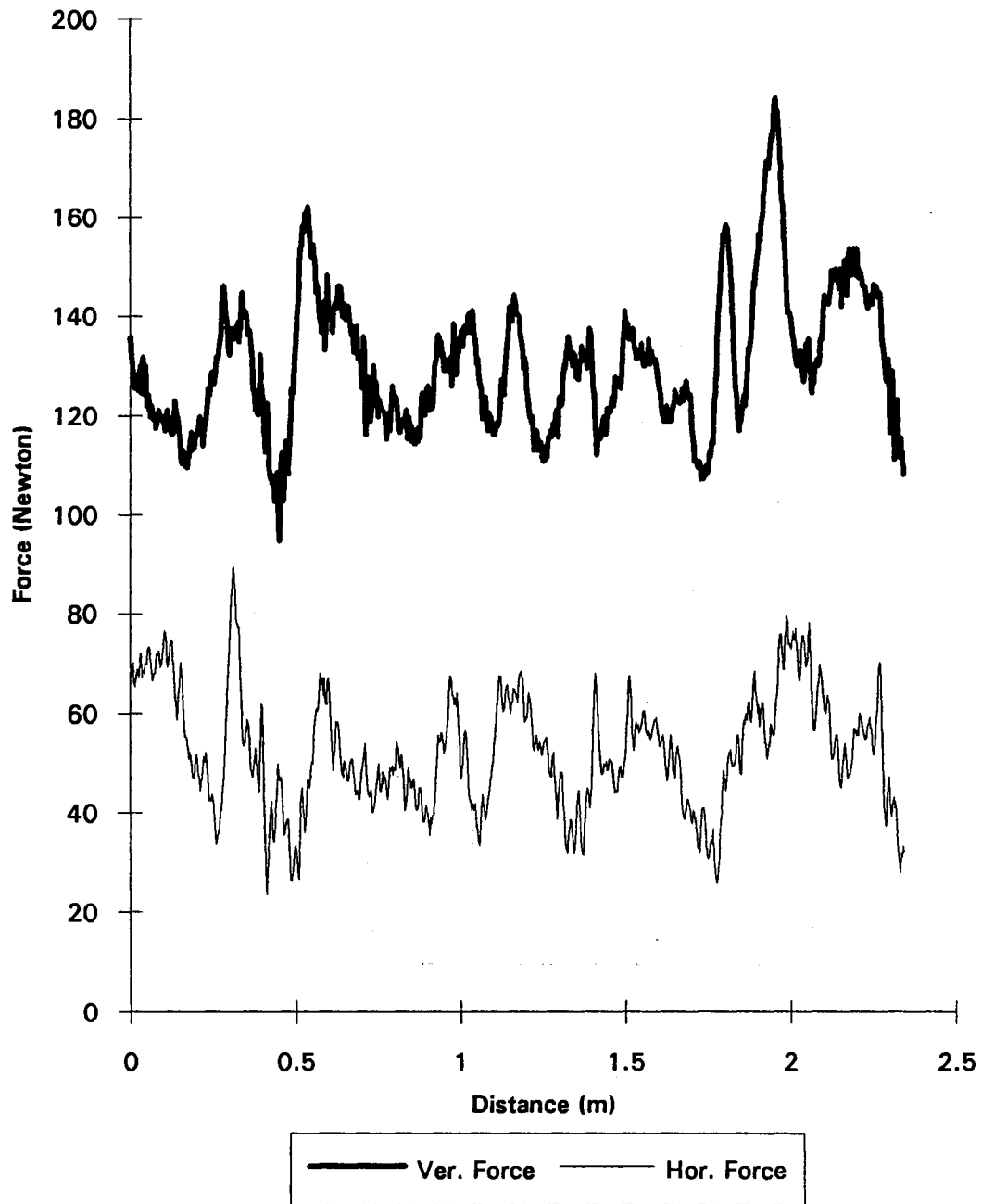


Figure 21. Forces Exerted on Press Wheel for Plot #105 of Field Experiment No. 2 with 10 kg Ballast and 51 mm Press Wheel.

A typical contour of the density profile of experiment no. 1 is shown in Figure 22. The contour is for sample #142 of field experiment no. 1 with 10 kg ballast and 25 mm press wheel. There was no clear density pattern, and no further analysis was possible. There was also a compacted layer section located about 60 mm below the surface in most of the samples. The compacted layer was another factor which may interfere with model prediction. There were numerous clods in these samples, which generated local high-density zones. Those clods were believed to act as rigid bodies at the load levels used here. This condition also complicated the modeling.

Second Field Experiment

Results of the second field experiment showed better density distribution pattern than that of the first experiment. After adjusting for increasing density with depth, errors between the measured and predicted density for four zones were calculated. Errors were very large, mostly in the range of 10% to 30%. Thus, results of the field experiments were not in a clear pattern to be modeled. The fourth zones were generally too close to the hard pan. The average properties and errors between the measured and predicted densities are shown in Table XIX. Usually, the errors of the fourth zone were the smallest. In this case, because the fourth zone was near the compacted layer, the errors for zone three, or the 25 mm X 25 mm square below the loading point, were reported. As an example, contours of the original density profile, predicted density profiles and prediction errors of sample #152 with 10 kg ballast and 51 mm press wheel are shown in Figure 23 to Figure 25. Although a consistent trend existed between the density values of compacted soil and the loading variables, the large variation of the field experiment data caused the model to fail to predict exact values.

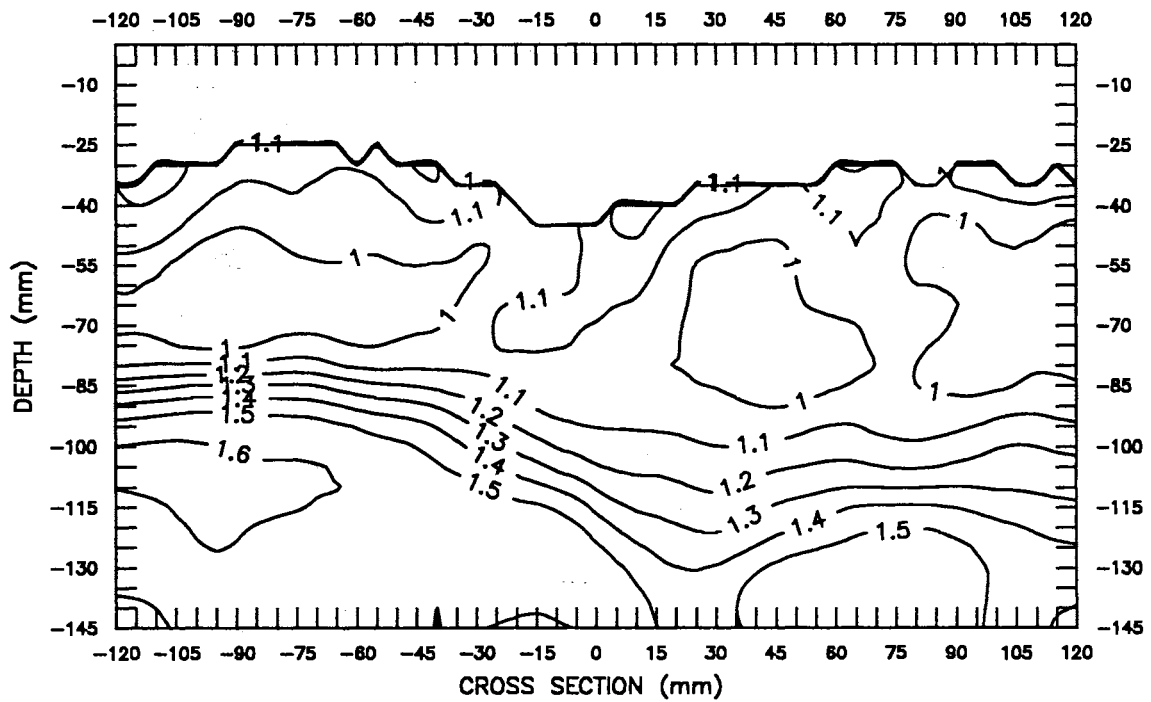


Figure 22. Contour of Density Profiles for Sample #142 of Field Experiment No. 1 with 10 kg Ballast and 25 mm Press Wheel.

TABLE XIX

AVERAGE PROPERTIES OF FIELD EXPERIMENT NO. 2 AND
PREDICTION ERRORS FOR ZONE 3

Width (mm)	Ballast (kg)	Reps	Sinkage (mm)	Area (mm ²)	Load (kPa)	MC (%)	Error (%)
25	10	6	32	2369	50.8	15.2	15.9
51	0	6	167	3614	11.2	14.4	21.9
51	5	6	22	4123	21.7	14.7	26.6
51	10	6	26	4484	30.8	17.0	29.0
51	15	6	37	5261	35.5	15.8	23.3
102	10	6	12	5648	25.4	16.5	30.4

Analysis of Soil Attenuation Coefficients

Validation of the gamma ray attenuation method in measuring soil density profile in soil samples can be accomplished by examining the soil attenuation coefficient. In this research, the density was not calculated directly from the soil attenuation coefficient. When converting the photon counts to density values, it was assumed the attenuation coefficients of soil and water were 0.0752 and 0.0831 cm²/g, respectively. Gravimetric water content was assumed 10% (dry base). The attenuation values used are the theoretical coefficients for quartz and water, respectively. Because of the less than ideal collimation and relatively high count rates used, it can be expected that the effective attenuation coefficients would be less than theoretical values. Initial density values were then divided by the ratio of average scanned density, ρ_I , to the measured average bulk density, ρ_R , for each sample. The ratio was:

$$Ratio = \frac{\rho_I}{\rho_R} = \frac{X(\mu_{sR} + \mu_w W_R)}{X(\mu_{sI} + \mu_w W_I)} \quad (63)$$

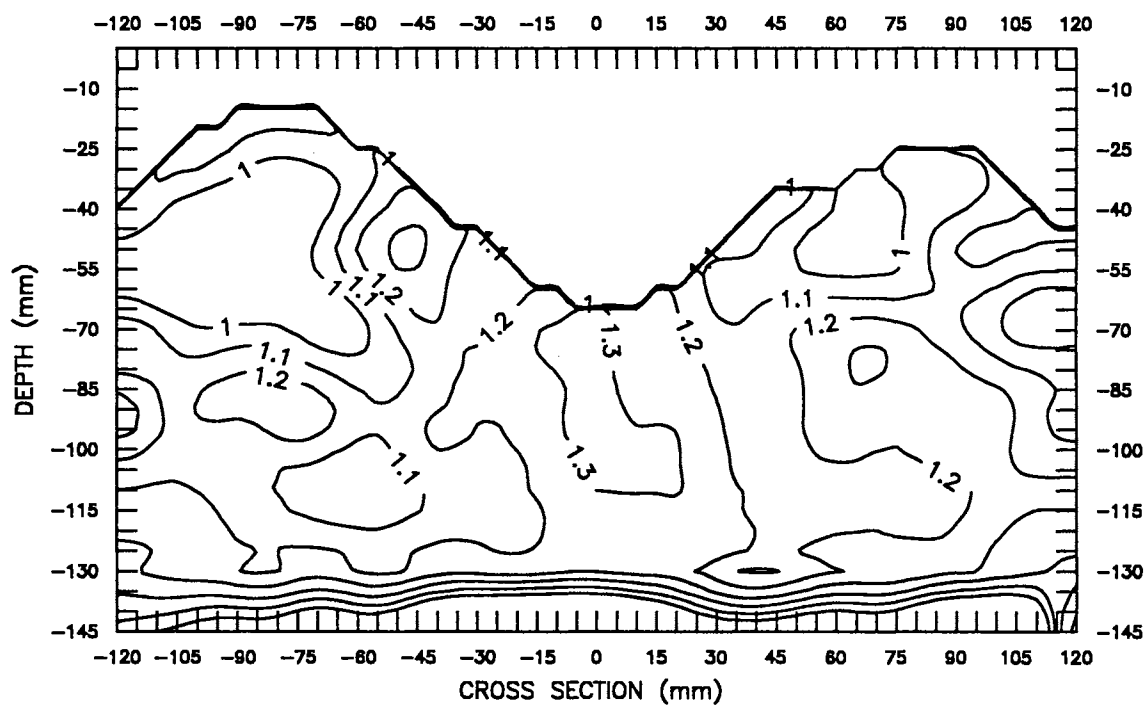


Figure 23. Contour of Original Density Profiles of Sample #152 of Field Experiment No. 2 with 10 kg Ballast and 25 mm Press Wheel.

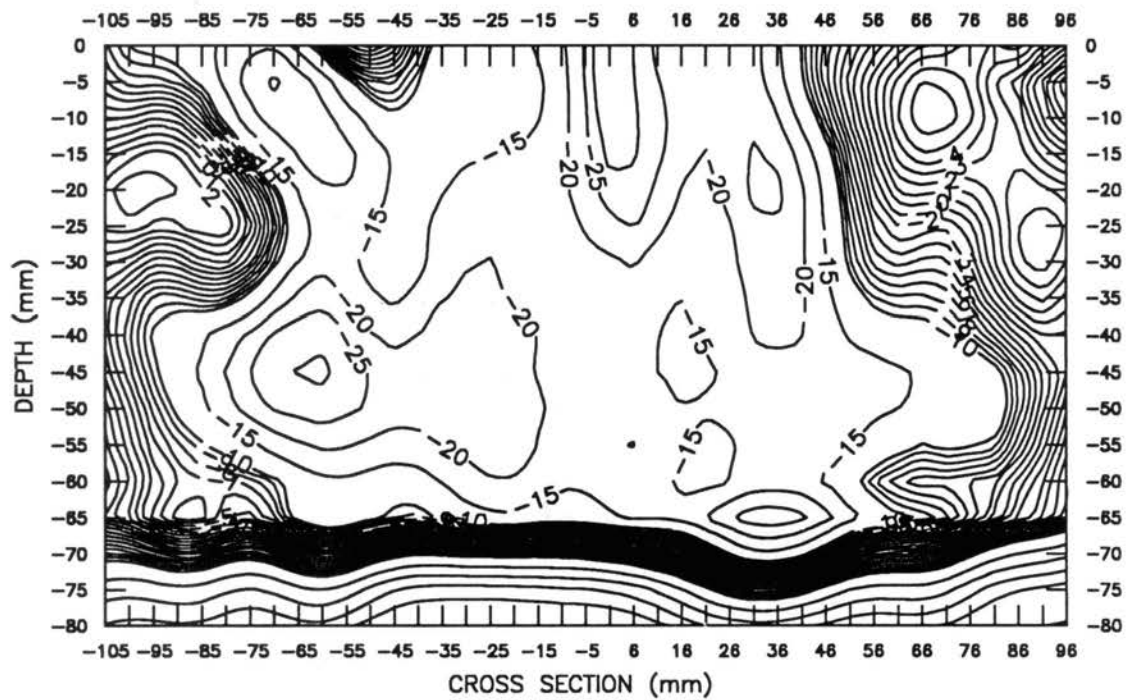


Figure 25. Contour of Simulation Errors of Sample #152 of Field Experiment No. 2 with 10 kg Ballast and 25 mm Press Wheel.

where μ_{sI} was the initially assumed soil attenuation coefficient, μ_{sR} was the actual soil attenuation coefficient, μ_w was the water attenuation coefficient, and W_I and W_R were the initially assumed and measured water contents (g/g), respectively.

Knowing the mass attenuation coefficient, μ_w , and actual water content of a sample, the soil attenuation coefficient was calculated as:

$$\mu_{sR} = \text{Ratio}(\mu_{sI} + \mu_w W_I) - \mu_w W_R \quad (64)$$

Each sample of an experiment generated one value, and the results are summarized in Table XX. Attenuation coefficients changed little and their standard deviations were typically less than 10% of the average values. As expected, they were lower than the originally assumed 0.0752 cm²/g, which was derived from the literature. Soil types seemed to influence μ_s , and calibration was necessary for the gamma ray system configuration and different soil types. After calibration of the soil attenuation coefficient, the gamma ray transmission method was adequate for testing density values in soil samples.

TABLE XX

AVERAGE SOIL ATTENUATION COEFFICIENTS (cm²/g)

	Field Test No. 1	Field Test No. 2	Soil Bin Test	Lab. Test
Soil Type	Zaneis Loam	Zaneis Loam	Asher Silty Clay Loam	Asher Silty Clay Loam
Avg. MC(%)	13.10	16.91	7.57	13.78
No. of Samples	28	36	12	12
μ_s Min	0.0554	0.0344	0.0521	0.0536
μ_s Max	0.0932	0.0756	0.0649	0.0550
μ_s Avg	0.0631	0.0627	0.0562	0.0544
μ_s Std	0.0081	0.0073	0.0046	0.0005

CHAPTER V

SUMMARY, CONCLUSIONS AND RECOMMENDATIONS

Summary

The effects of load and track width on the density profile in soil samples were evaluated for three kinds of experiments; namely, the laboratory test, the soil bin test and field tests. Field tests consisted of two separate experiments. Soil samples were packed directly into rectangular samplers in the laboratory test. In the field and soil bin experiments, the compacted soil was collected by inserting open-bottom samplers down into the soil.

Density profiles of soil samples were evaluated using gamma ray techniques. The profiles were similar in shape to the theoretical stress distribution in soil described by Boussinesq's equation. This equation was modified by adding two parameters, A and B, to fit the density profiles for different density levels and various loading conditions. Parameters A and B were related to density level, but B was also related to load and track width. Parameter A controlled the maximum width the iso-density lines spread, while parameter B influenced the shape of the iso-density lines. Four zones were considered when calculating the fitting errors. The zone which coincided with the seed zone had the least error. The fitted results were satisfactory for the laboratory test, and therefore, this modified equation was treated as the model for density distribution under

compaction of the press wheel.

However, subsequent soil bin test data did not fit the model as well as the laboratory test data. One possible reason was that the packing effort in preparation of the soil bin compacted the lower layer more than the top layer, and density profiles increased linearly with depth. The other reason may be that vibration, while transporting samples to the scanning lab, caused the linear trend of increasing density with depth. After correcting for linear trend, the density profile become more consistent with the model.

Data from the field experiments were so variable that the results could not fit into the model, even though about 72 samples were collected. However, a consistent trend existed between the density values of compacted soil and the loading variables.

Area enclosed by an iso-density line was analyzed as the function of load, loading width and density level. For a specified density level, the area increased if the load increased. When using the same ballast with different track widths, the actual applied load was different, in terms of load per unit area. This contributed to complexity of the compaction analysis. Furthermore, the track width also influenced the maximum width to which the compaction could spread horizontally. For these reasons, the area enclosed by an iso-density line, as influenced by changing track width, was more complex than the case of changing loads. Generally, a wider track compacted a greater area, but to a lesser degrees or lower density. On the other hand, narrower tracks compacted a smaller area, but to a greater density.

Maximum penetration depth of a specific density level was a function of load, density level and parameter B, which related to load, track width, and density level. Higher loads caused the compacted zone to penetrate deeper for the same track width and

density level; narrower tracks penetrated deeper for the same ballast and density level.

The ratio of the maximum width that the compaction can spread horizontally to the maximum depth that the compaction can penetrate was determined. This ratio defined the geometric characteristics of the "bulb" shape of iso-density lines, and was a function of density level. As density increased, the "bulb" became narrower, and vice versa.

Conclusions

From the laboratory and soil bin experiments and resulting data analysis, the following conclusions were reached:

1. The relationship between density profile in the soil and loading variables could be predicted by modifying Boussinesq's stress distribution equation with two parameters A and B. This relationship adequately described the density profile for areas influenced by loading variables, within the density range encountered in the experiments.

(a) Parameter A varies for different density levels, and is linearly related to density. It determines the maximum horizontal width that an iso-density line can spread.

(b) Parameter B relates to track width, load and density level. The relation is logarithmic. It determines the shape of an iso-density line in soil.

(c) Simulation of density values in soil using the derived model was successful for the seed zone, especially under the controlled conditions of the laboratory experiment. In field experiments, the model did not adequately predict the density distribution, because the data from these experiments were so variable that no clear density distribution pattern existed. Errors may also have been

introduced during transporting samples.

2. Geometric characteristics of an iso-density line were analyzed as a function of load and track width. This analysis is especially important for understanding the compaction prediction in terms of grain drill design and press wheel ballast selection.

(a) The area enclosed by an iso-density line increases as the applied load increases for applicable density ranges. In the case of the same load, narrower wheel tracks cause less low-density compaction, but cause more high-density compaction. In the case of wider tracks, the result is reversed.

(b) The depth of maximum penetration of a specified density level is a function of load, parameter B and the specified density level. Higher loads cause deeper penetration for the same density level. In the case of the same load, wider tracks cause deeper penetration of a low iso-density line, but shallower penetration of high iso-density line than do narrower tracks.

(c) The horizontal compaction width is proportional to the maximum penetration depth, with the ratio a function of the parameter A. Higher loads and wider tracks cause a wider compacted zone. However, the compaction level (density level) that a wider track can cause is less than that of a narrower track with the same load.

3. Moisture content is a factor influencing the compaction in terms of density levels. A correction factor should be used to compensate for the effect. Sinkage of the press wheel is another important factor to be considered, because it influences the contact area between soil surface and press wheel and subsequently influences the actual load (pressure) applied to the soil surface.

4. The gamma ray technique is a good method for evaluating density profiles in

soil samples. However, the soil attenuation coefficient should be calibrated for different system configurations and soil types.

5. The modified Boussinesq's equation adequately predicts the soil compaction around seed zone for the soil bin conditions, after compensating the effect of moisture content. The field compaction data collected in this research are so variable that no clear density pattern can be detected. Thus, modeling the soil compaction of field conditions is impossible.

6. Vertically transporting soil samples can cause changes in soil density profile and thus, should be avoided.

Recommendations for Future Research

The conclusions were based essentially on the laboratory experiment. The loading condition was static in nature and was different from the dynamic loading in grain drills. Therefore, future research should be conducted using real press wheels or equipment which resembles the press wheel with a dynamically applied load.

The density range in this research was basically in the range of 1.2-1.4 g/cm³ which is not very different from some density levels resulting from natural soil consolidation process. The density pattern cannot be easily detected if the results are too variable, or soil samples contain large aggregates. Therefore, future research should be conducted in a soil bin to closely control the experimental material.

The sinkage of the press wheel should be examined closely, for it greatly influences the loading condition and density pattern. The sinkage may be related to load and forward speed. Its effect may also depend on the initial density, or at least the surface density. This may warrant including the initial density values in the model.

Moisture content should be included in future modeling as a factor, not just to be used as a correction factor after a model is completed. Low moisture content tends to increase the soil strength and results in low density compaction, but the relationship may not be linear.

Soil type does not seem to be a major factor in modeling soil strength according to past research, especially compared to the effect of moisture content. Before the previous questions are closely examined, soil type should not be included in modeling to hold the research to a manageable size.

Horizontally transporting soil samples appeared to be better than vertical transport. Vibrating or shaking samples should be avoided, since it will change the sample density profile.

REFERENCES

- Abernathy, G. H. 1967. Soil density modification with furrow openers of simple geometric shape. Ph.D Thesis, Oklahoma State University, Stillwater, OK 74078.
- Ayers, P.D. 1987. Utilizing the torsional shear test to determine soil strength-properties relationships. *Soil and Tillage Research* 10:373-380.
- Ayers, P.D. and H.D. Bowen. 1987. Predicting soil density using cone penetration resistance and moisture profiles. *Transactions of the ASAE* 30(5):1331-1336.
- Ayers, P.D. and H.D. Bowen. 1988. Laboratory investigation of nuclear density gauge operation. *Transactions of the ASAE* 31(3): 658-661.
- Ayers, P.D. and J. Van Riper. 1991. Stress distribution under a uniformly loaded rectangular area in agricultural soils. *Transaction of the ASAE* 34(3):706-710.
- Bailey, A.C. 1986. A model for agricultural soil compaction. *Journal of Agricultural Engineering Research* 33:257-262.
- Bailey, A.C. and C.E. Johnson. 1988. A soil compaction model for cylindrical stress states. ASAE Paper No. 88-1018, ASAE, St. Joseph, MI 49085.
- Bailey, A.C. and G.E. Vanden Berg. 1968. Yielding by compaction and shear in unsaturated soils. *Transactions of the ASAE* 30(5):1231-1236.
- Ball, B.C. and M.F. O'Sullivan. 1982. Soil strength and crop emergence in direct drilled and plowed cereal seedbeds in seven field experiments. *Journal of Soil Science* 33(4):609-622.
- Bertuzzi, P., L. Bruckler, Y. Gabilly and J.C. Gaudu. 1987. Calibration, field-testing, and error analysis of a gamma-ray probe for in-situ measurement of dry bulk density. *Soil Science* 144(6):425-436.
- Blackwell, P.S., J.P. Graham, J.V. Armstrong, M.A. Ward, K.R. Howse, C.J. Dawson, and A.R. Butler. 1986. Compaction of a silt loam soil by agricultural vehicles. I. Effects upon soil conditions. *Soil Tillage Res* 7:97-116.

- Boussinesq, J.V. 1885. Application des potentiels à l'étude de l'équilibre et du mouvement des solides élastiques, Paris, Gauthier-Villars.
- Brown, O.B., M.L. Stone and J.E. Gazin. 1993. Accuracy of gamma ray computerized tomography in porous media. *Water Resources Research*, Vol. 29, No. 2, p. 479-486.
- Brown, O.B., M.L. Stone, J.E. Gazin and S.R. Clinkscales. 1994. Gamma ray tomography measurements of soil density variations in soil cores. *Tomography of Soil-Water-Root Processes*. SSSA Special Publication Number 36, p.87-97.
- Chancellor, W.J. 1976. Compaction of soil by agricultural equipment. Bulletin 1881. Richmond, CA: University of California.
- Chancellor, W.J., R.H. Schmidt and W. Soehne. 1962. Laboratory measurement of soil compaction and plastic flow, *Transaction of the ASAE*, 5:235-239.
- Chaplin, J., M. Lueders and D. Rugg. 1986. A study of compaction and crop yields in loamy sand soil after seven years of reduced tillage. *Transactions of the ASAE* 29(2):389-392.
- Chi, L. and R.L. Kushwaha. 1988a. Three dimensional finite element interaction between soil and tillage tool. ASAE Paper No. 88-1611, ASAE, St. Joseph, MI 49085.
- Chi, L. and R.L. Kushwaha. 1988b. Study of mechanical properties of agricultural soil for non-linear f.e. model. ASAE Paper No. 88-1610, ASAE, St. Joseph, MI 49085.
- Chi, L. and R.L. Kushwaha. 1990. Finite element analysis of soil forces on different tillage tool shapes. ASAE Paper No. 89-1103, ASAE, St. Joseph, MI 49085.
- Chi, L., S. Tessier and C. Laguë. 1993a. Finite element prediction of soil compaction induced by various running gears. *Transaction of the ASAE* 36(3):629-636.
- Chi, L., S. Tessier and C. Laguë. 1993b. Finite element modeling of soil compaction by liquid manure spreaders. *Transaction of the ASAE* 36(3):637-644.
- Chu, Y.N., C.G. Coble and W.R. Jordan. 1991a. Cotton emergence force as affected by soil temperature, moisture, and compression. *Crop Science* 31:405-409.
- Chu, Y.N., C.G. Coble and W.R. Jordan. 1991b. Hypocotyl elongation and swelling of cotton as affected by soil temperature, moisture, and physical impedance. *Crop Science* 31:410-415.
- Craig, R.F. 1983. *Soil Mechanics*, 3rd Ed. Van Nostrand Reinhold Co. Ltd., United Kingdom.

- Ehlers, W., U. Köpke, F. Hesse and W. Böhm. 1983. Penetration resistance and root growth of oats in tilled and untilled loess soil. *Soil & Tillage Research* 3:261-275.
- Ellington, A. 1986. Effects of deep ripping, direct drilling, gypsum and lime on soils, wheat growth and yield. *Soil Tillage Res.* 8:29-49.
- Erbach, D.C., J.E. Morrison Jr. and D.E. Wilkins. 1983. Equipment modification and innovation for conservation tillage. *Journal of Soil Water Conservation* 38(3):182-185.
- Gill, W.R. and G.E. Vanden Berg. 1967. *Soil Dynamics in Tillage and Traction*, Agricultural Handbook No. 316. Agricultural Research Service, United States Department of Agriculture.
- Golden Software, Inc. *Surfer, Version 4 Reference Manual*, © 1989. Golden, Co.
- Goyal, M.R., G.L. Nelson, T.G. Carpenter, L.O. Drew and A.W. Leissa. 1982. Stresses generated in soil curst by emerging dicots. *Transaction of the ASAE* 25(3):556-562.
- Graham, J.P., P.S. Blackwell, J.V. Armstrong, D.G. Christian, K.R. Howse, C.J. Dawson and A.R. Butler. 1986. Compaction of a silt loam by wheeled agricultural vehicles. II. Effects on growth and yield of direct-drilled winter wheat. *Soil Tillage Res.* 7:189-203.
- Grisso, R.D., C.E. Johnson and A.C. Bailey. 1987. Soil compaction by continuous deviatoric stress. *Transactions of the ASAE* 30(5):1293-1301.
- Gupta, C.P. and R. Visvanathan. 1993. Dynamic behavior of saturated soil under impact loading. *Transaction of the ASAE* 36(4):1001-1007.
- Hamblin, A.P., D. Tennant and H. Cochrane. 1982. Tillage and the growth of a wheat crop in a loamy sand. *Aust. J. Agric. Res.* 33(6):887-897.
- Hanson, T.L., H.P. Johnson and D.F. Young. 1967. Dynamic shearing resistance of soils. *Transaction of the ASAE* 10(4):439-443.
- Hoag, D. L. and R. R. Yoerger. 1974. Designing load rings for measurement. *Transactions of the ASAE.* 17(2):251-253,261.
- Holtz, R.D. and W.D. Kovacs. 1981. *An Introduction to Geotechnical Engineering*. Prentice-Hall, Inc. Englewood Cliffs, NJ:
- Johnson, C.E. and E.C. Burt. 1986. A method of predicting soil stress state under tires. ASAE Paper No. 86-1059. St. Joseph, MI: ASAE.

- Johnson, C.E. and E.C. Burt. 1990. A method of predicting soil stress state under tires. Transaction of the ASAE 33(3):713-717.
- Johnson, C.E., D.W. Wright and A.C. Bailey. 1982. Compaction characteristics of some soil mixtures. ASAE Paper No. 82-1543, ASAE, St. Joseph, MI 49085.
- Jumikis, A.R. 1984. Soil Mechanics, Robert E. Krieger Pub. Co., Inc., Malabar, Florida. p. 326-336
- Koolen, A.J. and H. Kuipers. 1983. Agricultural Soil Mechanics, Advanced Series in Agricultural Sciences 13. Springer-Verlag, New York, N.Y.
- Korcher, M.F. and J.D. Summers. 1988. Wave propagation theory for evaluating dynamic soil stress-strain models. Transactions of the ASAE 31(3):683-691.
- Luo, X. and L.G. Wells. 1992. Evaluation of gamma ray attenuation for measuring soil bulk density: Part 1. Laboratory investigation. Transaction of the ASAE 35(1):17-32.
- Larson, W.E. and R.R. Allmaras. 1971. Chapter 8. Management factors and natural forces as related to compaction. In Compaction of Agricultural Soils, p.406-407. American Society of Agricultural Engineers, St. Joseph, Michigan.
- MathSoft, Inc., MathCad, Version 3.1, © 1986-1992. Cambridge, MA.
- Morrison, J.E. Jr. 1989. Factors affecting plant establishment with a no-tillage planter opener. Applied Engineering in Agriculture 5(3):316-318.
- Nassehzadeh-Tabrizi, A. and L.S. Willardson. 1981. Effects of vibration and soil moisture on the draft of a model mole plow. Transaction of ASAE 24(6):1490-1495.
- Ohu, J.O., G.S.V. Rahgavan, E. McKyes, K.A. Stewart and M.A. Fanous. 1985. The effects of soil compaction and organic matter on the growth of bush beans. Transactions of the ASAE 28(4):1056-1061.
- Perumpral, J.V. 1983. Cone penetrometer application - a review. ASAE Paper No. 83-1549, ASAE, St. Joseph, MI 49085.
- Pollock, D. Jr, J.V. Perumpral and T. Kuppusamy. 1986. Finite element analysis of multipass effects of vehicles on soil compaction. Transactions of the ASAE 29(1):45-50.
- Press, W.H., S.A. Teukolsky, W.T. Vetterling and B.P. Flannery. 1992. Numerical Recipes in C, the Art of Scientific Computing, 2nd Edition. Cambridge University Press. p.362-367.

- Schafer, R.L., A.C. Bailey, C.E. Johnson and R.L. Raper. 1991. A rationale for modeling soil compaction behavior: an engineering mechanics approach. *Transaction of the ASAE* 34(4):1609-1617.
- Scholefiel, D., P. M. Patto and D.M. Hall. 1985. Laboratory research on the compressibility of four topsoils from grassland. *Soil Tillage Res.* 6:1-16.
- Soehne, W. 1958. Fundamentals of pressure distribution and soil compaction under tractor tires. *Agricultural Engineering* 39:276-281, 190.
- Taylor, H.M. 1971. Effects of soil strength on seedling emergence, root growth and crop yield. Contribution from the Soil and Water Conservation Res. Division, ARS, USDA, in Cooperation with the Alabama Agricultural Experiments Station, Auburn University, Auburn, Alabama.
- Taylor, H.M. and H.R. Gardener. 1963. Penetration of cotton seedling taproots as influenced by bulk density, moisture content, and strength of soil. *Soil Science* 96(3):153-156.
- Taylor, H.M. and R.R. Bruce. 1968. Effects of soil strength on root growth and crop yield in the southern United States. *Ninth International Congress of Soil Science* 1:803-811.
- Van Bavel, C.H.M., N. Underwood and S.R. Ragar. 1957. Transmission of gamma radiation by soil and soil densitometry. *Soil Sci. Soc. Am. Proc.* 21:588-591.
- ✓ Voorhees, W.B., D.A. Farrell and W.E. Larson. 1975. Soil strength and aeration effects on root elongation. *Soil Sci. Soc. Amer. Proc.* 39(5) 948-953.
- Whiteley, G.M. and A.R. Dexter. 1982. Root development and growth of oilseed, wheat and pea crops on tilled and non-tilled soil. *Soil & Tillage Research* 2:379-393.
- Wolf, D. and A. Hadas. 1984. Soil compaction effects on cotton emergence. *Transaction of the ASAE* 27(3):655-659.
- Young, S.C, C.E. Johnson and R.L, Schafer. 1988. Quantifying soil physical condition for tillage control applications. *Transactions of the ASAE* 31(3):662-667.

APPENDIX A
PROGRAMS FOR DATA ACQUISITION AND PROCESSING

APPENDIX A-1

Program for Measuring Forces on Press Wheel and Coultter

```
{ *****
This program has been written to read inputs from drill force
sensors and speed sensor.
***** }
```

```
Program Drill(input,output,file1);
Uses Dos;           { FOR DOS INTERFACE }
{$I PCIHEAD.PAS}   { DEFINE THE PCI-20026S-3 ENTITIES. }
{$I P26.PAS}
```

```
Var
  file1                : Text;
  filename, filename1 : string;
  FS                   : PathStr;
  Segmt                : word;
  i, j, Vect, Gain, ZChn, Range, CTChn, RGChn, Ovf,
  DCT, RCT, num        : Integer;
  Adata :array[1..4,1..1024] of integer;
  Adata0 :array[1..4,1..50] of integer;
  Chn :array[1..4] of integer;
  Freq1, Freq2         : Real;
  choice, done         : Char;
```

```
{** Define a general purpose error processing routine. **}
```

```
Procedure ErrorRoutine(ErrorString : String);
```

```
Var
  ErrorCode : Integer ;
Begin { ErrorRoutine }
  ErrorCode := ErrSys ;
  If ErrorCode < > 0 Then
  Begin
    WriteLn(ErrorString, ' ',ErrorCode);
    Halt;
  End ; { If ErrorCode < > 0 Then }
End ; { ErrorRoutine }
```

```
{
*****
Define the main program
*****
}
```

```

Begin { Sample05 }

{
* Setup the PCI-20026S-3 dispatch vector.
}
Vect := $61 ;
SetVec (Vect) ;

{ *****
Initialize the PCI-20026S-3 system. This call must be made
prior to calling any other PCI-20026S-3 instruction.
*****}
SysInit ;

{*****
Segmt, defined below, contains the base address of the PCI-20041C-3.
Init(segmt) must be called once for each carrier or board in the system,
each with its own address.
*****}
Segmt := $CD00 ;
Init (Segmt) ;

{*****
Check for a system error. During debug, call ErrSys often, possibly after
every call to the PCI-20026S-3. It is a good idea to leave a few ErrSys
calls in a finished program to monitor the status of the system.
*****}
ErrorRoutine ('ERROR FOUND DURING Init') ;

{*****
Configure analog input channel 0 to a gain of 10 with no auto zero
channel. Configure the frequency channel also.
*****}
Gain := 10 ;
ZChn := -1 ;
Range := 5 ;
num := 1024;
Chn[1] := 2; Chn[2]:=5; Chn[3]:=4; Chn[4]:=3;
RCT := 1000;
CTChn := 0;
RGChn := 0;
{
***** Collecting Data *****
}
choice := 'y'; { Choice=y means continue to collect data }
while ((choice = 'y') or (choice = 'Y')) do
begin

```

```

{
***** set up file name etc *****
}
done := 'n'; { done = n means filename not set yet }
while ((done = 'n') or (done = 'N')) do
begin
  writeln;
  writeln;
  write('Plot Number? > ');
  readln(filename1);
  filename := filename1 + '.dat';
  assign(file1, filename);
  FS := FSearch(filename, GetEnv('PATH'));
  if (FS = '') then { new filename input}
  begin
    rewrite(file1);
    done := 'y';
  end
  else { filename existed already}
  begin
    writeln(filename, ' Already Existed');
    writeln('R: Replace');
    writeln('C: Cancel');
    write('Choice An Option > ');
    readln(choice);
    if ((choice = 'R') or (choice = 'r')) then begin
      rewrite(file1);
      done := 'y';
    end
    else begin
      done := 'n';
    end;
  end;
end;
end;
{
***** Finish setting up file name *****
}

{
***** Zero Readings *****
}
write('Press [S] to Collect Zero Readings > ');
done := ' ';
while not ((done = 's') or (done = 'S')) do begin
  readln(done);
end;

```

```

for i:=1 to 50 do begin
  for j:=1 to 4 do begin
    CnfAI (Chn[j], Gain, ZChn, Range) ;
    Adata0[j,i] := ReadCh (_AI, Chn[j]) ;
  end;
end;

{
***** Collecting *****
}
writeln;
write('Press [S] to Start Collecting > ');
done := ' ';
while not ((done = 's') or (done = 'S')) do begin
  readln(done);
end;

writeln(' Collecting ...');
{
***** Measuring 1st Speed *****
}
writeln('...begin...');
Ovf := ReadFrq(CTChn, RGChn, RCT, DCT);
Freq1 := DCT*1000.0/RCT;

{
***** Measure Coulter V. & H. *****
}
for i:=1 to num do begin
  for j:=1 to 2 do begin
    CnfAI (Chn[j], Gain, ZChn, Range) ;
    Adata[j,i] := ReadCh (_AI, Chn[j]) ;
  end;
end;

{
***** Measure Press Wheel V. & H. *****
}
for i:=1 to num do begin
  for j:=3 to 4 do begin
    CnfAI (Chn[j], Gain, ZChn, Range) ;
    Adata[j,i] := ReadCh (_AI, Chn[j]) ;
  end;
end;

{***** Measuring 2nd Speed *****}

```

```

Ovf := ReadFrq(CTChn, RGChn, RCT, DCT);
Freq2 := DCT*1000.0/RCT;

writeln('..end..');
{
***** Storing the results *****
}

writeln(' ... Storing {', filename, '} ...');
writeln(file1, "FILENAME="',',',', filename, "'");
writeln(file1);
writeln(file1, "Freq1 =",',',', Freq1:6:1,',',', "Freq2 =",',',', Freq2:6:1);
writeln(file1);
writeln(file1, "***** Zero Reading *****");
for i:= 1 to 50 do begin
  for j:= 1 to 4 do begin
    write(file1, Adata0[j,i], ',');
  end;
  writeln(file1);
end;

writeln(file1);
writeln(file1, "***** DATA Reading *****");
for i:= 1 to num do begin
  for j:= 1 to 4 do begin
    write(file1, Adata[j,i], ',');
  end;
  writeln(file1);
end;
close(file1);

{
***** Continue Collecting ? *****
}
choice := 'n';
write(' Continue ... ? (y,n) > ');
readln(choice);
if ((choice = 'y') or (choice = 'Y')) then
begin { check disk space }
  if (DiskFree(0) < 20000) then begin
    writeln(' disk space is full');
    choice := 'n';
  end;
end;

end; {end of collecting data}
End.

```


APPENDIX A-2

Program for Constructing Density Profile from Scanning Data

```

{
*****
This program is to read input data from original scanner readings and
change them into a file of data readable by surfer program. The output
file contains x, y and data. Values of y are negative, and data are soil
density assumed the soil (mu) is 0.0752, Water (mu) is 0.0831 and
moisture content is 10%. Those parameters are to be modified later.
Max is the maximum I number in the first five rows which is used as
the reference number.
*****
}

Program convert(input,output,file1,file2);

Var
  file1,file2           : Text;
  filein, fileout,fintemp : string;
  i, plane, row, f1, f2, f3 : integer;
  MAX,temp             : real;
  data                 : array[1..31] of real;
  choice, done         : char;

{
*****
Main program begins
*****
}

BEGIN {begin main program}
{
*****
Set file names
*****
}
choice:='y';
while ((choice = 'y') or (choice = 'Y')) do begin
  writeln('input file name?');
  readln(filein);
{
for f1:=1 to 3 do begin
for f2:=1 to 6 do begin
for f3:=1 to 2 do begin

```

```

filein:= chr(f1+48)+chr(f2+48)+chr(f3+48);
}
fileout:= 'c:\li\surdata3\' + filein + '.dat';
assign(file2, fileout);
rewrite(file2);
writeln;

for plane:=1 to 49 do begin
  i:=plane;
  if i < 10 then
    fintemp:=filein+chr(i+48)+' .tst'
  else
    fintemp:=filein+chr((i div 10)+48)+chr(i mod 10 +48)+' .tst';

  assign(file1,fintemp);
  reset(file1);
  writeln('converting file: ',fintemp);

  MAX:=0;
  for row:=1 to 30 do begin
    readln(file1,data[row]);
    if((data[row] > MAX) and (row < 6)) then
      MAX := data[row];
  end;
  close(file1);

{
*****
writing the calculated soil density data into new file
*****
}
for row:=1 to 30 do begin
  temp:= -ln(data[row]/MAX)/7.6/(0.0752+0.0831*0.1);
  writeln(file2, (5*(plane-1)-120):3, ' ', -5*(row-1):4, ' ', temp:6:3);
end;
end; {end of for plane:=1 to 49}
close(file2);

writeln('Continue converting another file (y/n)?');
readln(choice);
end; {end of while}
{
end;
end;
end;
}
END.

```

APPENDIX A-3

Program for Simulating Density in Soil Samples

```

/*
*****
* Program "regres.c" is to simulate zone density data. The interested
* zone is defined by x_length and y_length. The density was calculated
* by density formula which is the function of two parameters A and B.
* A is related to density and B is related to track width, load and density.
* These two parameters are defined by constant from regression analysis
* of data of this test. The boundary file data was used to determine the
* lowest point on soil surface, i.e., the load applied point. The property
* file, containing data of undisturbed limits of soil sample, the weights
* and wheel width for each sample and other property. The final errors
* in total area and three different zones are calculated and both in net
* errors and absolute errors.
*****
*/

#include < alloc.h >
#include < conio.h >
#include < dos.h >
#include < math.h >
#include < mem.h >
#include < stdio.h >
#include < stdlib.h >
#include < string.h >

#define UP_LIMIT 0 // limits of row and columns of sample
#define DOWN_LIMIT 31
#define RIGHT_LIMIT 49
#define LEFT_LIMIT 0
#define RECORDS RIGHT_LIMIT
#define X_LENGTH 200 // Zone1, the area of interest in mm
#define Y_LENGTH 85
#define a0 3.7228 // parameter A's components
#define a1 (-2.04386)
#define b0 1.6245 // parameter B's components
#define b1 1.723974
#define b2 0.166978
#define b3 (-12.9968)
#define yoff0 3.2052553 // parameter Yoffset's components
#define yoff1 0.00040086
#define MAXIT 1000 //max iterations using N-R method
#define ACCURACY 0.0001 //accuracy for N-R to stop

```

```

#define LBOUND 0.25    //Low and High bounds for N-R to search
#define HBOUND 2.5
#define LZONE2 60      //define limits for zone 2-4
#define LZONE3 30
#define LZONE4 25
#define LZONE4_DOWN 25

typedef struct {        // structure for surface boundary file
    int x,y;
    float density;
} boundary_line;

boundary_line b_line_point[RECORDS];

FILE *fin_d, *fin_b, *fout_d, *fout_err, *f_property;
int x0, y0;           // applied point
float force, width, xl0,xl1,xr0,xr1;
float x_coor,y_coor,cal_den;
float cohesion, adhesion;
float density[RIGHT_LIMIT][DOWN_LIMIT];
char fin_den[30], fout_data[30], tfname[5], prefix_in[30], prefix_out[30], fin_bln[30];

void find_furrow(void);
void funcd (float, float *, float *);
void open_file(void);
void read_data(void);
void read_property(void);
float rtsafe(void(*funcd)(float, float *, float *), float, float,float);
void write_zone(void);

void main()
{
    char i,j, f1, f2, f3, option="";

    strcpy(prefix_in, "2mth"); // prefix of density input file name
    strcpy(prefix_out,"regr4"); // prefix of output file name

    /* open file of property data */
    f_property = fopen("property.dat","r");
    if(!f_property) {
        printf("can't open property file\n");
        exit(1);
    }

    /* open file for storing error */
    fout_err = fopen("regr4err.dat","w");
    if(!fout_err) {

```

```

printf("can't open error file\n");
exit(1);
}

/* print out title line to error file */
fprintf(fout_err,"Sample T_net_Err T_abs_Err Z1_net_Err Z1_abs_Err
Z2_net_Err Z2_abs_Err Z3_net_Err Z3_abs_Err\n");

/* determine to handle all files or individual file */

while (!(option=='a' || option=='A' || option=='s' || option=='S')){
  clrscr();
  printf("Calculate for all or single file?(a/s)\n");
  scanf("%c",&option);
}

if (option == 'a' || option == 'A'){ /* all files */
  for (f1=1;f1<2;f1++){
    for (f2=1;f2<7;f2++){
      for (f3=1;f3<3;f3++){
        tfname[0]=f1+48;
        tfname[1]=f2+48;
        tfname[2]=f3+48;
        tfname[3]='\0';
        printf("working on file %s\n",tfname);

        open_file();
        read_data();
        read_property();
        find_furrow();
        write_zone();

        fclose(fin_d);
        fclose(fin_b);
        fclose(fout_d);
      }
    }
  }
}
else { /* handling single file */
  option = 'y';
  while(option == 'y' || option == 'Y') {
    printf("which soil sample to calculate?\n");
    scanf("%s",tfname);

    open_file();
    read_data();

```

```

    read_property();
    find_furrow();
    write_zone();

    fclose(fin_d);
    fclose(fin_b);
    fclose(fout_d);
    printf("Do another file (y/n)?\n");
    scanf("%s",&option);
}
}
fclose(f_property);
fclose(fout_err);
}

/* find out the lowest point along the boundary file */

void find_furrow()
{
    int i,j,tempi,temp_fx,temp_delta, dx,dy;

    x0 = -120;
    y0 = 0;
    tempi=RECORDS/2;

    for (i=0;i<RECORDS;i++) {
        dx=b_line_point[i].x;
        dy=b_line_point[i].y;
        if (dy < y0 && dx >= -50 && dx <= 50) {
            y0 = dy;
            tempi = i;
        }
    }

    /* find the center of x with same y values */
    temp_fx=tempi;
    while (y0 == b_line_point[tempi+1].y)
        tempi++;
    temp_delta=tempi-temp_fx;
    if((temp_delta % 2) == 0)
        x0=b_line_point[temp_fx+temp_delta/2].x;
    else {
        x0=(b_line_point[temp_fx+temp_delta/2].x+
            b_line_point[temp_fx+temp_delta/2+1].x)/2.0;
    }
}
}

```

```

/*
  Calculate the regressed density values for given track width, force and
  coordinates x and y. Because parameters A and B are related to density,
  the calculation must be in iteration steps.
  The given force is in kPa and y_offset are in mm.
*/

void funcd(float den, float *fn, float *df)
{
  double y_offset,temp, b_temp;
  double a, b, da, db, x_coor1, y_coor1;

  y_offset = yoff0+yoff1*pow(width, 2.5);

  x_coor1 = x_coor;
  y_coor1 = y_coor-y_offset;

  a = a0+a1*den;

  b_temp = exp(b0)*pow(width,b1)*pow(force,b2);
  b = b_temp*pow(den,b3);
  da = a1;
  db = b_temp*b3*pow(den, b3-1.0);

  temp = 1+pow(x_coor1/a/y_coor1,2.0);

  *fn = den-b*force/pow(y_coor1,2.0)/pow(temp,2.5);
  *df = 1-db*force/pow(y_coor1,2.0)/pow(temp,2.5)-5.0*da*b*force*
      pow(x_coor1,2.0)/pow(a,3.0)/pow(y_coor1,4.0)/pow(temp,3.5);
}

/*
  open the soil density and sample boundary files
*/

void open_file(void)
{
  strcpy(fin_den,prefix_in);    // open density file
  strcat(fin_den,tfname);
  strcat(fin_den, ".dat");

  fin_d = fopen(fin_den,"r");
  if(!fin_d) {
    printf("can't open infile %s err = %d\n",fin_den, ferror(fin_d));
    exit(1);
  }
}

```

```

strcpy(fin_bln,tfname);    /* open boundary file */
strcat(fin_bln,".bln");

fin_b = fopen(fin_bln,"r");
if(!fin_b)
{
    printf("can't open infile %s err = %d\n",fin_bln, ferror(fin_b));
    exit(1);
}

/* open output data file */
strcpy(fout_data,prefix_out);    // open density file
strcat(fout_data,tfname);
strcat(fout_data,".dat");

fout_d = fopen(fout_data,"w");
if(!fout_d) {
    printf("can't open output file %s\n", fout_data);
    exit(1);
}
}

/*
read in the data of density file
*/

void read_data(void)
{
    int i,j, dx, dy, feer;
    float dd;
    char dummy[81];

    /* read the data of boundary file */

    for (i=0;i<RECORDS;i++) {
        feer=fscanf(fin_b, "%d %d %f",&dx, &dy, &dd);
        if(feer == -1){
            printf("reading error when read boundary file\n");
            exit(1);
        }
        b_line_point[i].x=dx;
        b_line_point[i].y=dy;
        b_line_point[i].density=dd;
        iffeof(fin_b) {
            printf("end of file, in reading boundary file\n");
            exit(1);
        }
    }
}

```



```

}

/* read the data of density file */

for (i=0;i<RECORDS;i++)
  for (j=0;j<DOWN_LIMIT;j++) {
    feer=fscanf(fin_d, "%d %d %f", &dx, &dy, &dd);
    if(feer == -1){
      printf("reading error when read density file\n");
      exit(1);
    }
    density[i][j]=dd;
  }
}

/*
  Read property data for each sample from the property data file.
  The property data file contains data for all samples.
*/

void read_property(void)
{
  char temp[80], file_str[10];

  /* read in the 4 limits of undisturbed part */
  do {
    if(fgets(temp, 80, f_property) == NULL){
      printf("can not find property data for\n");
      exit (0);
    };
    sscanf(temp, "%s %d %d %d %d %f %f %f %f",
      file_str,&x10,&x11,&xr0,&xr1,&force,&width,&cohesion,&adhesion);
  } while (strcmp(file_str,tfname));
  rewind(f_property);
}

/*
  Using combination of Newton-Raphson and bisection, find the root
  of a function bracketed between x1 and x2. The root, return as
  the function value rtsafe, will be refined until its accuracy
  is know within +-xacc. funcd is a user-supplied routine that returns
  both the function value and the first derivative of the function.
*/

float rtsafe(void (*funcd)(float, float *, float *), float x1, float x2,float xacc) {
  int j;
  float df, dx, dxold, f,fh,fl;

```

```

float temp,xh,xl,rts;

(*funcd)(x1,&fl,&df);
(*funcd)(x2,&fh,&df);
if ((fl>0.0 && fh>0.0) || (fl<0.0 && fh<0.0)) {
    printf("Root must be bracketed in rtsafe\n");
    exit(1);
}
if (fl == 0.0) return x1;
if (fh == 0.0) return x2;

if (fl < 0.0) { // Orient the search so that f(x1)<0 .
    xl=x1;
    xh=x2;
}
else {
    xh=x1;
    xl=x2;
}

rts=0.5*(x1+x2); // Initialize the guess for root,
dxold=fabs(x2-x1); // the step size before last,
dx=dxold; // and the last step.

(*funcd)(rts,&f,&df);

for (j=1; j<=MAXIT; j++) { // Loop over allowed iterations

    if (((rts-xh)*df-f)*((rts-xl)*df-f) >= 0.0) // Bisection if Newton out of range
        || (fabs(2.0*f) > fabs(dxold*df)) { // or not decreasing fast enough
        dxold=dx;
        dx=0.5*(xh-xl);
        rts=xl+dx;
        if (xl == rts) return rts; // Change in root is negligible.
    } // Newton step acceptable. Take it.
    else {
        dxold=dx;
        dx=f/df;
        temp=rts;
        rts -= dx;
        if (temp == rts) return rts;
    }
}

if (fabs(dx) < xacc) return rts; // Convergence criterion met

(*funcd)(rts,&f,&df); //One new function evaluation per iter.

```

```

    if (f<0.0) // Maintain the bracket on the root
        xl=rts;
    else
        xh=rts;
}
printf("Maximum number of iterations exceeded in rtsafe\n");
return 999.9;
}

/*
    Simulate density values and write the x, y, obs_den, cal_den and
    error into files for the interested zone areas
*/

void write_zone(void)
{
    int i,j, ii, jj, total_count, zone2_count, zone3_count, zone4_count;
    float error, total_net_err, total_abs_err, zone2_net_err, zone2_abs_err;
    float zone3_net_err, zone3_abs_err, zone4_net_err, zone4_abs_err;

    total_count=0;
    zone2_count=0;
    zone3_count=0;
    zone4_count=0;
    total_net_err=0.0;
    total_abs_err=0.0;
    zone2_net_err=0.0;
    zone2_abs_err=0.0;
    zone3_net_err=0.0;
    zone3_abs_err=0.0;
    zone4_net_err=0.0;
    zone4_abs_err=0.0;

    for (j=(-y0)/5;j<((-y0)/5+Y_LENGTH/5)&&j<DOWN_LIMIT;j++){
        y_coor=-5*j-y0;

        for (i=(x0-X_LENGTH/2+120)/5;i<=(x0+X_LENGTH/2+120)/5;i++){
            x_coor=((float)i-RIGHT_LIMIT/2.0)*5.0-x0;

            /* Call rtsafe to simulate density for point (x_coor, y_coor)*/
            cal_den = rtsafe(funcd, LBOUND, HBOUND, ACCURACY);

            error=(density[i][j]-cal_den)/density[i][j]*100;

            fprintf(fout_d,"%7.11f %7.11f %7.31f %7.31f %7.21f\n",
                x_coor,y_coor, cal_den, density[i][j], error);

```

```

total_net_err += error;
total_abs_err += fabs(error);
total_count ++;

/* Calculate errors for zone 2 */
if ((fabs(x_coor) < LZONE2/2.0+0.1)&&(fabs(y_coor) < LZONE2+0.1)){
    zone2_net_err += error;
    zone2_abs_err += fabs(error);
    zone2_count ++;
}

/* Calculate errors for zone 3 */
if ((fabs(x_coor) < LZONE3/2.0+0.1)&&(fabs(y_coor) < LZONE3+0.1)){
    zone3_net_err += error;
    zone3_abs_err += fabs(error);
    zone3_count ++;
}

/* Calculate errors for zone 4 */
if ((fabs(x_coor) < LZONE4/2.0+0.1)&&(fabs(y_coor) > LZONE4-0.1)&&
    (fabs(y_coor) < LZONE4+LZONE4_DOWN+0.1)){
    zone4_net_err += error;
    zone4_abs_err += fabs(error);
    zone4_count ++;
}
}
}

total_net_err /= total_count;
total_abs_err /= total_count;
zone2_net_err /= zone2_count;
zone2_abs_err /= zone2_count;
zone3_net_err /= zone3_count;
zone3_abs_err /= zone3_count;
zone4_net_err /= zone4_count;
zone4_abs_err /= zone4_count;

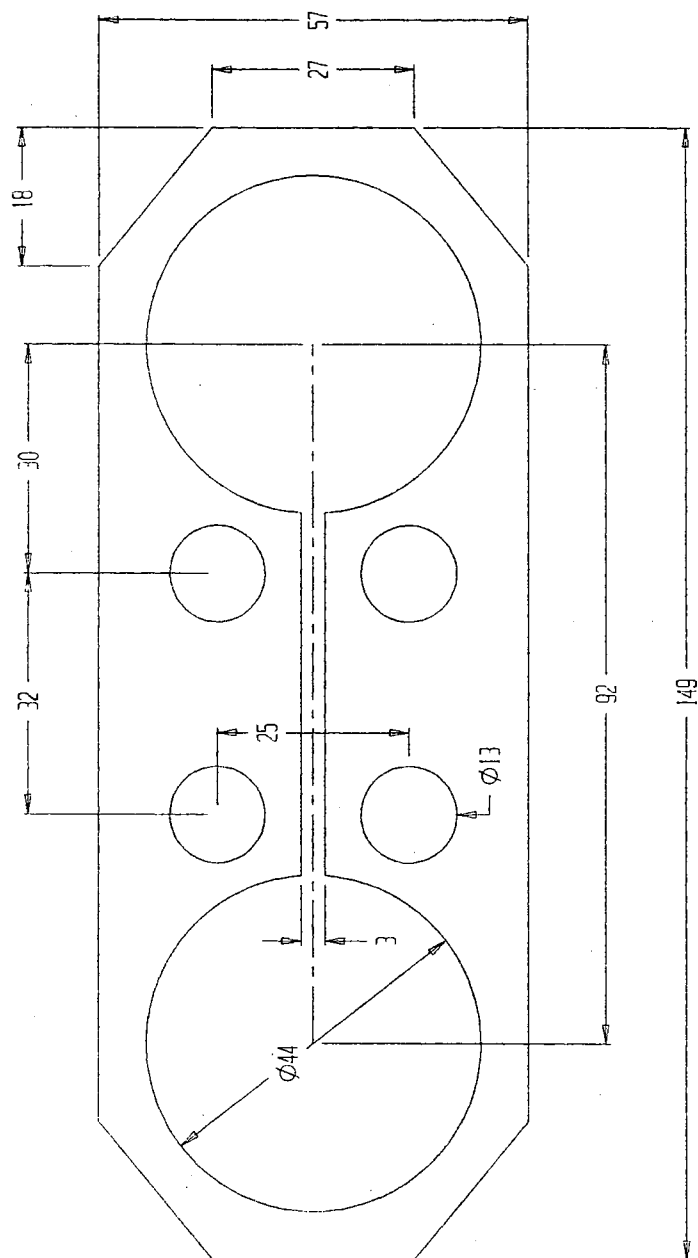
fprintf(fout_err, "%s %8.3f %8.3f %8.3f %8.3f %8.3f %8.3f %8.3f %8.3f\n",
    tfname, total_net_err, total_abs_err, zone2_net_err, zone2_abs_err,
    zone3_net_err, zone3_abs_err, zone4_net_err, zone4_abs_err);
}

```

APPENDIX B
DESIGN DRAWINGS FOR FORCE TRANSDUCER,
CALIBRATION BRACKETS

APPENDIX B-1

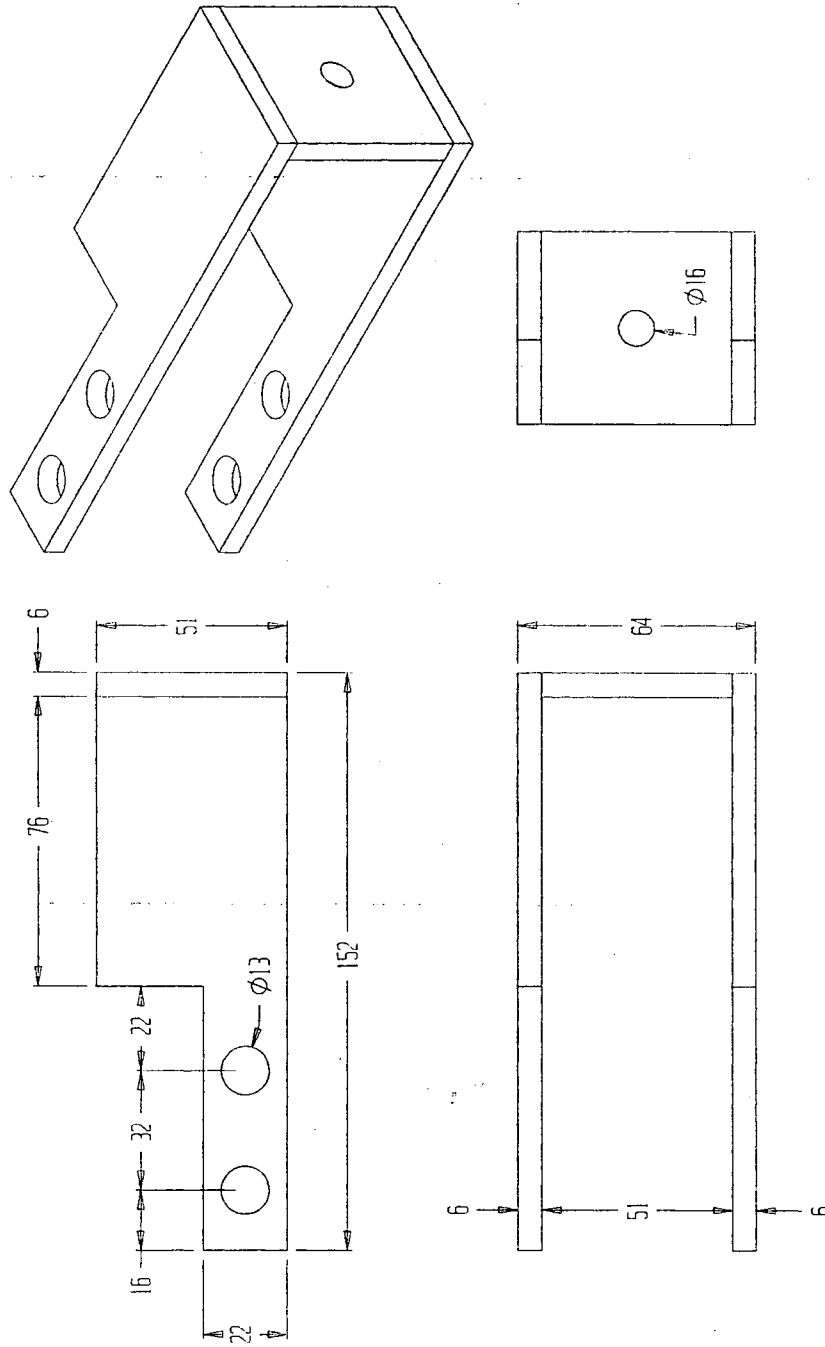
Design Drawing of Extended Circular Ring Loadcell



Note: Machine three pieces 38 mm thick
All dimensions are in millimeters
Use aluminum

APPENDIX B-2

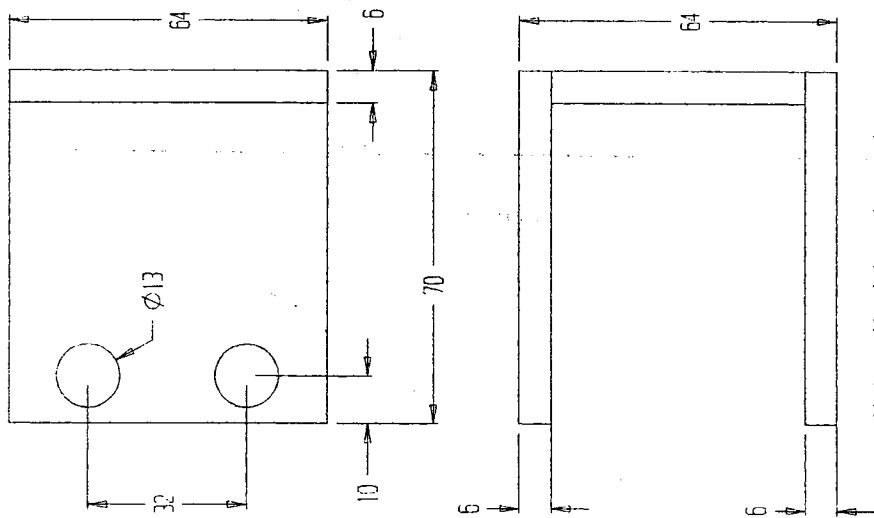
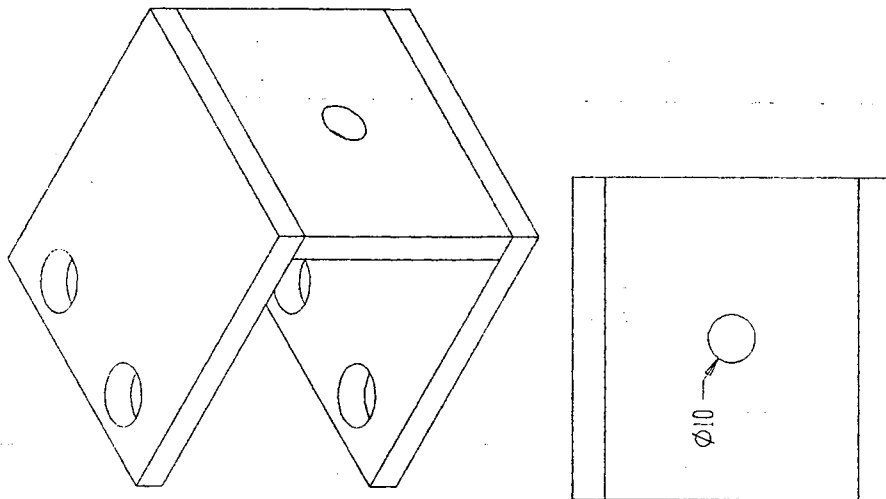
Design Drawing of Loadcell Calibration Bracket for Horizontal Force



Note: Make two pieces
All dimensions are in millimeters

APPENDIX B-3

Design Drawing of Loadcell Calibration Bracket for Vertical Force



Note: Machine two pieces
All dimensions are in millimeters

APPENDIX B-4

Calibration of Loadcells

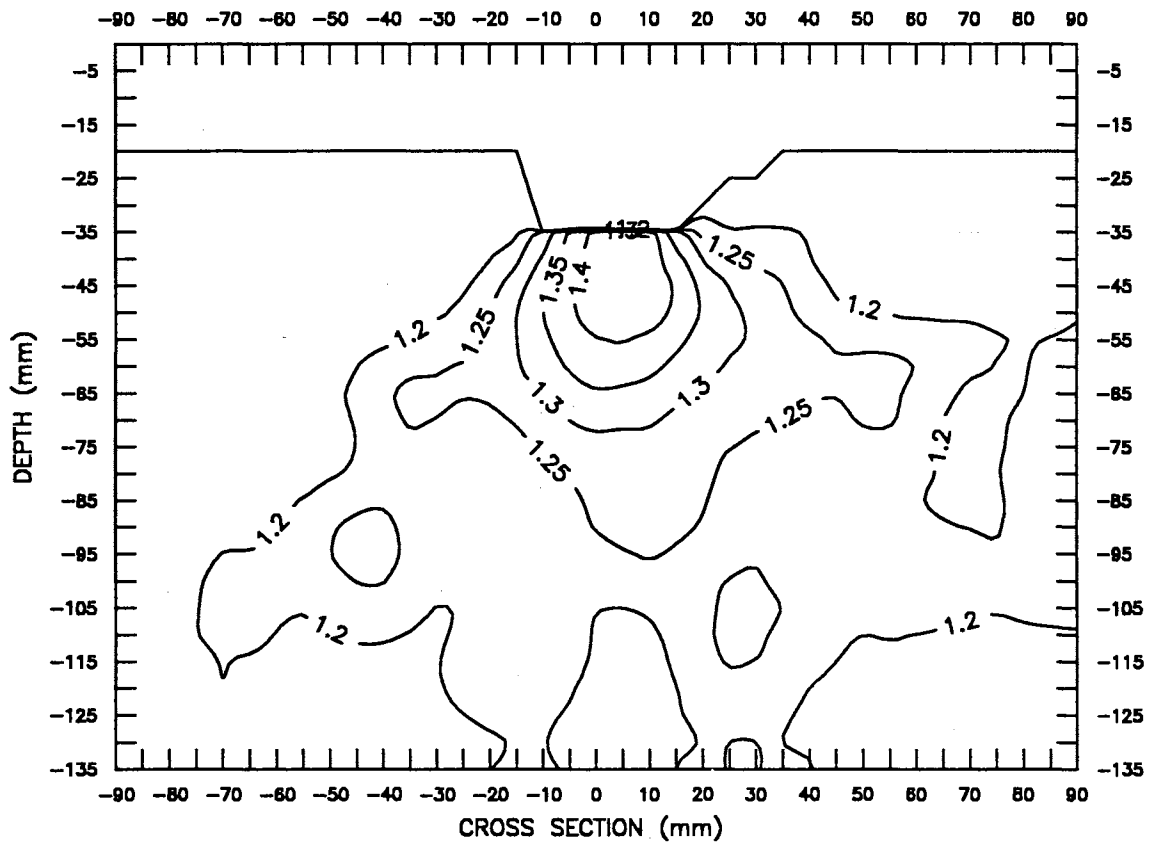
Load (Newton)	A/D Readings			
	WV	WH	CV	CH
0	1751	2048	116	2203
22	1786	2373	143	2238
44	1821	2338	170	2271
67	1856	2303	197	2306
89	1890	2268	225	2340
111	1927	2233	251	2374
133	1961	2198	278	2408
155	1997	2163	304	2442
177	2032	2129	332	2477
199	2065	2094	359	2511

APPENDIX C

**CONTOUR MAPS OF ORIGINAL DENSITY PROFILES OF LABORATORY
EXPERIMENT SAMPLES**

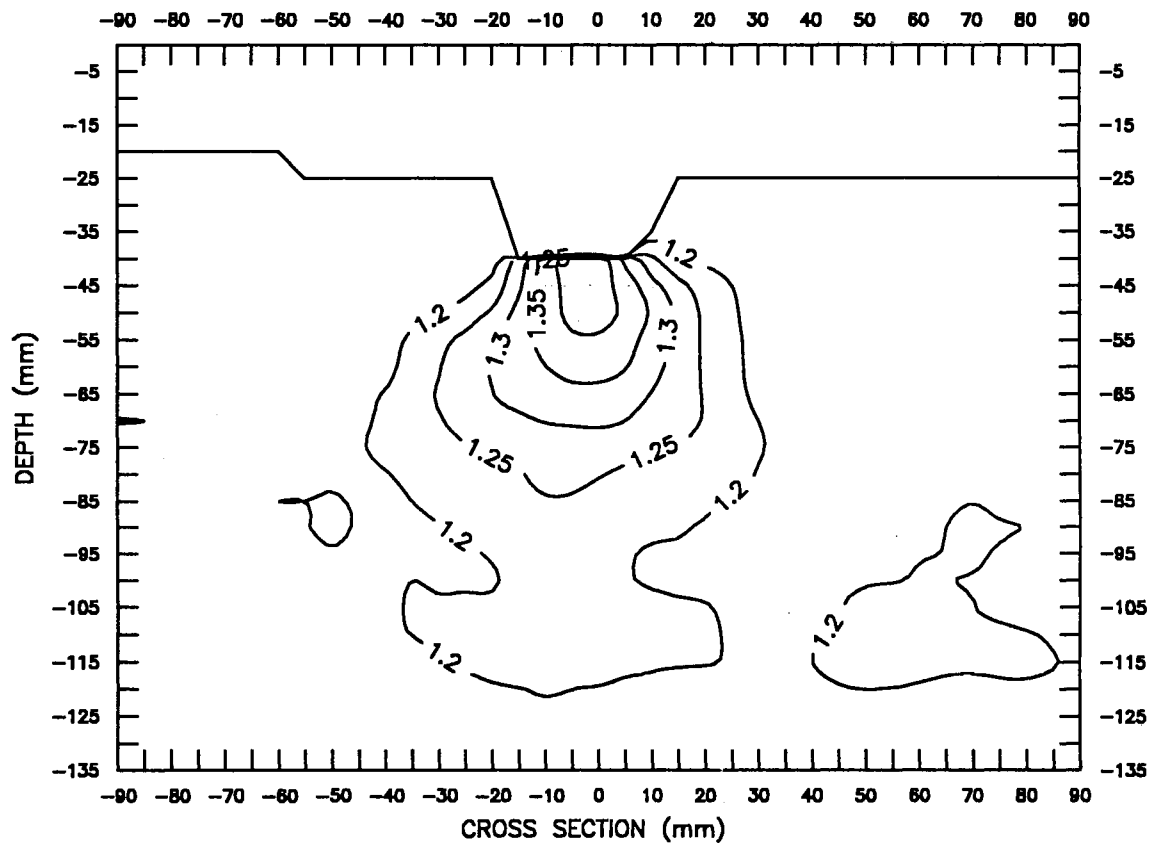
APPENDIX C-1

Contour Map of Laboratory Experiment Sample 111
with 25 mm Track and 5 kg Ballast



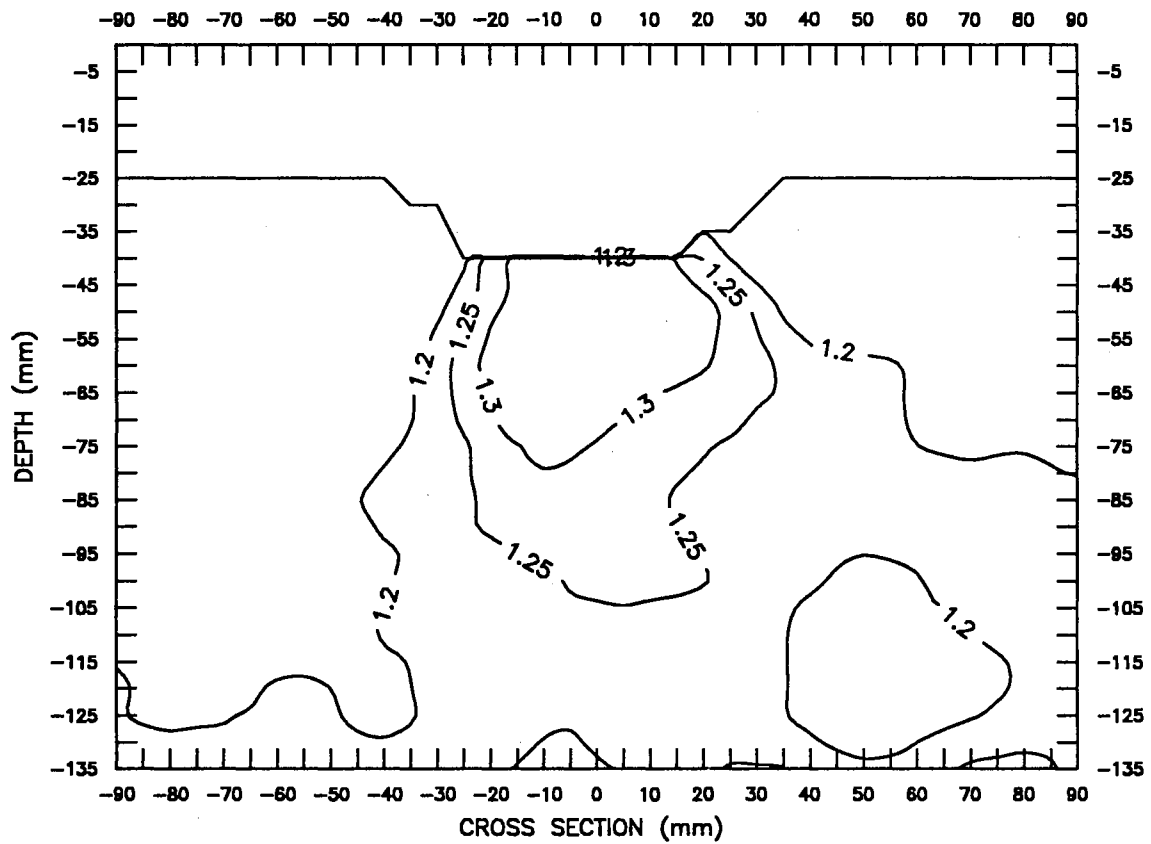
APPENDIX C-2

Contour Map of Laboratory Experiment Sample 112
with 25 mm Track and 5 kg Ballast

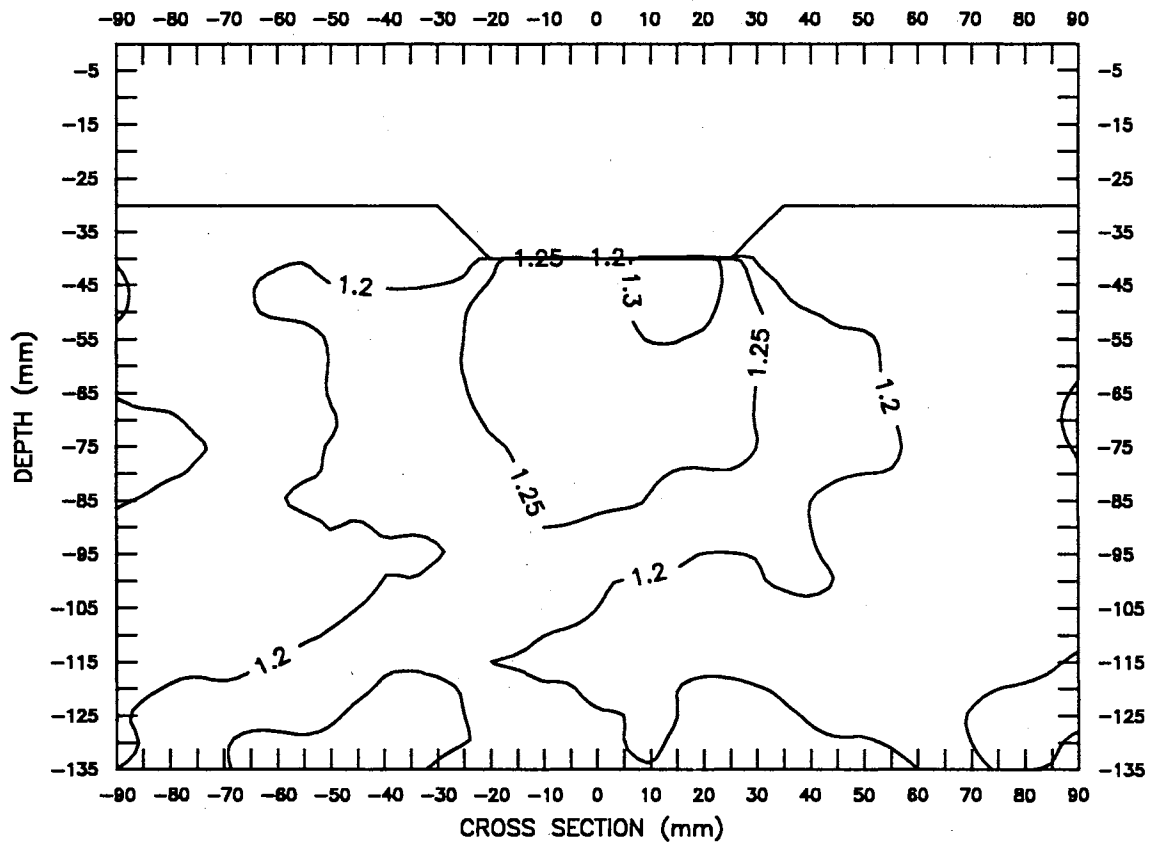


APPENDIX C-3

Contour Map of Laboratory Experiment Sample 121
with 51 mm Track and 5 kg Ballast

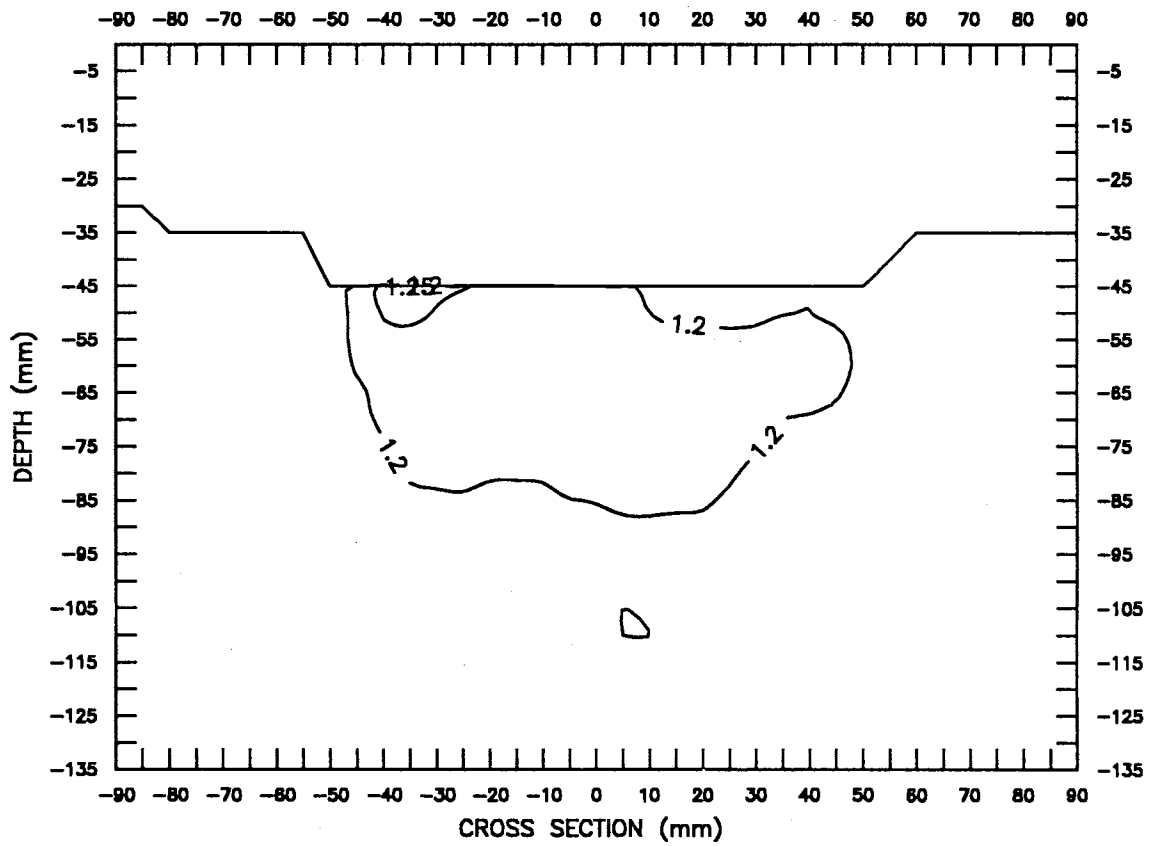


APPENDIX C-4

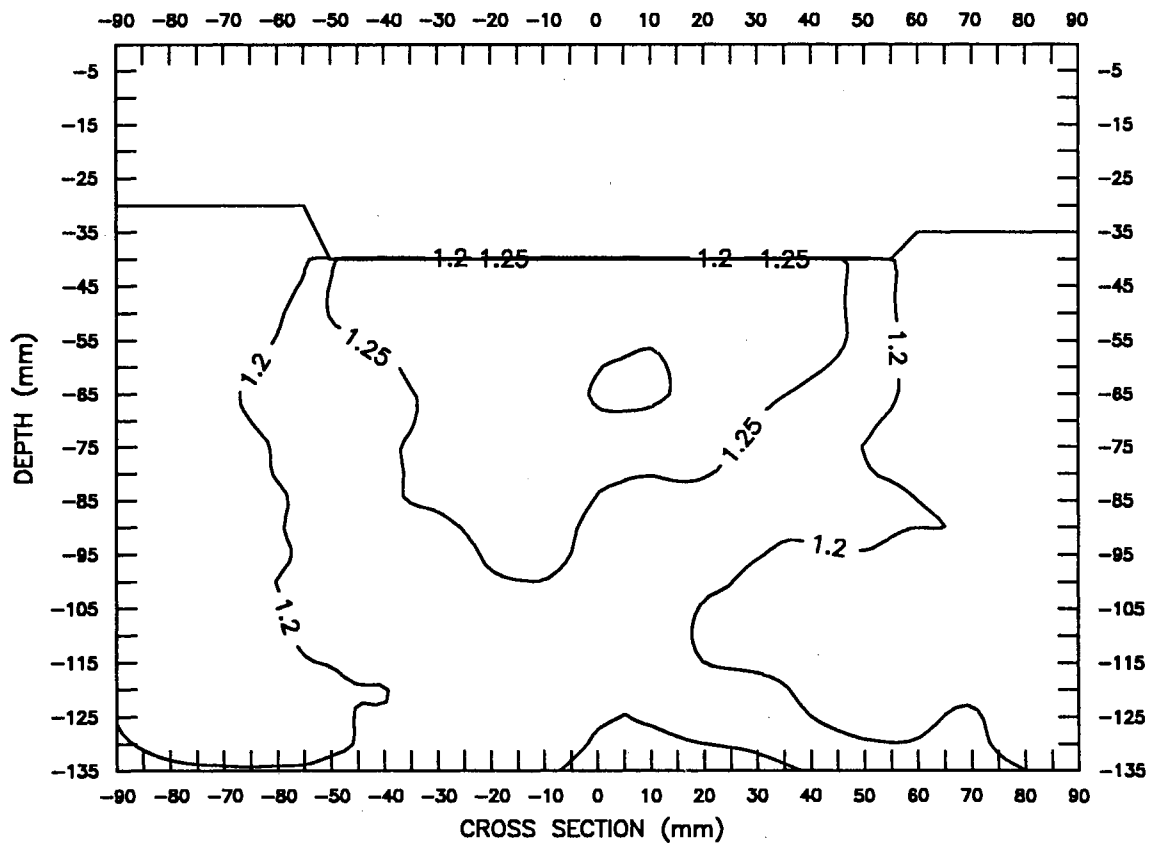
Contour Map of Laboratory Experiment Sample 122
with 51 mm Track and 5 kg Ballast

APPENDIX C-5

Contour Map of Laboratory Experiment Sample 131
with 102 mm Track and 5 kg Ballast

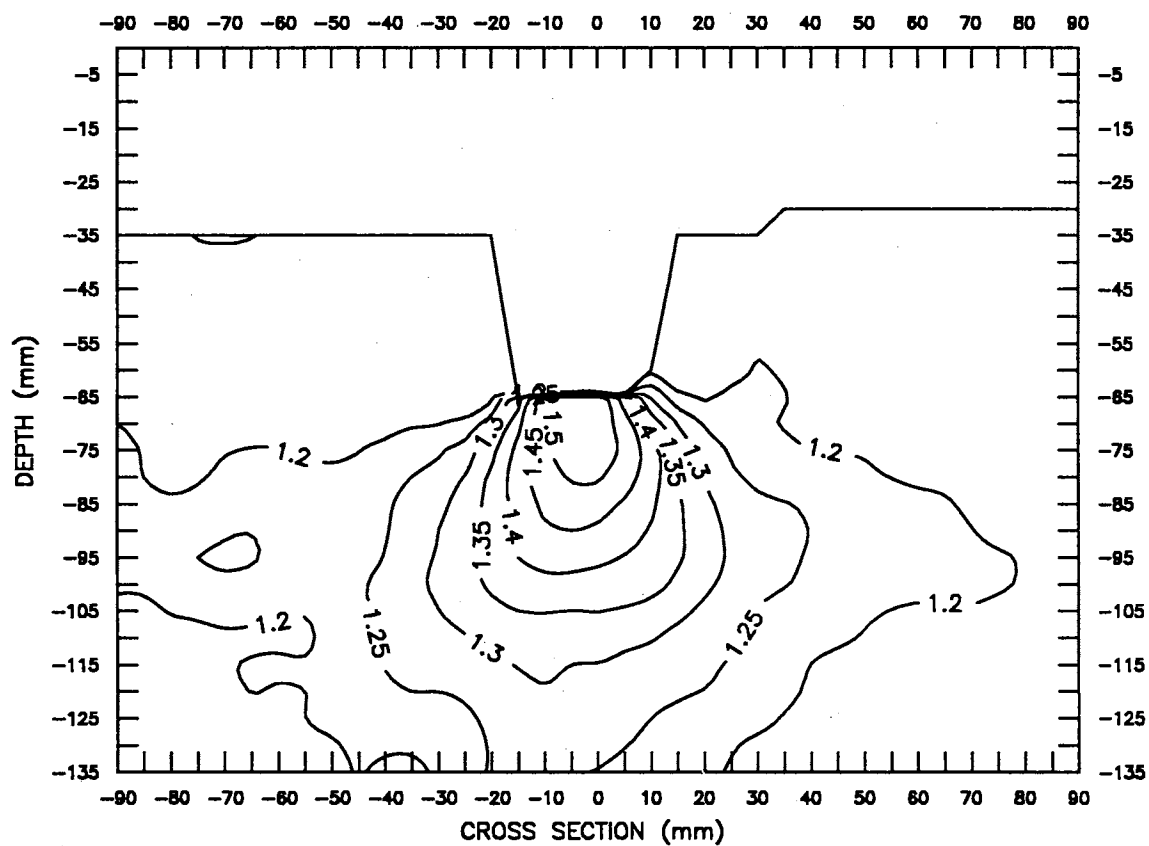


APPENDIX C-6

Contour Map of Laboratory Experiment Sample 132
with 102 mm Track and 5 kg Ballast

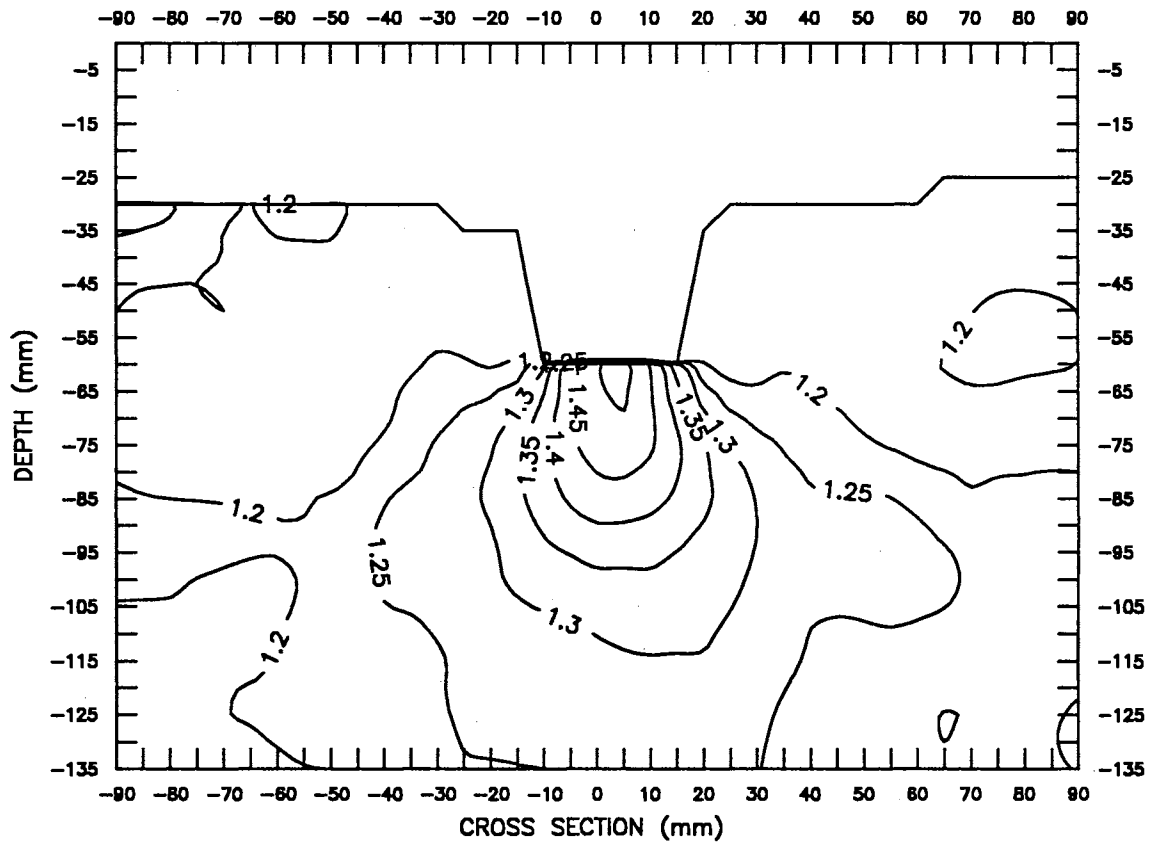
APPENDIX C-7

Contour Map of Laboratory Experiment Sample 141
with 25 mm Track and 10 kg Ballast



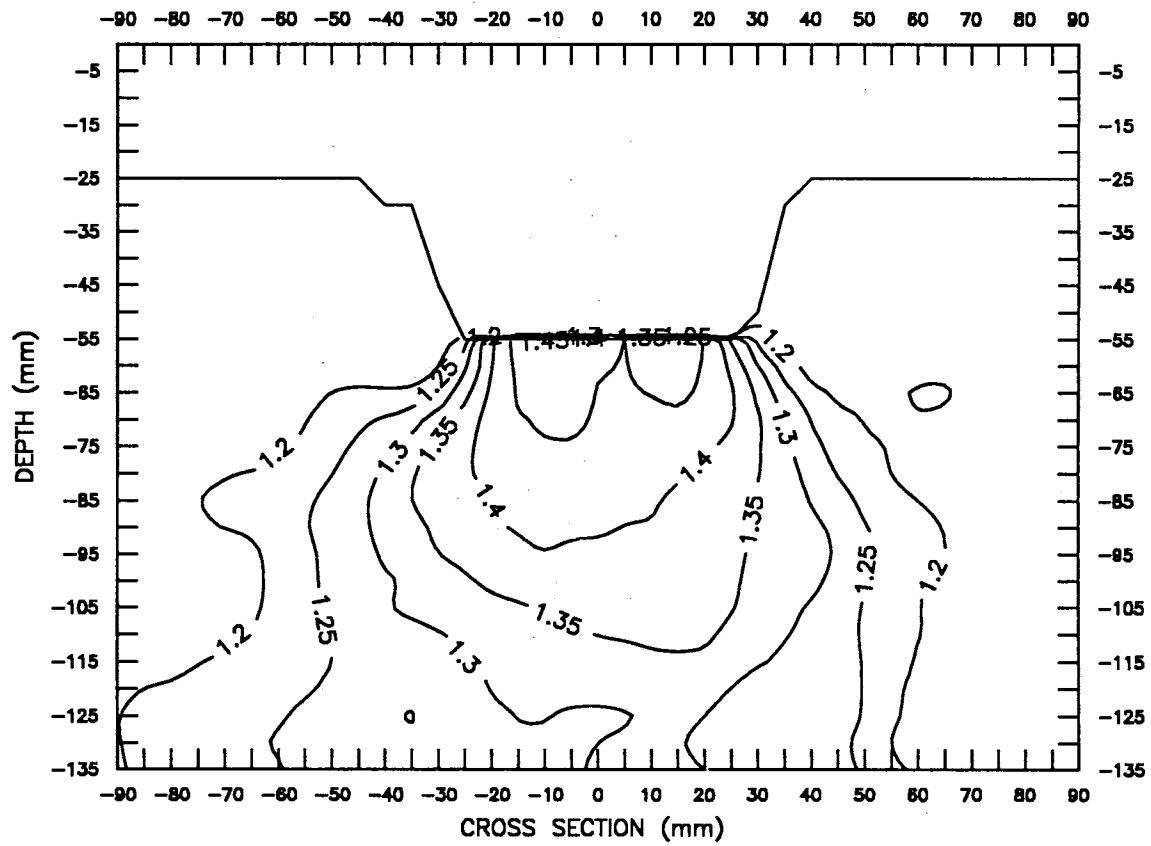
APPENDIX C-8

Contour Map of Laboratory Experiment Sample 142
with 25 mm Track and 10 kg Ballast

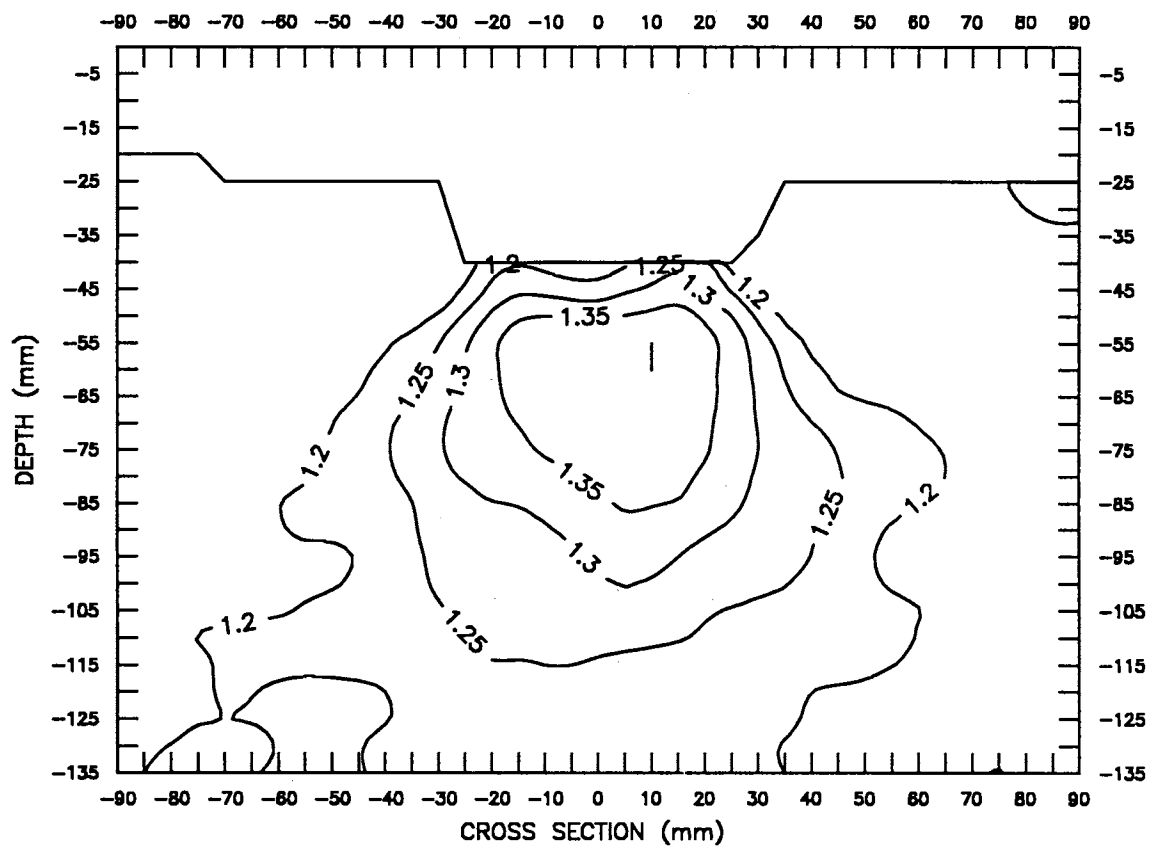


APPENDIX C-9

Contour Map of Laboratory Experiment Sample 151
with 51 mm Track and 10 kg Ballast

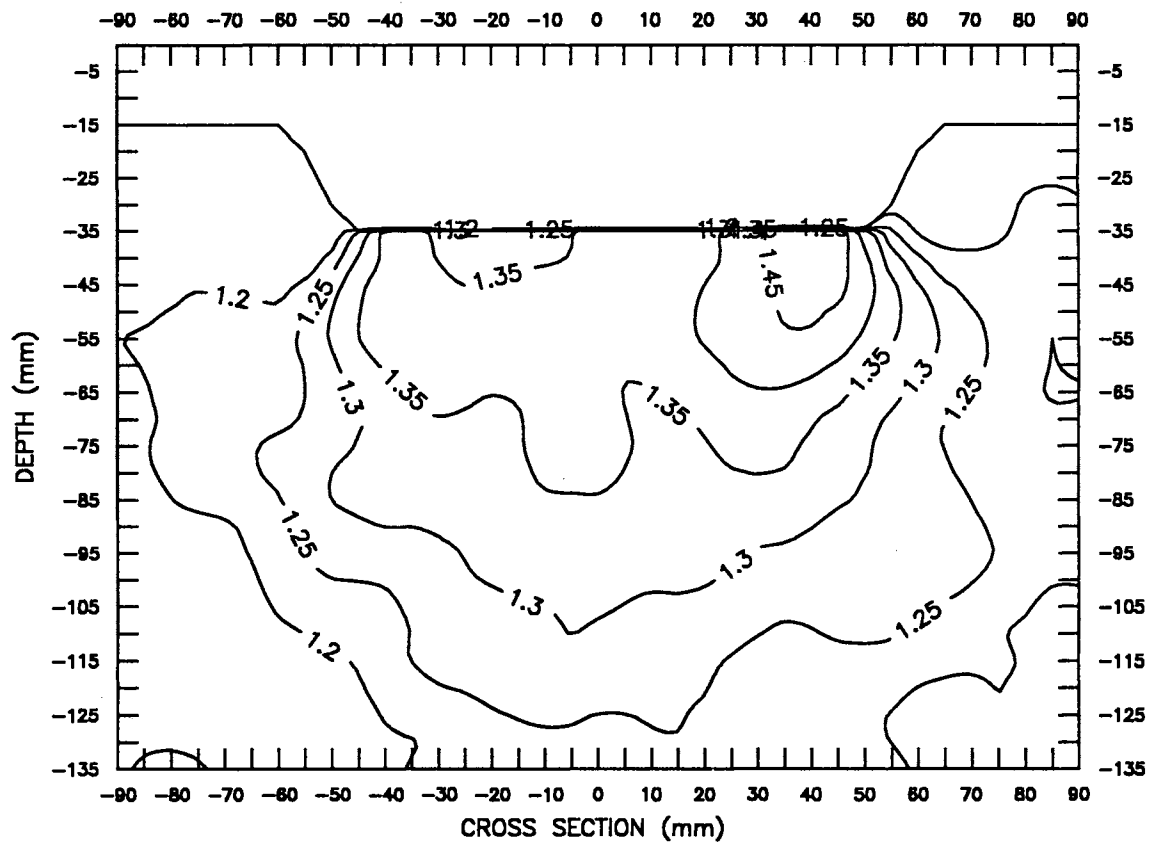


APPENDIX C-10

Contour Map of Laboratory Experiment Sample 152
with 51 mm Track and 10 kg Ballast

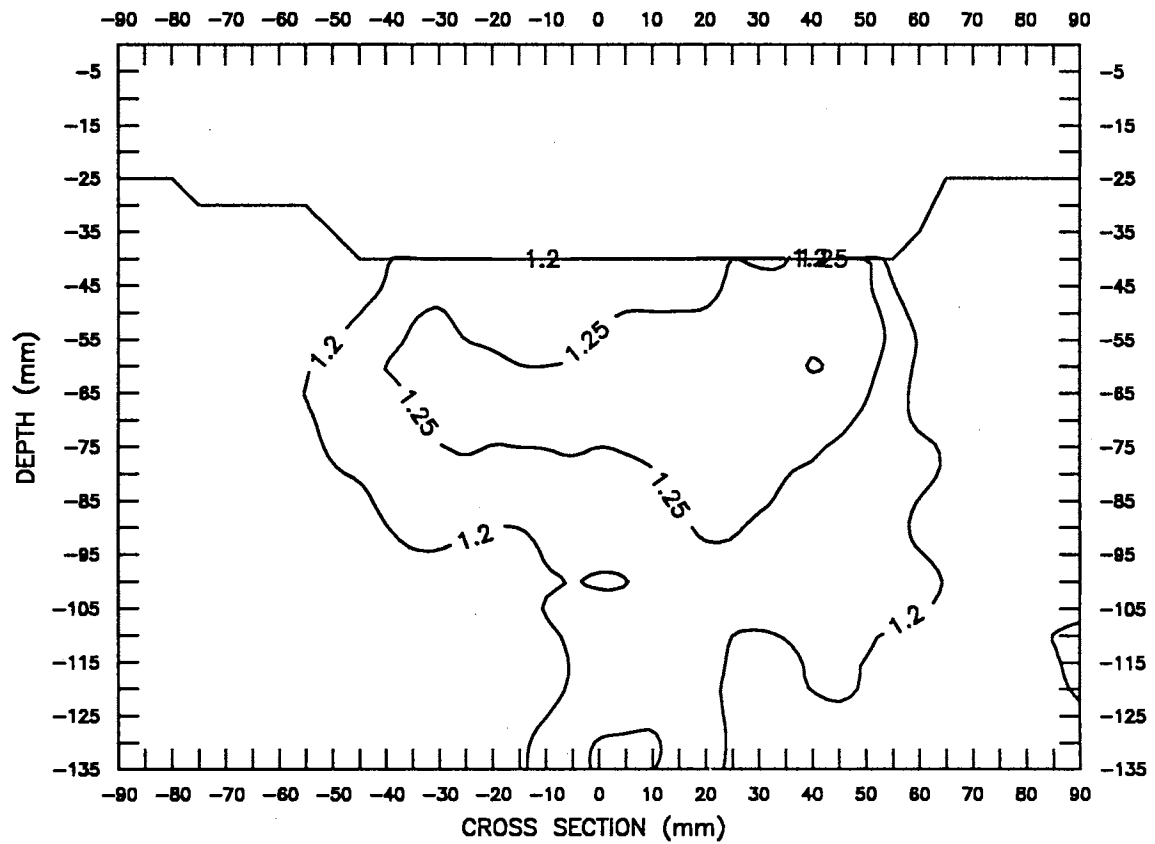
APPENDIX C-11

Contour Map of Laboratory Experiment Sample 161
with 102 mm Track and 10 kg Ballast



APPENDIX C-12

Contour Map of Laboratory Experiment Sample 162
with 102 mm Track and 10 kg Ballast

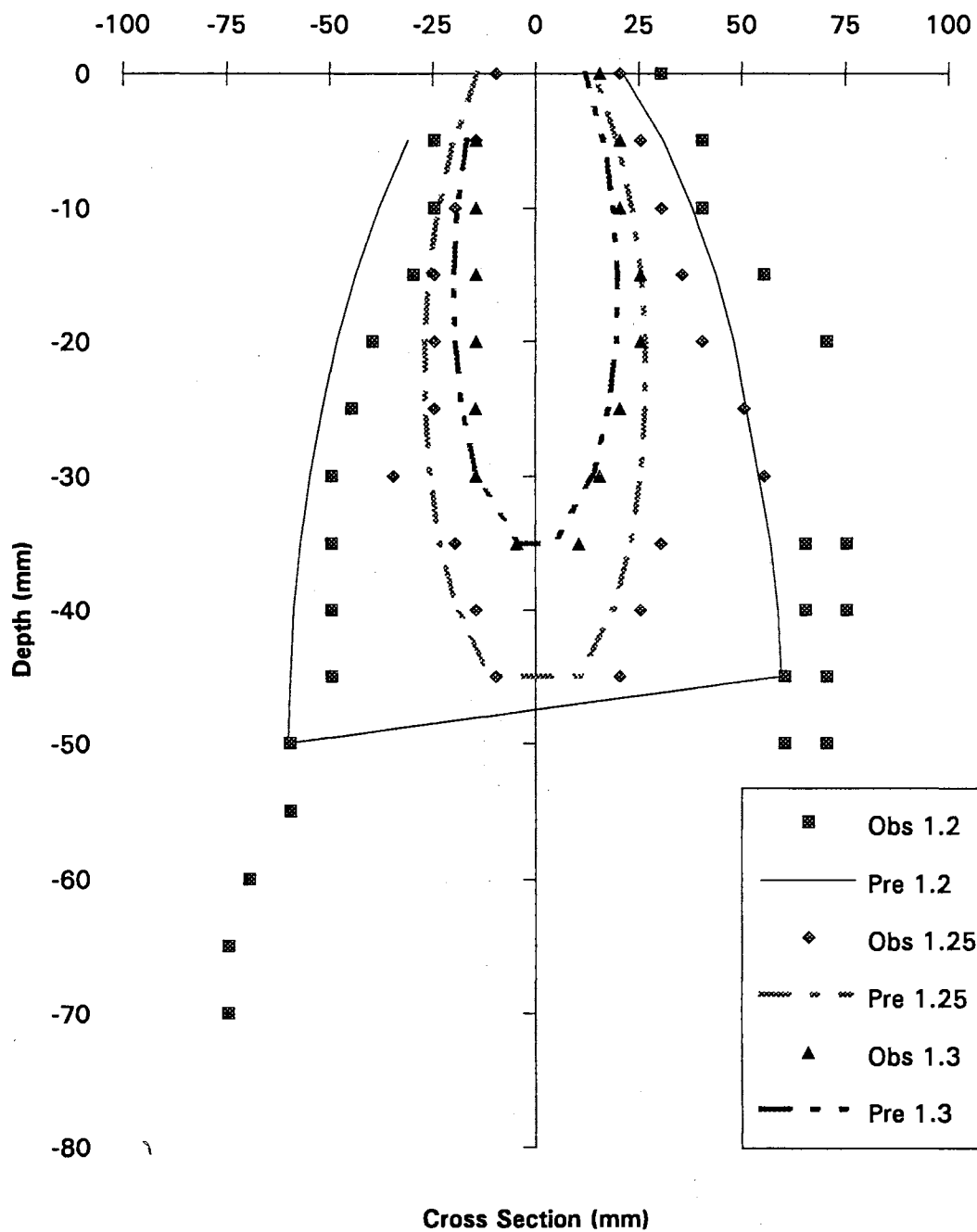


APPENDIX D

**FIGURES OF FITTING LABORATORY EXPERIMENT SAMPLES FOR DENSITY
LEVEL OF 1.2, 1.25 AND 1.3 g/cm³**

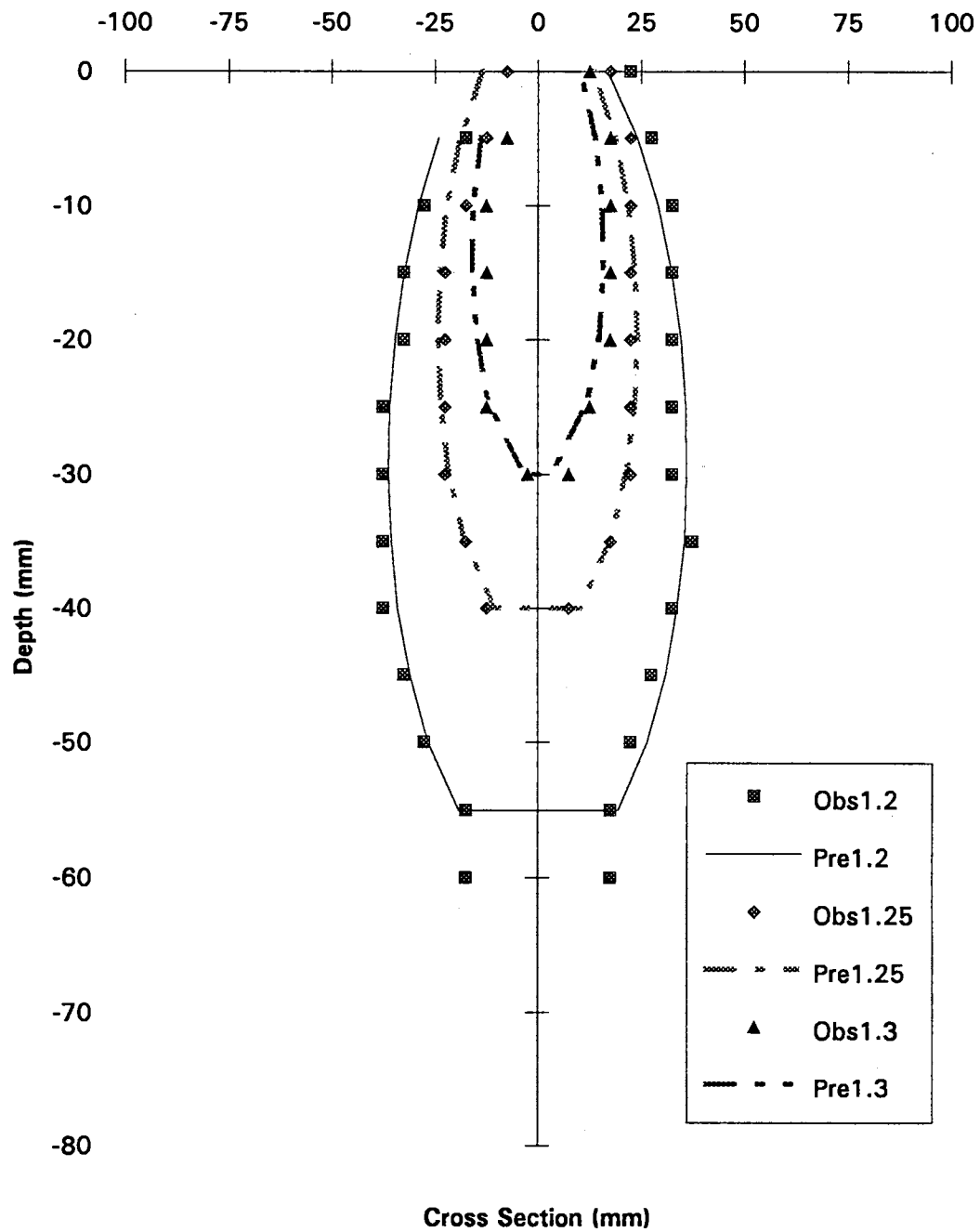
APPENDIX D-1

Fitting of Laboratory Experiment Sample 111
with 25 mm Track and 5 kg Ballast



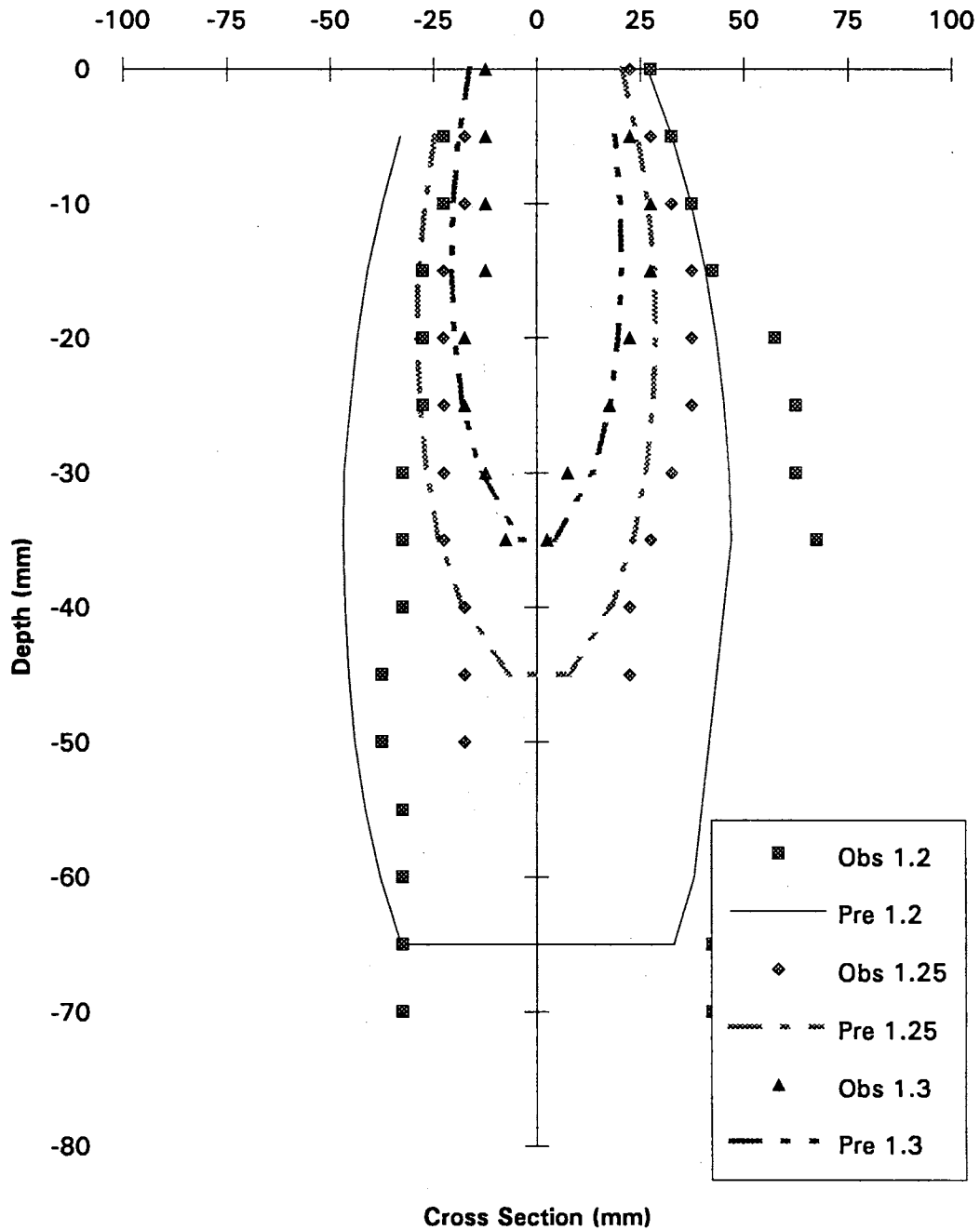
APPENDIX D-2

Fitting of Laboratory Experiment Sample 112
with 25 mm Track and 5 kg Ballast

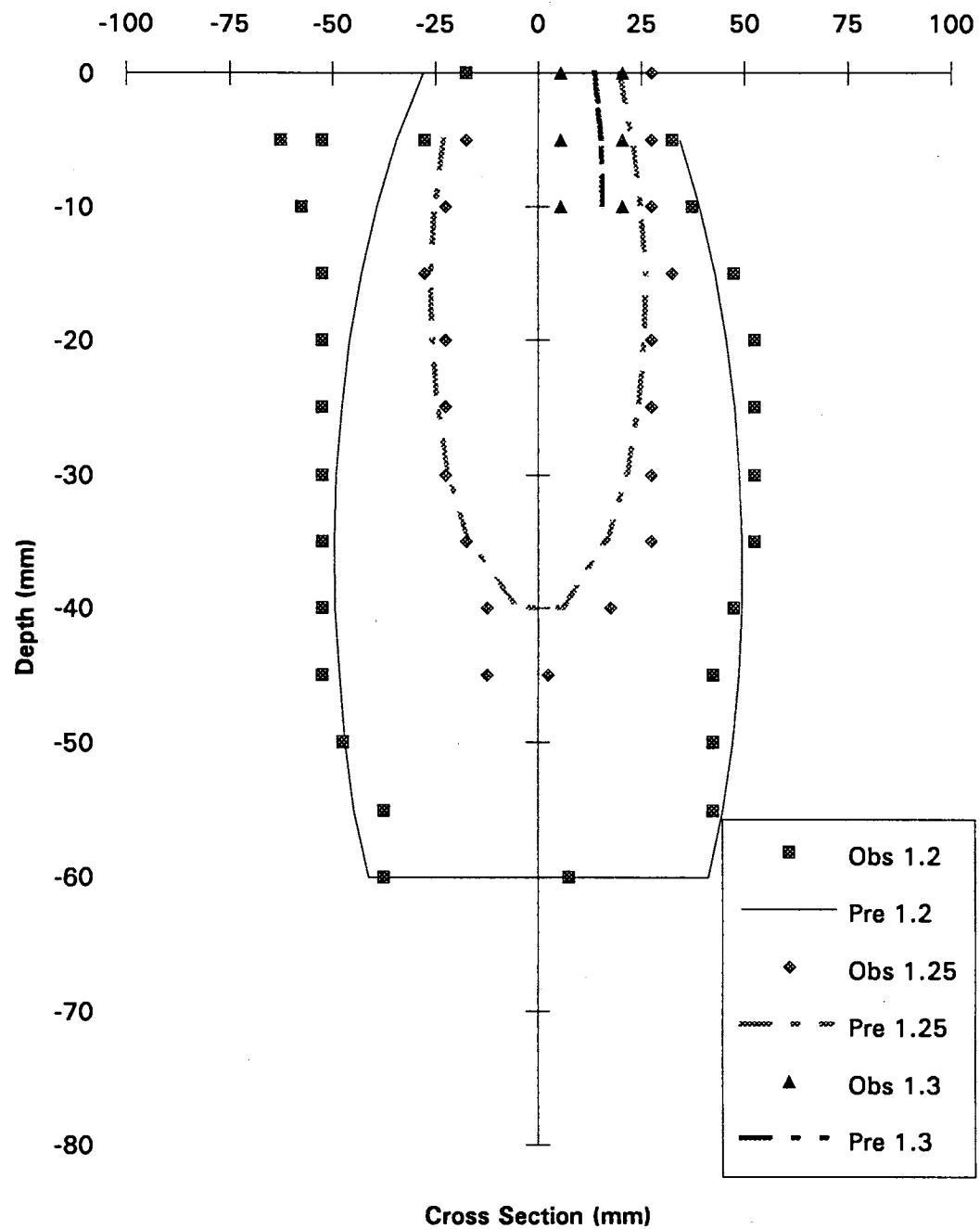


APPENDIX D-3

Fitting of Laboratory Experiment Sample 121
with 51 mm Track and 5 kg Ballast

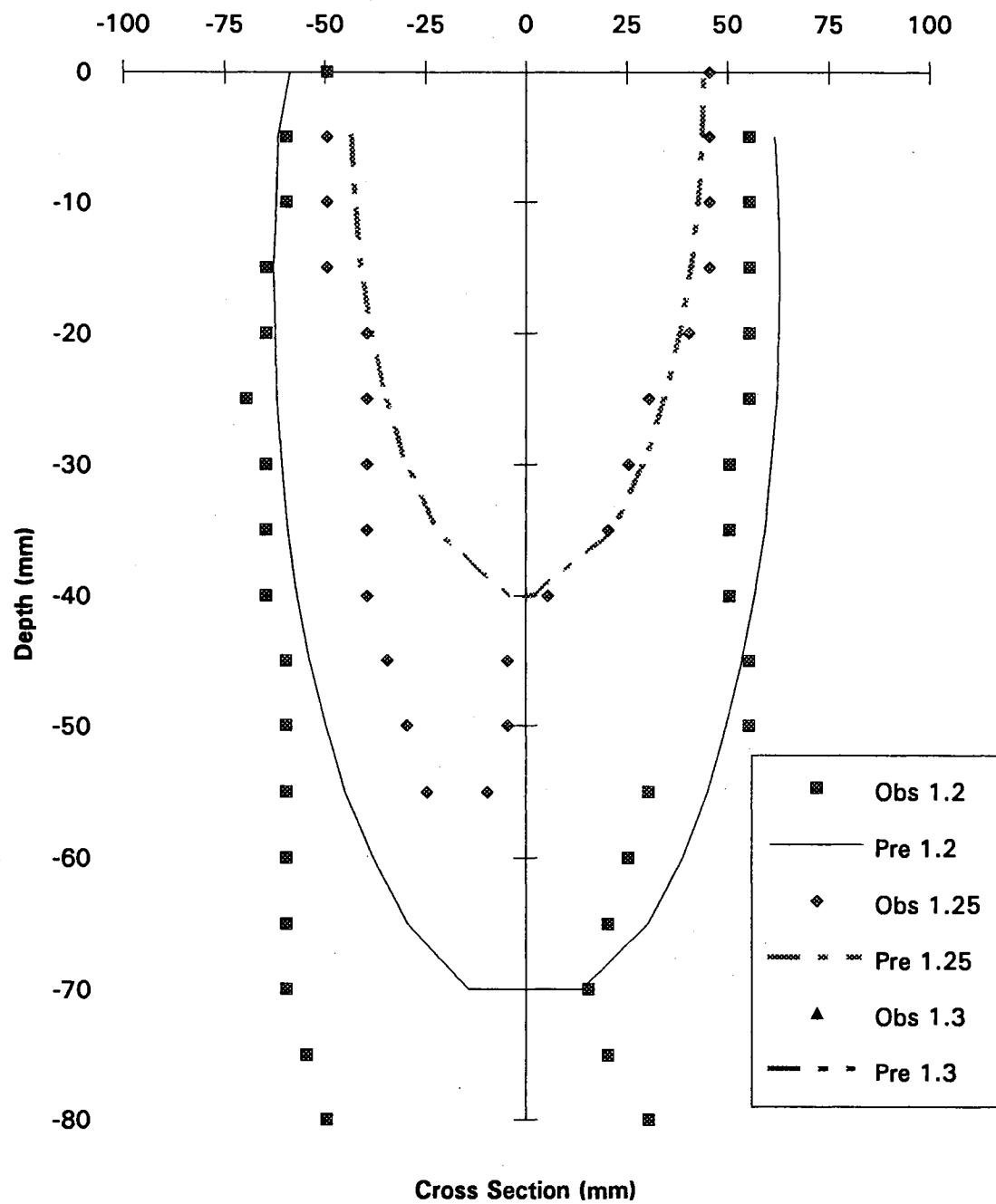


APPENDIX D-4

Fitting of Laboratory Experiment Sample 122
with 51 mm Track and 5 kg Ballast

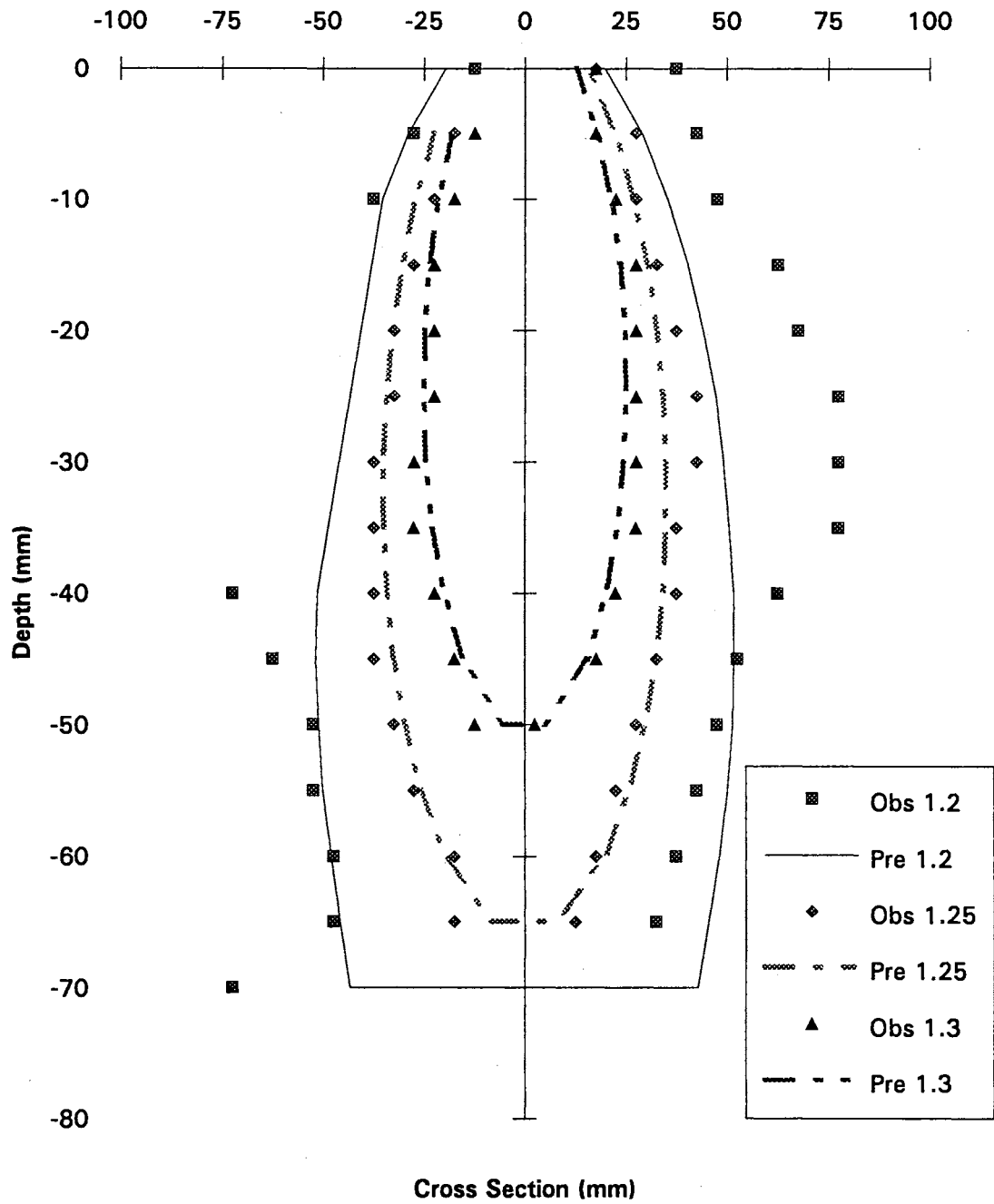
APPENDIX D-6

Fitting of Laboratory Experiment Sample 132
with 102 mm Track and 5 kg Ballast



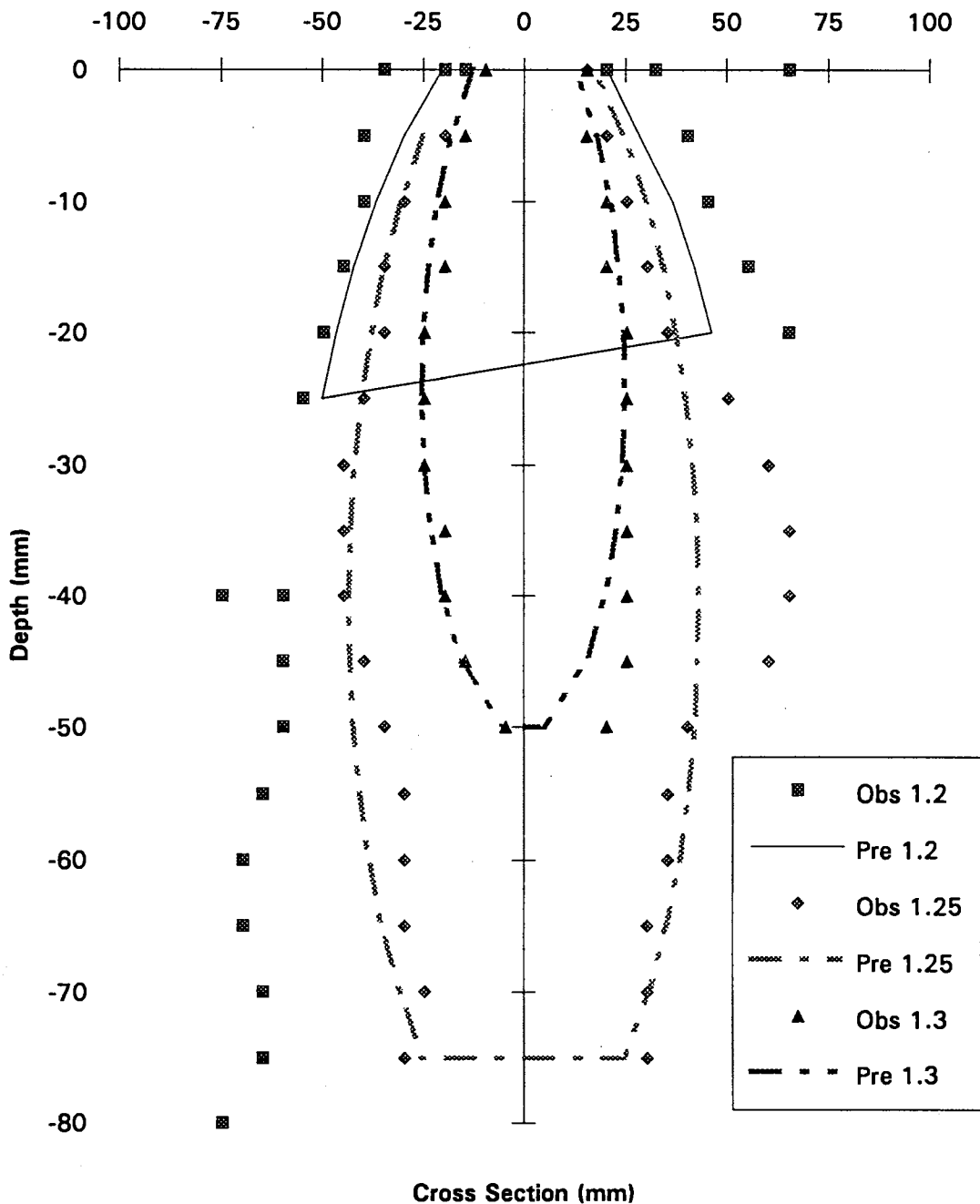
APPENDIX D-7

Fitting of Laboratory Experiment Sample 141
with 25 mm Track and 10 kg Ballast



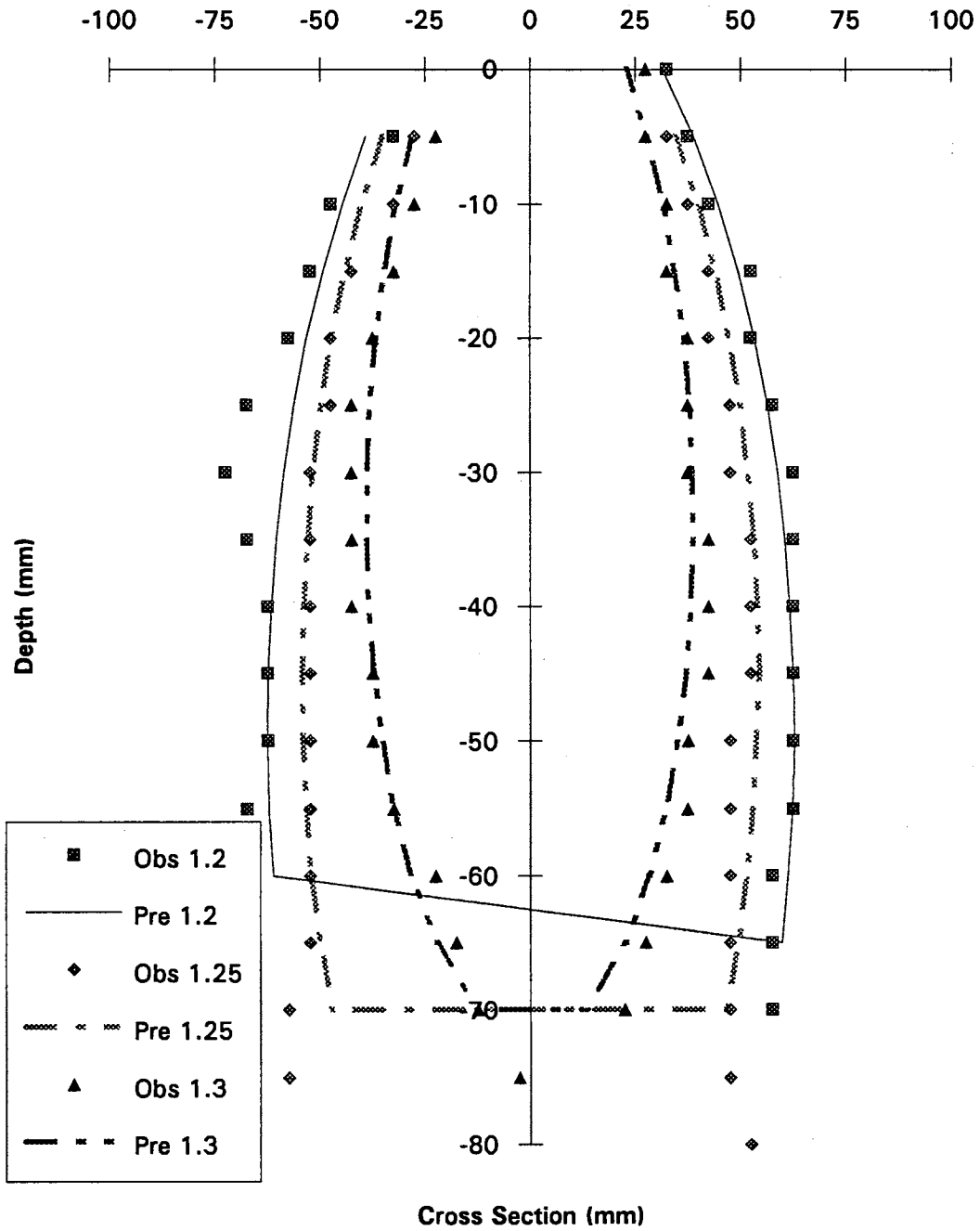
APPENDIX D-8

Fitting of Laboratory Experiment Sample 142
with 25 mm Track and 10 kg Ballast



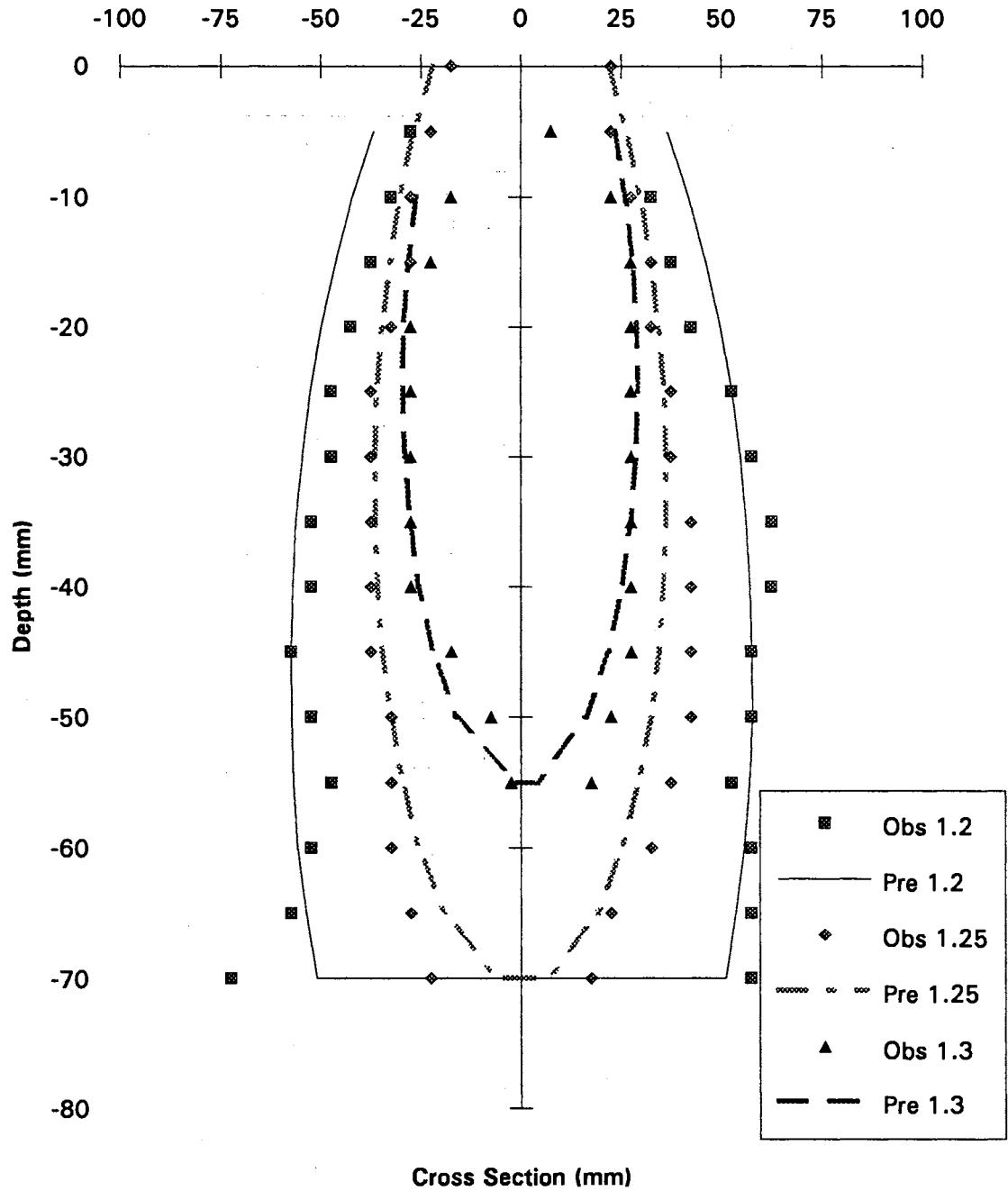
APPENDIX D-9

Fitting of Laboratory Experiment Sample 151
with 51 mm Track and 10 kg Ballast



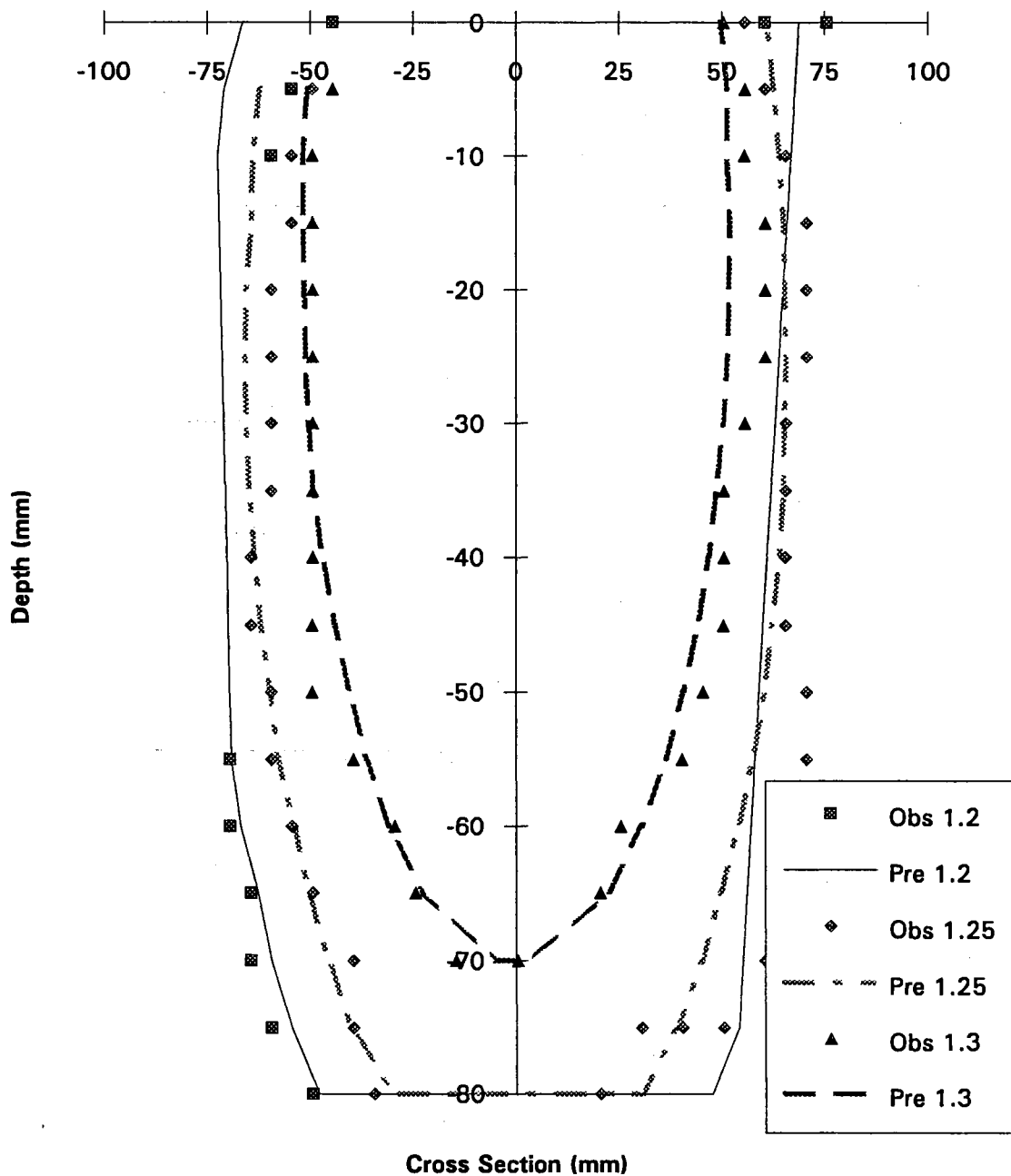
APPENDIX D-10

Fitting of Laboratory Experiment Sample 152
with 51 mm Track and 10 kg Ballast



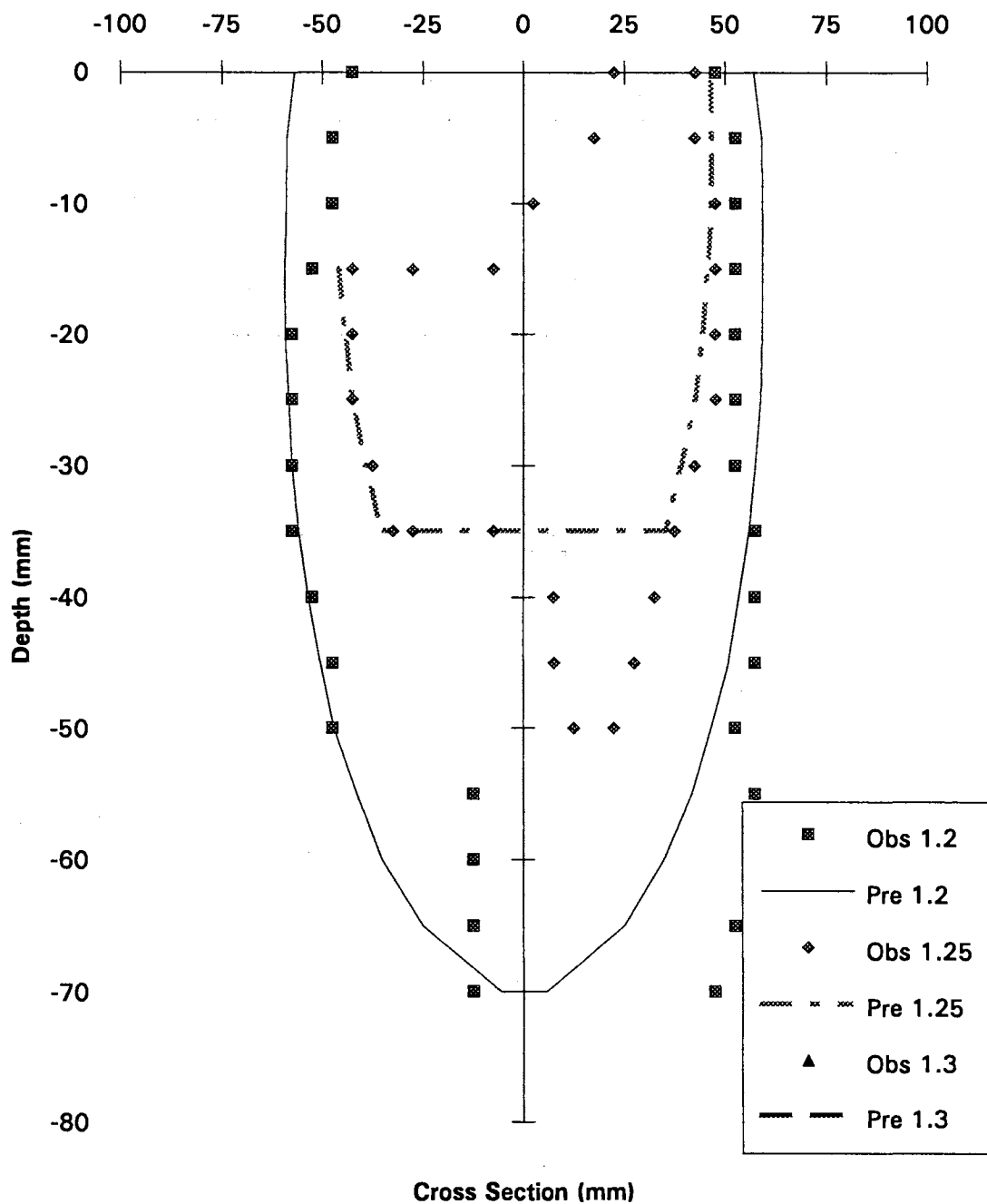
APPENDIX D-11

Fitting of Laboratory Experiment Sample 161
with 102 mm Track and 10 kg Ballast



APPENDIX D-12

Fitting of Laboratory Experiment Sample 162
with 102 mm Track and 10 kg Ballast



APPENDIX E

MAPS OF EXPERIMENTAL DESIGNS

APPENDIX E-1

Design of Field Experiment No. 1

I	I	I	I	I	I
1	1	1	1	1	1
2	2	2	1	2	3
1	2	3	3	4	3
101	102	103	104	105	106
A L L E Y					
I	I	I	I	I	I
2	2	2	2	2	2
1	2	3	2	2	2
3	1	3	3	2	4
201	202	203	204	205	206
A L L E Y					
I	I	I	I	I	I
3	3	3	3	3	3
2	3	2	1	2	2
4	3	2	3	3	1
301	302	303	304	305	306

APPENDIX E-2

Design of Field Experiment No. 2

II 1 1 3	II 1 2 2	II 1 2 1	II 1 2 4	II 1 2 3	II 1 3 3
101	102	103	104	105	106
A L L E Y					
II 2 1 3	II 2 3 3	II 2 2 3	II 2 2 1	II 2 2 2	II 2 2 4
201	202	203	204	205	206
A L L E Y					
II 3 3 3	II 3 1 3	II 3 2 1	II 3 2 2	II 3 2 4	II 3 2 3
301	302	303	304	305	306

APPENDIX E-3

Design of Soil Bin Experiment

III	III	III	III	III	III
1	1	1	1	1	1
1	3	2	2	2	2
3	3	1	2	3	4
101	102	103	104	105	106

APPENDIX E-4

Design of Laboratory Experiment

IV	IV	IV	IV	IV	IV
1	1	1	1	1	1
1	2	3	1	2	3
2	2	2	3	3	3
101	102	103	104	105	106

VITA²

WANGXING LI

Candidate for the Degree of

Doctor of Philosophy

Thesis: **COMPACTION ANALYSIS OF AGRICULTURAL SOIL
USING GAMMA RAY TECHNIQUES**

Major Field: **Biosystems Engineering**

Biographical:

Personal Data: Born in Beijing, People's Republic of China, May 15, 1961, the son of Jingxian Li and Enrong Pan.

Education: Graduated from Dayushu High School, Yanqing, Beijing, P.R. China, in August 1978; received a Bachelor of Science degree in Agricultural Engineering from Jilin University of Technology, P.R. China; received a Master of Science degree in Agricultural Engineering from the University of Nebraska-Lincoln; completed the requirements for the Doctor of Philosophy degree at Oklahoma State University in December, 1994.

Professional Experience: Graduate Research Assistant, Oklahoma State University Biosystems and Agricultural Engineering Department, spring 1987 to summer 1991 and fall 1992; Graduate Teaching Assistant, Oklahoma State University Agricultural Engineering Department, spring 1993; Member of American Society of Agricultural Engineers, Alpha Epsilon.